AL-FARABI KAZAKH NATIONAL UNIVERSITY

UDC: 620.193.4 (043.3)

On manuscript rights

ZELLELE DANIEL MEKONNEN

Electrochemical synthesis and functional properties of metal and alloy-based composition coatings

8D07110 Material Science and Technology of New Materials

Dissertation for the degree of Doctor of Philosophy (PhD)

Scientific consultants:
Dr. Sc. Professor
Yar-Mukhamedova Gulmira Sharifovna

PhD, Assistant Professor
Rutkowska-Gorczyca Malgorzata

Republic of Kazakhstan
Almaty, 2026

CONTENTS

ABBREVIATIONS **4**
INTRODUCTION **5**
1 LITERATURE REVIEW **8**
1.1 Electrochemical synthesis 8
1.2 Historical development 9
1.3 Electrochemical cell 11
1.4 Electrodeposition and its methods 13
1.5 Direct current electrodeposition 16
1.6 Pulse current electrodeposition 17
1.7 Jet electrodeposition 19
1.8 Electrodeposition of composite coatings 19
1.9 Common types of composite coatings and their functional properties 21
1.10 Electrodeposition process parameters for composite coatings and their effect 28
1.11 Formulation of research objectives 34
1.12 Conclusion and trends 37
2 RESEARCH METHODS **39**
2.1 Scanning Electron Microscopy (SEM) and Energy Dispersive X-ray Spectroscopy (EDS) 40
2.2 Raman Spectroscopy 42
2.3 Mechanical properties testing 46
2.4 Scanning Probe Microscopy and Atomic Force Microscopy (AFM) 47
2.5 X-ray Diffraction 48
2.6 Optical Microscopy 50
2.7 Electrochemical testing 51
2.8 Relevance to composition coatings 52
3 SYNTHESIS AND FUNCTIONAL PROPERTIES OF METAL AND ALLOY-BASED COMPOSITION COATINGS **53**
3.1 Morphology and corrosion resistance of electrodeposited chromium-graphene composite coatings under varying temperatures **53**
3.1.1 Experimental 54
3.1.2 Synthesis of graphene 54
3.1.3 Electrodeposition process 55
3.1.4 Characterization methods 56
3.1.5 Characterization of graphene 56
3.1.6 Effect of varying deposition temperature on surface morphology and carbon content of coatings 58
3.1.7 Grain sizes and microhardness 62
3.1.8 Effect of deposition temperature on corrosion resistance properties 65
3.1.9 Summary 67
3.2 Characterization of microstructural and surface properties of nickel-copper coatings electrodeposited at high current density on AISI 304 substrate **69**
3.2.1 Substrate preparation 70
3.2.2 Electrolyte, deposition conditions and characterization methods 70

3.2.3 Surface morphology and elemental composition 72
3.2.4 XRD analysis: Phase identification and texture analysis 74
3.2.5 AFM surface topography analysis 76
3.2.6 Microhardness analysis 78
3.2.7 Corrosion properties 79
3.2.8 Summary 80
3.3. Electrodeposition of binary and ternary Cobalt-Vanadium alloy coatings.. 82
3.3.1 Research methods 83
3.3.2 Formation of coatings by direct (stationary) electrolysis 85
3.3.3 Electrodeposition of ternary Co-Fe-V alloys 85
3.3.4 Structural characteristics of Co-V coatings 86
3.3.5 Formation of Co-V coatings in pulse electrodeposition mode 88
3.3.6 Effect of pulse parameters on alloy composition and efficiency 89
3.3.7 Electrocatalytic properties toward the hydrogen evolution reaction (HER) 90
3.3.8 Microhardness and mechanical properties 92
3.3.9 Deposition from vanadyl sulfate-containing electrolytes 92
3.3.10 Corrosion resistance 95
3.3.11 Summary 95
4 CONCLUSIONS 96
LIST OF REFERENCES USED 97

ABBREVIATIONS

DC	Direct Current
PC	Pulse Current
PRC	Pulse Reverse Current
PED	Pulse Electrodeposition
GO	Graphene Oxide
RGO	Reduced Graphene Oxide
H_2SO_4	Sulfuric Acid
$KMnO_4$	Potassium Permanganate
H_3PO_4	Phosphoric Acid
AFM	Atomic Force Microscopy
XRD	X-ray Diffraction
SEM	Scanning Electron Microscope
EDS	Energy Dispersive Spectroscopy
EDAX	Energy Dispersive X-ray Spectroscopy
EIS	Electrochemical Impedance Spectroscopy
SCE	Saturated Calomel Electrode
NaOH	Sodium Hydroxide
CO_2	Carbon Dioxide
NiO	Nickel Oxide
NO_2	Nitrogen Dioxide
CVD	Chemical Vapor Deposition
PVD	Physical Vapor Deposition
H_2O_2	Hydrogen Peroxide
HCl	Hydrochloric Acid
Zn_SO_4	Zinc Sulfate
Cu_SO_4	Copper Sulfate
Ni_2SO_4	Nickel Sulfate
CNT	Carbon Nanotubes
WC	Tungsten Carbide
Al_2O_3	Aluminum Oxide
TiC	Titanium Carbide
TiB	Titanium Bromide
HER	Hydrogen Evolution Reaction
KCl	Potassium Chloride
SiC	Silicon Carbide
NaCl	Sodium Chloride
HV	Hardness Value
MMC	Metal Matrix Composite
rpm	Revolution Per Minute
mm	Millimeter
µm	Micrometer
nm	Nanometer

INTRODUCTION

Actuality of the research topic

The actuality/relevance of this dissertation is determined by the growing global demand for advanced surface engineering technologies that enhance the durability, functionality, and service life of engineering materials. Metal and alloy-based composition coatings play a critical role in modern industries by providing protection against corrosion, wear, oxidation, and mechanical damage, which are among the main causes of premature failure of structural components.

Electrochemical synthesis is one of the most versatile and cost-effective methods for producing various types of functional coatings, offering precise control over chemical composition, microstructure, thickness and surface morphology. Compared to conventional coating technologies, electrochemical methods are known to provide advantages such as low energy consumption, environmental compatibility, scalability and the ability to form complex multi component and composite coating systems. However, even though it has been extensively used in lab scale and industrially, there remain unresolved and ongoing scientific challenges related to controlling phase formation, amount and density of defects formed, internal stresses, and structure-property relationships in metal and alloy-based composition coatings. The rapid development of oil and gas, transport, energy, and chemical industries has intensified the need for high-performance coatings capable of operating under aggressive environments, including high humidity, elevated temperatures, and corrosive media. Particularly, infrastructure and equipment used in harsh climate and industrial conditions require surface protection systems with improved corrosion resistance, mechanical strength, and functional stability. This issue is especially relevant for countries with extensive industrial infrastructure and challenging environmental conditions. In the context of sustainable development, the replacement of toxic and environmentally hazardous coating technologies with greener electrochemical processes is of strategic importance. The development of electrodeposition technologies that reduce the use of hazardous substances while simultaneously improving coating performance directly supports global environmental and industrial safety goals.

Therefore, the research on electrochemical synthesis and functional properties of metal and alloy-based composition coatings is highly relevant both from a scientific and applied point of view, as it contributes to the development of advanced materials with improved performance characteristics, extended service life, and reduced environmental impact. The results of this work can be widely applied in mechanical engineering, energy systems, transport infrastructure, and chemical equipment as well as other key industrial sectors.

Objective of the dissertation work

To develop, optimize, and characterize electrochemically synthesized metal and alloy-based composition coatings (Chromium-Graphene, Nickel-Copper, Cobalt-Vanadium), and to establish their structure-property relationships in terms of functional characteristics.

Research tasks

To achieve this objective, it is necessary to carry out these research tasks:

● To design and optimize electrochemical deposition parameters (electrolyte composition, pH, current density, temperature) for producing uniform and adherent metal and alloy-based composite coatings on various substrates and to investigate the influence of electrochemical synthesis conditions on the nucleation, growth, and microstructural evolution of the coatings.

● To characterize the morphological, structural, and compositional features of the deposited coatings using SEM/EDS, XRD, AFM, and related surface analytical techniques and to evaluate key functional properties of the coatings such as hardness and corrosion resistance and how they correlate with the synthesis parameters and microstructure.

● To establish structure-property relationships that explain how electrochemical synthesis routes affect the coating quality and functional performance and to propose optimized electrochemical strategies for producing high-performance protective and functional coatings suitable for industrial applications.

Main provisions for defense

1. The morphology, microhardness, and content of the dispersed phase in the synthesized chromium–graphene electrolytic coatings are determined by the deposition temperature. This is manifested in the formation of a nanocrystalline structure (25–26 nm) at deposition temperatures of 288–303 (±2) K, a nanocrystalline structure (19 nm) at 318 (±2) K, and a cracked and microporous structure at 303 (±2) K.

2. In coatings consisting of binary Ni–Cu alloys, control over crystal size, grain texture, and porosity can be achieved by varying the current density, thereby enabling the purposeful formation of nanocrystalline and amorphous–crystalline structures and optimization of mechanical properties and corrosion resistance for specified operating conditions.

3. The corrosion-electrochemical and mechanical characteristics of composite electrolytic coatings based on binary Co-V alloys depend on the deposition mode (direct current or pulsed). An increase in the content of the refractory component is associated with an increase in current efficiency and with the chemical reduction of vanadium during the pause period under pulsed electrodeposition conditions.

Scientific novelty and significance

A comprehensive study has been carried out on the processes governing microstructure formation and physicochemical properties of chromium-based composite coatings structured with graphene, as well as composite electrolytic coatings from binary Ni-Cu and Co-V alloys obtained by electrochemical synthesis on AISI 304 steel substrates.

A new approach to controlling crystal size in binary Co-V systems has been developed, based on variation of current density and deposition modes (direct current and pulsed) for multicomponent coatings. As a result of this, a new electrolyte was developed, and a utility model patent titled *"Method for Depositing Cobalt-Vanadium Alloy"* was obtained (Republic of Kazakhstan Patent No. 11879, dated March 6, 2026).

For the first time, the mechanisms of co-deposition of nickel with copper and cobalt with vanadium into alloys have been established, and the influence of electrolyte composition and deposition regimes on component content, structure, properties, and efficiency of the electrodeposition process for Ni-Cu and Co-V coatings has been substantiated.

Based on quantitative analysis of experimental data on oxidation kinetics, as well as the results of physical and mechanical property tests, a phenomenological model describing the formation of the microstructure of chromium-graphene composite coatings has been proposed.

Personal contribution of the doctoral student

The doctoral student's personal contribution includes setting the goals and objectives of the work, writing reviews, conducting experiments, cooperating with colleagues, processing and analyzing results, formulating conclusions, and writing articles.

Publications

As part of the dissertation research work and the experimental data obtained from it, the doctoral student, under the guidance of scientific consultants, has authored, co-authored and published a total of 18 manuscripts including 4 articles in scientific journals of the Scopus database with high impact factor, 5 articles on journals in Kazakhstan Citation Database (National Center of Scientific and Technology Evaluation), 6 abstracts and conference proceedings in national and international conferences, 1 monograph, and 2 utility model patents.

Volume and structure of the dissertation

The dissertation contains a list of abbreviations, an introduction, literature review, materials and methods, results and analyses consisting of three subjects, conclusions and a list of references. The work is presented on 113 pages containing 52 figures, 16 tables and 216 bibliographical references.

1 LITERATURE REVIEW

Materials play a crucial role in the realm of engineering and technology, serving as the foundational pillars upon which advancements are built. The interaction of materials, precisely their electrochemical, mechanical, and thermal properties, initiate at the surface. However, the surfaces of materials are constantly under pressure from corrosion and wear, leading to significant amount of losses within various applications and industries. To overcome these issues, utilizing surface properties enhancement methods and technologies have become necessity. In recent years, significant advancements in the fields of metallurgy and materials science have been observed, resulting in the development of new engineering materials with enhanced functional properties. The process of producing these materials consists of complex procedures aimed at altering their inherent characteristics. This requires careful consideration of both the economic aspects and environmental implications of the material being produced. As a result, the importance of materials in engineering and technology cannot be overstated. By leveraging surface property enhancement technologies and embracing the latest scientific developments, it is possible to continue to push the boundaries of what is possible in the world of materials science.

1.1 Electrochemical synthesis

Electrochemical synthesis is a versatile and environmentally friendly method that has gained significant attention in recent years for the production of various organic and inorganic chemical compounds in an electrochemical cell. It is achieved by passing an electrical current between two electrodes separated by an electrolyte, making the synthesis take place at the electrode-electrolyte interface. It is versatile and transformative field at the intersection of chemistry and electrochemistry, enabling the precise control and manipulation of chemical reactions using electrical energy and it involves using this electrical energy to trigger chemical reactions at electrodes, creating new compounds or materials. One of the key areas of focus in electrochemical synthesis is the development of novel materials for energy storage applications. Lv et al. [1] reviewed the progress in synthesizing nano-/microstructured materials for supercapacitors using various electrochemical techniques. These techniques include cyclic voltammetry, potentiostatic deposition, galvanostatic deposition, pulse deposition, and electrophoretic deposition, highlighting the importance of nanostructured materials in enhancing the performance of supercapacitors. Another significant area of research in electrochemical synthesis is the development of metal-organic frameworks (MOFs). V. et al. [2] provided a review on the direct electrochemical synthesis of MOFs, emphasizing the importance of this method in producing MOFs with specific properties for various applications, and discussing the challenges and opportunities in the electrochemical synthesis of MOFs. Electrochemical synthesis has also been utilized in the production of pharmaceutical compounds and fine chemicals. Li et al. [3] demonstrated the electrochemical synthesis of α, α-dihaloacetophenones from terminal alkyne derivatives, showcasing the potential of electrochemistry in the synthesis of complex organic molecules. Similarly, Zhao et al. [4] reported an electrochemical method for the synthesis of benzimidazoles via dehydrogenative cyclization of amidines, highlighting the simplicity and efficiency

of the electrochemical approach. In the field of catalysis, electrochemical synthesis has shown promise in the development of efficient catalysts for various reactions. Jimenez-Villegas et al. [5] presented SnO_2-supported single metal atoms as a bifunctional catalyst for the electrochemical synthesis of H_2O_2, demonstrating the potential of electrocatalysis in green chemistry. Ye et al. [6] reviewed the electrochemical synthesis of cooper-based catalysts for the reduction of CO_2 to C^{2+} products, showcasing the importance of electrochemistry in sustainable catalysis. Furthermore, electrochemical synthesis has been applied in the production of ammonia, a green energy carrier. Wu et al. [7] discussed the progress and challenges in the electrochemical synthesis of ammonia, highlighting the potential of electrochemistry in the sustainable production of ammonia for various applications. Moreover, Wang et al. [8] also provided a compressive review on the electrochemical synthesis of ammonia and its direct utilization in ammonia fuel cells, with an emphasis on the importance of electrochemical methods in terms of the development of alternative energy sources. Overall, the literature on electrochemical synthesis demonstrates the versatility and potential of this method in various fields, including energy storage, catalysis, pharmaceuticals, and green energy production. The advancements in electrochemical techniques and materials synthesis pave the way for the development of sustainable and efficient processes for the production of valuable compounds. Further research in this area is essential to unlock the full potential of electrochemical synthesis for future applications.

1.2 Historical Development

The historical development of electrochemical synthesis marked by several key milestones that have significantly influenced both scientific understanding and industrial applications. From the foundational discoveries in the late 18th century to modern advancements in organic and inorganic chemistry, electrochemical synthesis has evolved to become a cornerstone of chemical processes. This progress is characterized by the vital contributions of pioneering scientists, the development of new methods and techniques, and application of electrochemistry in diverse fields and disciplines. The crucial milestones include the discovery of bioelectricity by Luigi Galvani in 1776, when experiments laid the groundwork of electrochemistry by demonstrating the electrical nature of biological phenomena, Alessandro Volta's invention of the voltaic pile in 1800, which provided the first continuous source of electric current enabling further experimentation and discovery, and Michael Faraday's laws of electrolysis formulated in the 1830s which established the quantitative relationship between electricity and chemical change forming the basis for electrochemical synthesis [9]. The mid-1800s saw the pioneering work of Kolbe, who utilized electrochemical methods for the synthesis of organic compounds, marking the beginning of electrochemical synthesis in organic chemistry. Over the decades, advancements in electrochemical tools have expanded the possibilities for carbon-carbon bond formations, enabling the total synthesis of various natural products. These developments have introduced mechanistic insights and unique bond formations that differ from conventional methods, significantly influencing the approach chemists take

towards synthesizing complex natural compounds [10]. The 20th century witnessed the expansion of electrocatalysis, with significant advancements in reactions such as CO_2 reduction and hydrogen evolution, facilitated by various electrocatalysts including metal oxides, carbon-based materials, alloys, noble metals, and platinum-based catalysts. The evolution of layered electrocatalytic materials and exploration of electrocatalysts without platinum also mark important progress in the field, showcasing the diverse approaches to enhancing electrochemical synthesis efficiency [11].

More recent developments in electrosynthesis have enabled the creation of selective organic reactions, such as site selective C-H functionalization, which are crucial for drug discovery and the synthesis of complex organic molecules [12]. Moreover, the electrochemical synthesis of complex compounds with transition elements has been refined by Frolov et al. [13] allowing for the development of new methods and the exploration of novel compound compositions. With establishing optimal conditions for electrochemical synthesis, including the concentration ranges of ligands, temperature, solvent choice, and gaseous medium, which significantly influence the yield and efficiency of the complex compounds formed. The use of rare earth metal anodes was introduced for the first time, leading to the synthesis of acetylacetones with distinct physical properties compared to previously synthesized analogues. It was demonstrated that anodic dissolution of metals enhances the decarboxylation of hydroxy acids, and the electrochemical synthesis method proved to be more efficient than conventional chemical synthesis, yielding higher substance yields and current efficiencies. This process allows for controlled synthesis under mild conditions, resulting in high purity and yield of the final products-marking significant advancements in electrochemical synthesis. More recent advances in electrochemical synthesis include nanotechnology [14] and green chemistry approaches [15]. The integration of nanotechnology has revolutionized electrochemical synthesis, enabling enhanced catalytic performance, increased surface area, and improved reaction kinetics. Nanostructured materials have opened up new possibilities for efficient and sustainable synthesis processes. Similarly, adopting green chemistry principles in electrochemical synthesis has gained momentum, leading to the development of sustainable processes that minimize waste generation, utilization of non-toxic reagents, and reduce energy consumption. Electrochemical methods contribute to the advancement of environmentally friendly synthesis routes.

Electrochemical synthesis offers precise control over reactions, high selectivity, and the ability to operate at mild conditions. It is also environmentally friendly, cost effective, and allows for utilization of renewable energy sources. While the historical trajectory of electrochemical synthesis highlights significant progress, it is important to recognize the ongoing challenges and opportunities in the field. Electrochemical synthesis may have limitations in scalability, electrolyte compatibility and electrode stability. Developing efficient electrode materials and improving energy efficiency are ongoing challenges. Overcoming these technological hurdles will pave the way for the widespread adoption of electrochemical synthesis in various sectors. The continuous development of new materials and techniques promises further advancements, particularly in sustainable energy and green chemistry applications. This dynamic field

remains at the forefront of scientific innovation, bridging traditional chemistry with modern technological needs. The future of electrochemical synthesis lies in the exploration of novel electrode materials, the integration of artificial intelligence, for reaction optimization, and the development of integrated systems for continuous production. Cross-disciplinary collaborations and innovation are key drivers for advancing the field.

In conclusion, electrochemical synthesis stands as a powerful tool for designing and producing a wide range of materials with tailored properties, offering sustainable and efficient solutions for various industrial processes. As research continues to push boundaries and address challenges, the future of electrochemical synthesis holds promise for driving innovations in diverse fields and contributing to a more environmentally and technologically advanced society.

1.3 Electrochemical cell

An electrochemical cell, where electrochemical synthesis happens, is a device that can generate electrical energy from the chemical reactions occurring in it, or use the electrical energy supplied to it facilitate chemical reactions in it. These devices are capable of converting chemical energy into electrical energy, or vice versa. A common example of an electrochemical cell is a standard 1.5 V cell which is used to power many electrical appliances such as TV remotes and clocks. These cells are widely used in various applications such as batteries, fuel cells, and sensors. The basic components of an electrochemical cell include two electrodes - an anode and a cathode, connected by an electrolyte solution. When the electrodes are connected through an external circuit, redox reactions occur at each electrode, generating an electric current that flows from the anode to the cathode.

There are two primary types of electrochemical cells: galvanic (voltaic) cells and electrolytic cells. Such cells capable of generating an electric current from the chemical reactions occurring in them are called galvanic cells or voltaic cells. Alternatively, the cells which cause chemical reactions to occur in them when an electric current is passed through them are called electrolytic cells. Both types of cells play a vital role in modern technology, providing power for portable electronic devices, electric vehicles, and renewable energy systems. The key differences between these two cells are presented in Table 1 below.

Table 1 - Key differences between galvanic cells and electrolytic cells

Galvanic(voltaic) cell	**Electrolytic cell**
Chemical energy is transformed into electrical energy	Electrical energy is transformed into chemical energy
The redox reactions that take place in these cells are spontaneous in nature	An input energy is required for the redox reactions to proceed, i.e., the reactions are non-spontaneous
The anode is negatively charged and the cathode is positively charged	These cells are positively charged anode and a negatively charged cathode
The electrons originate from the species that undergo oxidation	Electrons originate from an external source (such as a battery)

One of the key concepts in electrochemical cells is the difference in electronegativity between the two electrodes. The anode is where oxidation occurs, leading to the loss of electrons, while the cathode is where reduction occurs, leading to the gain of electrons. This flow of electrons creates a potential difference, or voltage, between the two electrodes. The amount of voltage produced by an electrochemical cell is determined by the types of electrodes and electrolyte used, as well as the conditions under which the cell operates. Figure 1 below shows a diagram detailing the different parts of an electrochemical cell.

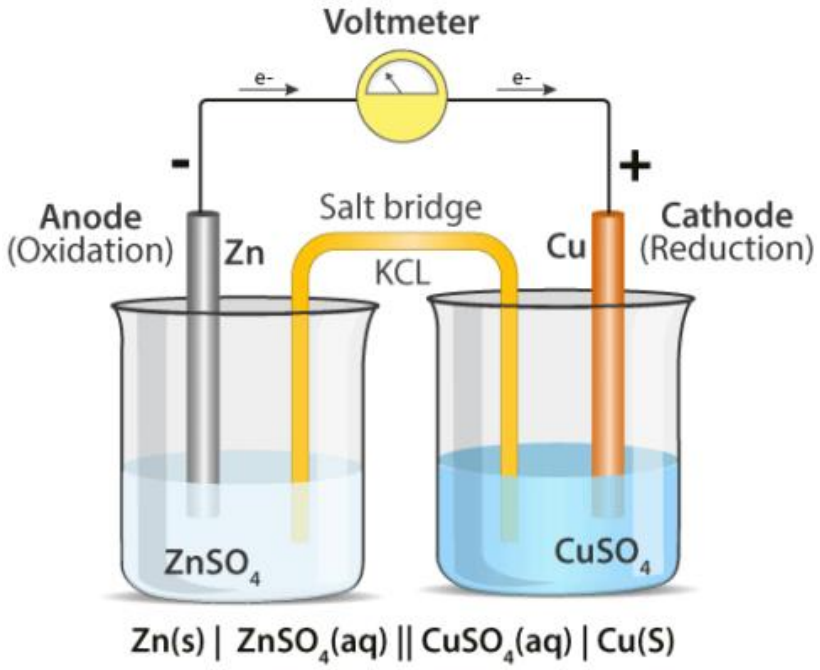


Figure 1 - An electrochemical cell

Electrochemical cells generally consist of a cathode and an anode. The key features of the cathode and the anode are tabulated below in Table 2.

Table 2 - Key features of anode and cathode in electrochemical cells

Cathode	**Anode**
Denoted by a positive sign since electrons are consumed here	Denoted by a negative sigh since electrons are liberated here
A reduction reaction occurs in the cathode of an electrochemical cell	On oxidation reaction occurs here
Electrons move into the cathode	Electrons move out of the anode

General convention dictates that the cathode must be represented on the right-hand side whereas the anode is represented on the left-hand side while denoting an electrochemical cell.

Overall, electrochemical cells are versatile devices that play a crucial role in converting chemical energy into electrical energy and vice versa. Understanding the

principles of redox reactions, electrode potentials, and cell construction is essential for designing and optimizing electrochemical cells for specific applications. As researchers continue to develop new materials and technologies, the potential for electrochemical cells to revolutionize energy storage and conversion is vast, offering a sustainable and efficient solution to our growing energy needs.

1.4 Electrodeposition and its methods

Electrodeposition is a widely used industrial electrochemical process known for its comparative simplicity and versatility in which a metal coating is deposited onto the surface of a substrate material via an electrolytic cell. It uses electric current to deposit metal or alloy layers on a substrate. The composition of the coating can be controlled by varying the electrolyte composition, the applied voltage, the current density, the deposition time, and other parameters. This synthesis method can be utilized to produce different kinds of coatings with a variety of functional properties, such as wear and corrosion resistance, catalytic activity, optical reflectivity, and electrical conductivity. Additionally, metal and alloy-based composition coatings prepared by electrochemical synthesis method have found various applications in the fields of energy, electronics, biomedicine, and engineering. The process of electrochemical synthesis involves passing a known magnitude of electric current through a defined electrolyte solution containing the metal ions to be deposited on a desired substrate, resulting them to plate out onto the conductive surface of the substrate. Electrodeposition offers numerous advantages including enhanced corrosion resistance, improved wear resistance, and decorative finishes. Furthermore, it allows for precise control over thickness and uniformity of the coating, making it ideal for various applications in industries such as automotive, electronics, aerospace and jewelry manufacturing, where it is used for corrosion protection, decorative finishes, and component fabrication. However, electrodeposition requires careful consideration of factors such as bath composition, current density, temperature, and agitation to ensure optimal results. Overall, electrodeposition plays a crucial role in modern manufacturing processes by providing high-quality coatings with excellent adhesion and durability and other desirable properties. The history of electrodeposition can be traced back to the early 1800s when researchers first began experimenting with using electrical currents to apply thin coatings of metal onto various substrates [16,17].

One of the earliest documented instances of electrodeposition occurred in England in 1805, when Italian chemist Luigi Valentino Brugnatelli successfully coated silver onto a copper surface using an electric current. Over the years, advancements in electrochemical science and technology have led to the development of more efficient and precise electrodeposition processes, allowing for the production of complex and high-quality metal coatings on a wide range of materials. The continuous evolution and refinement of electrodeposition techniques highlight its importance as a versatile and essential process in modern industrial applications.

The electrodeposition technique offers distinct advantages over other coating methods, like chemical vapor deposition (CVD), physical vapor deposition (PVD),

electrodeposition, thermal spray, sol-gel methods and laser electron beam surface treatment for several reasons [18-20]:

1) It requires low initial investment while maintaining high rate of production
2) It's compatibility with a wide range of substrates having various shapes and sizes
3) It's possibility for the production of nanocomposite materials with grain sizes as small as 10 nm. Besides, process parameters can carefully be controlled to obtain fine grain sizes and required coating functional properties.
4) Coatings produced by electrodeposition require no additional processing and can be applied to usage immediately.
5) The concept and application procedure of electrodeposition is straightforward and can be easily implemented in both laboratory and industrial set ups with minimal technological barriers.
6) Coatings produced by electrodeposition have been found to demonstrate superior desirable mechanical, corrosion and wear resistance properties.

Generally, electrodeposition stands out as a cost-effective, simple, versatile and efficient method for producing high quality metal and alloy-based coatings with desirable properties for various applications.

Electrodeposition is an electrochemical process based on the underlying principle that a layer of coating, whether single or multi layered, forms as a result of electrochemical reactions between the electrode and the electrolyte. This results in the deposition of ions contained in the electrolyte bath. The process takes advantage of the unique properties of materials in their metastable state, achieved through the reduction of grain size on the nanoscale. In this metastable state, the grain boundaries contain a higher proportion of atoms compared to those inside the grains [7]. These materials, known as nanocomposites, consist of nanoparticles and exhibit superior properties when compared to traditional grain-sized materials. In some cases, nanocomposite materials offer entirely new properties altogether.

A simplified schematic of the electrode position setup is shown in Figure 2a. For this particular example, the electrochemical cell consists of an electrolyte containing Ni^{2+} ions with the cathode polarized negatively to promote nickel reduction on the substrate surface. The anode is polarized positively and undergoes oxidation, releasing Ni^{2+} ions back into the bath, thereby compensating for the ions consumed at the cathode. This process can be described by the fundamental reduction reaction:

$$Ni^{2+}(aq) + 2e^- \rightleftharpoons Ni(s)$$

When an anode is composed of nickel, the oxidation reaction occurring at its surface effectively replenishes Ni^{2+} ions in the electrolyte, thereby maintaining bath composition and ensuring a stable deposition process.

In laboratory research, electrochemical studies of nickel electrodeposition, as well as controlled preparation of coatings for property evaluation, are often conducted using a three-electrode electrochemical cell (Figure 2b). This configuration comprises the working electrode (WE), counter electrode (CE), and reference electrode (RE).

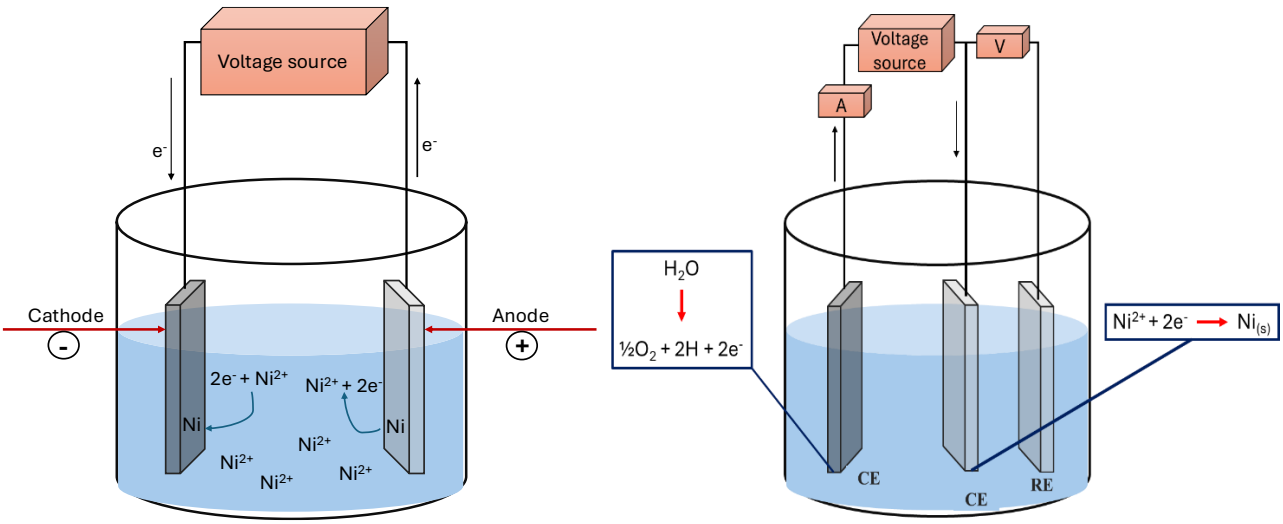


Figure 2 – a) Schematic representation of a two-electrode electrochemical cell, b) Schematic representation of a three-electrode electrochemical cell

The working electrode corresponds to the substrate of interest, on which nickel reduction occurs. The reference electrode provides stable and constant potential, enabling precise measurement of electrode potentials between the working electrode and difference electrode through a voltmeter. The counter electrode serves to complete the circuit and supply the required current, which flows only between the counter electrode and working electrode and is measured with an ammeter. Typically, inert materials such as platinum are employed for the counter electrode to avoid introducing unwanted products into the electrolyte. Is this setup, the reduction of Ni^{2+} ions to metallic nickel takes place at the working electrode surface according to Equation 1, while the oxidation of water occurs at the counter electrode, as described by the following:

$$H_2O \rightleftharpoons \frac{1}{2}O_2 + 2H^+ + 2e^-$$

This oxidation reaction provides the electrons required for nickel reduction at the working electrode/electrolyte interface ensuring charge balance within the system.

Nanocomposite materials with grain sizes below 100 nm have garnered significant attention from researchers and scientists worldwide. To increase production efficiency and reduce costs, various electrodeposition synthesis methods have been developed over the years. These methods range from basic direct current setups to more advanced techniques such as pulse plating, jet electrodeposition, and pulse reverse current methods [21-23].

Electrodeposited composite coatings present a superior option compared to single metal coatings, as they have the capability to blend the advantageous characteristics of various materials. By integrating a dispersed phase such as ceramic nanoparticles, these coatings can achieve improved mechanical strength, corrosion resistance, and customized functionalities. With continuous advancements in material combinations and deposition methods, composite coatings are positioned to have a significant impact on a wide range of industrial applications. For instance, it was found out that incorporating SiC nanoparticles to Ni-Mn alloys significantly improved the

microhardness and wear resistance of the coating compared to a pure nickel coating [24]. This makes them ideal for components subjected to high friction and wear. It is also explored in [25] that Zn-TiC/TiB composite coatings exhibited superior corrosion resistance in a chloride medium compared to a pure zinc coating. This synergy between the metal matrix and the dispersed phase offers better protection against environmental degradation. By incorporating TiO_2 nanoparticles, electrodeposited Ni-TiO_2 coatings achieved a composite coating with enhanced photocatalytic activity [26]. This demonstrates the ability to tailor the properties of the coating for specific applications beyond just protection. Recent advancements allow for precise control over the microstructure of the composite coating. Pulse current deposition techniques for nano-composite coatings was explored in [25]. This method led to a refined microstructure and increased incorporation rate of the secondary phase, leading to improved overall performance.

Electrodeposition, one technique of electrochemical synthesis, is the process by which an applied current or potential is used to deposit a film of metal or alloy by the reduction of metallic ions onto a conductive working substrate. The electrodeposition of particulates along with a metal or alloy leads to the formation of a composite. It involves using an electric current to deposit a thin layer of metal onto a workpiece, to achieve desired properties such as corrosion resistance, improved wear characteristics, and enhanced aesthetics. It is an important technology which helps to coat widely available and inexpensive base materials with layers of different metals with superior properties to extend their applications which would have been expensive otherwise. Electrodeposition offers a versatile toolbox for creating thin films and coatings on a target substrate. But how to apply the electrical current to achieve the desired results can vary. A breakdown of the different electrodeposition methods is presented in the following sections.

1.5 Direct current electrodeposition

This is the simplest, most basic and widely used method. A constant direct current is applied, causing positively charged ions (cations) in the electrolyte solution to migrate towards the negatively charged electrode (cathode – the electrode where the coating is wanted). At the cathode, the cations are reduced to their elemental form, depositing as a thin film on the substrate. This technique is further categorized into two types based on the orientation of the electrodes in the electrolyte bath during the electrodeposition process: namely the conventional electro co-deposition (CECD), and sediment co-deposition techniques (SCD). In conventional electro co-deposition, the electrodes are positioned vertically in the electrolyte bath, while in sediment co-deposition, they are positioned horizontally. These orientations impose forces which put great influence on the nanoparticle adsorption into the alloy matrix during the process of electrodeposition. In a study conducted to investigate the effect of co-deposition technique and particle size on the microhardness and corrosion resistance properties of Ni-Co/SiC composite coatings [27], Bakhit et al. found out that the two main forces involved during SCD electro co-deposition (electrophoresis force and gravitational pull), produce higher corrosion resistance properties compared to conventional electro co-deposition, which only relies on gravitational pull. The

technique of direct current electrodeposition has comparative advantages over other coating methods due to its simplicity in terms of setup and operation as well as availability of well established vast technical and reliable process. Hessam et al. showed that [28] DC setups are easier to design, operate, and maintain compared to those requiring precise control of pulse parameters in pulse current (PC) and pulse reverse current (PRC) methods. The results demonstrated that PC electrodeposited films have porous morphology with smaller crystallite size and high donor density in comparison with DC electrodeposited films that include equiaxed particles in their morphologies. This translates to lower initial investment and operational costs. In a separate study, Borkar [29] reported that all direct current deposited nickel and nickel nanocomposite coatings resulted much stronger and less random crystallographic textures when compared to coatings obtained using pulse current and pulse reverse current deposition methods.

Direct current electrodeposition is the conventional method where a constant current or potential is continuously applied during the deposition process to coat the desired materials. Figure 3 below illustrates the schematic of the direct current application and the typical growth process associated with it. The DC technique primarily involves two variables: the applied potential/current and the deposition time, while the precursor concentration and electrolyte pH are common variables. By adjusting these parameters, the morphology, composition, and thickness of the deposit can be modified. In DC deposition, the continuous application of constant potential/current results in film deposition without any relaxation, promoting the growth of existing nuclei rather than generating new nucleation sites, which leads to a rough and porous deposit.

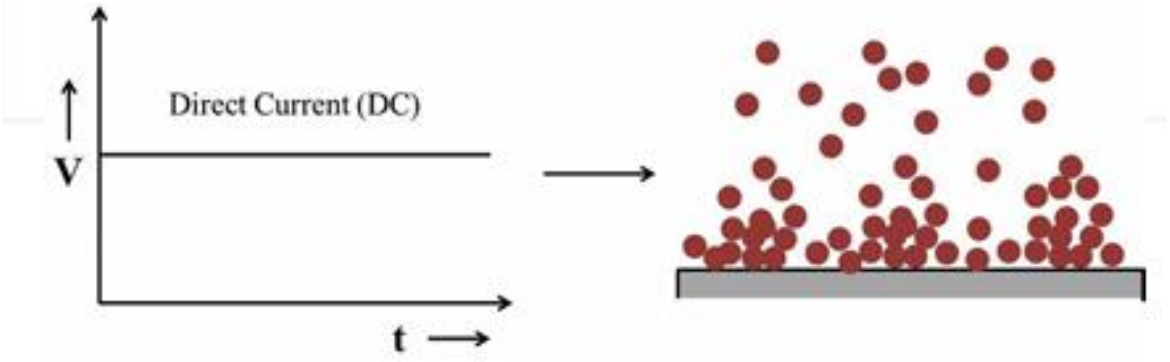


Figure 3 – Schematic diagram of direct current electrodeposition and expected growth process of the deposit [30, p. 112]

In spite of the fact that it has its own several disadvantages, DC electrodeposition is still a leading technique for the production of single element deposits and binary alloys [31].

1.6. Pulse electrodeposition

Pulse electrodeposition technique introduces a new kind of phase in the electrodeposition of alloys, metals and metal matrix composites. Unlike the conventional direct current electrodeposition method, it offers significantly superior flexibility in terms of adjusting essential deposition parameters, such as peak current

density (Ip), pulse current on time (t_{on}) and pulse current off time (t_{off}). This flexibility helps allow for producing unique combinations of microstructure and combination in the deposited coatings. The average current density (I_a) can be achieved through various combinations of different peak current densities, pulse current on and off times [32]. Moreover, current in pulse electrodeposition can be efficiently changed between two distinctly different values, resulting in a series of pulses with equal amplitude, duration and polarity separated by zero current magnitude [33]. Figures 4 and 5 below demonstrate a typical pulse current waveform where the current value alternates between a positive current value (Ip) for the duration of t_{on} and a zero (0) current value for the duration of t_{off}.

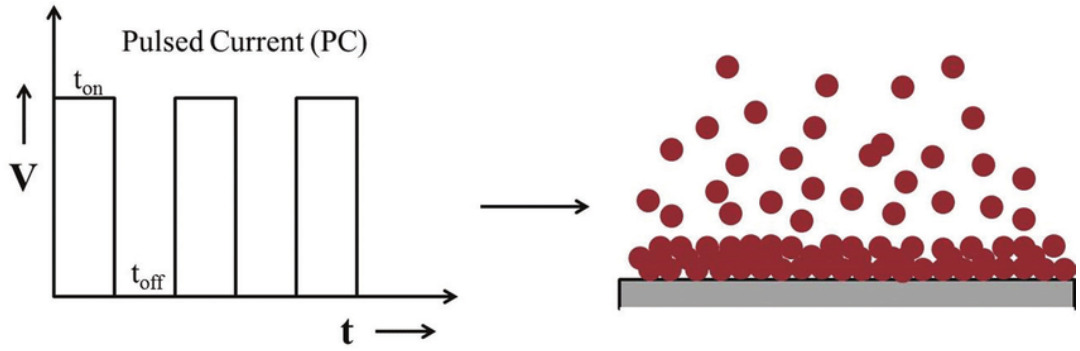


Figure 4 - Schematic of pulse electrodeposition and expected growth process of the deposit [30, p. 113]

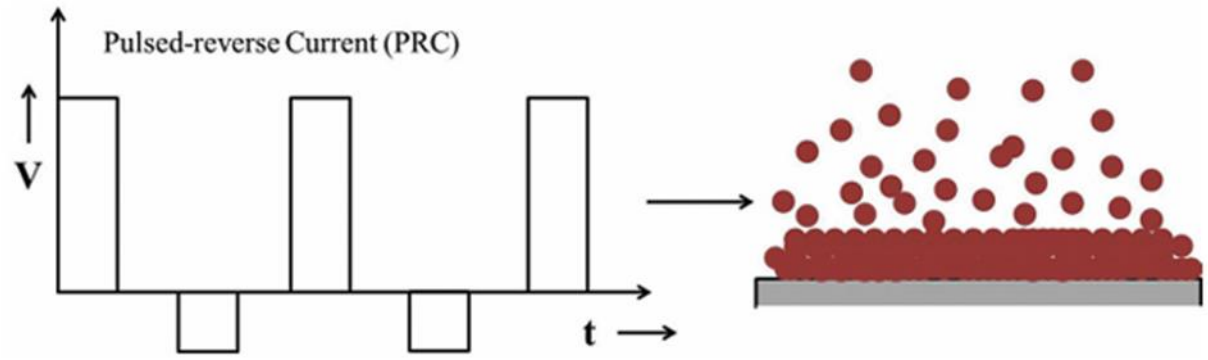


Figure 5 - Schematic of pulse reverse electrodeposition and expected growth process of the deposit [30 p. 114]

The concepts of pulse current and pulse reverse current electrodeposition techniques are illustrated below:

- In pulse electrodeposition, during the t_{off} period, the electric double layer found around the cathode electrode discharges, which allows ions to pass through and reach the surface of the cathode. However, in pulse current electroception, this electric double layer prevents ions from reaching the surface of the cathode.
- While electrodeposition process happens, high current density regions in the electrolyte bath experience greater ion depletion when compared to areas with low current density. During the t_{off} period, ions tend to migrate to these

depleted regions resulting in a more uniform ion distribution for deposition when t_{on} pulse occurs.

Pulse electrodeposition technique enables the synthesis of various coatings with controlled coating thickness, microstructure and composition by adjusting pulse parameter mentioned above. Pulse current and pulse reverse current electrodeposition techniques offer several advantages and have their own disadvantages in comparison to direct current electrodeposition. The advantages include limiting current density significantly improves by replacing metal ions in the diffusion layer during off time, reduced process limitations due to flexibility in pulse parameters, inability to produce lower porosity fine grained deposits with reduced stress, inability to improve deposit adhesion and creating uniform thickness, and enhance deposition rate as well as physical and mechanical properties of deposits. Conversely, these techniques have limitations like more expensive pulse generators than direct current units, requirements related to careful advance planning and a series of procedures to achieve optimal results.

1.7 Jet electrodeposition

In jet electrodeposition method, a stream of electroplating solution is directly aimed at the surface of the cathode. An electrical field exists between the cathode (substrate) and anode (positioned in the nozzle of the setup). Figure 6 below illustrates the schematic of setup configuration of jet electrodeposition.

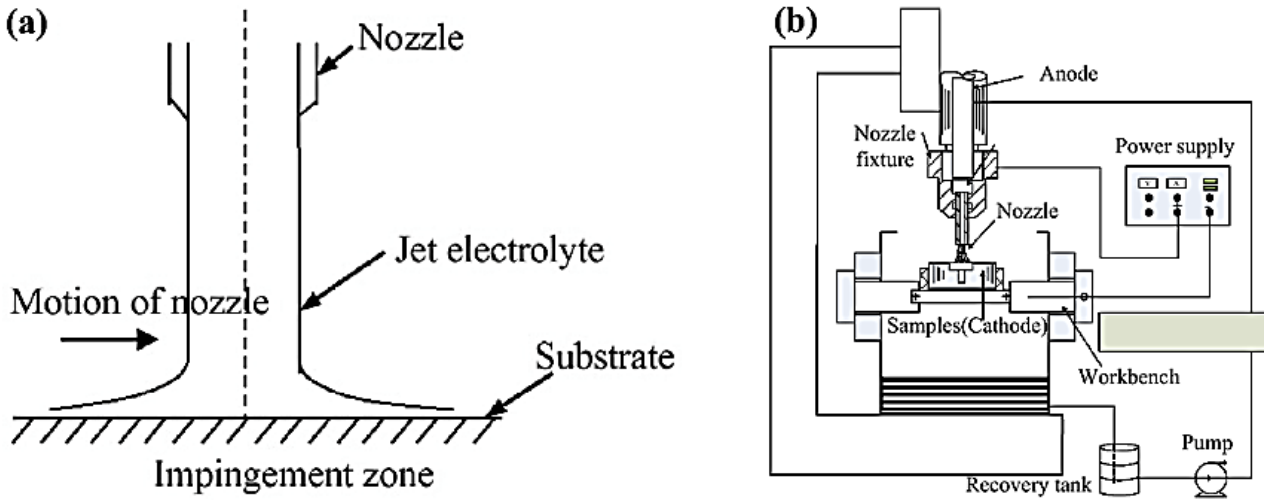


Figure 6 – Schematic diagram of jet electrodeposition method [35, p. 13920]

As the electroplating solution flows, electric current is passed through the solution stream to the surface of the substrate. This facilitates deposition on the surface of the substrate (cathode) where the overflow of the jet occurs. Jet electrodeposition is known to be a rapid electrodeposition technique which offers numerous advantages compared to other coating techniques, such as higher deposition rates and effective refinement of grain sizes of the coatings [36,37].

1.8. Electrodeposition of composite coatings

Electrodeposition of composite coatings (co-deposition) involves the incorporation of fine particles of metallic, non-metallic compounds, or polymeric

materials from an electrolytic of electroless bath into the electrocoated layer. The purpose of this process include enhanced materials properties such as hardness, corrosion and wear resistance, lubrication, tensile and yield strength, and fracture toughness [38, 39]. Well-dispersed nanoparticles within the composites enhance mechanical properties and are also well-suited for applications in microdevices [39].

Co-deposition of fine particles into metal matrix deposits involves two common processes. Thes processes are physical dispersion of particles in the electrolyte bath and electrophoretic migration of fine particles [40]. Composite electrocoating integrates both micron and sub-micron particles of metallic and non-metallic compounds into the coated layer. For composite electrodeposition, two models have been developed Guglielmi and Kurozaki. According to Guglielmi's model, composite electrodeposition occurs in two different steps. At the start, solid particles are surrounded by a cloud of adsorbed ions during electrodeposition. These solid particles are not strongly adsorbed onto the cathode substrate due van der Waals forces as they approach in the first step. In the next step, these loosely adsorbed solid particles are strongly adsorbed onto the cathode substrate surface by coulombic forces and subsequently become trapped within the metal matrix. A fundamental drawback of this model is the absence of consideration for effects of mass transfer during the process of electrodeposition. On the other hand, a model developed by Kurozaki, a widely accepted one, considers the transfer of solid particles from the solution to the cathode substrate surface through agitation [44]. This model demonstrates a process consisting of three steps:

1. Uniformly dispersed solid particles are transferred to the electric double layer via mechanical agitation
2. Charged solid particles to the cathode surface through electrophoresis
3. At the cathode substrate surface, solid particles become adsorbed due to coulombic forces that exist between them and adsorbed anions and subsequently incorporated into the metal matrix deposit.

One of the most commonly and widely used mechanisms of composite electrodeposition process comprises of five steps [45], shown in Figure 7 below.

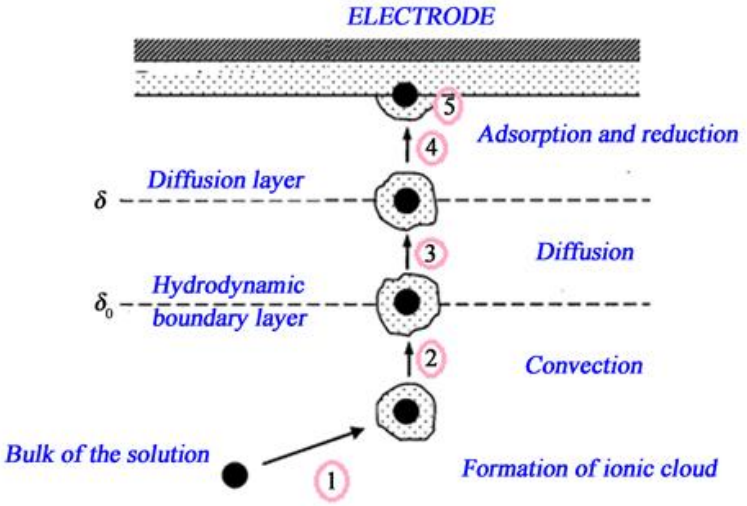


Figure 7. A five-step reaction schematic description of co-deposition process [45, p. 82]

The whole process involves the formation of ionic clouds around the solid particles (bulk electrolyte, typically covering centimeters); convectional movement towards the cathode substrate surface (convection layer, typically a few millimeters thick); diffusion through a concentration boundary layer (diffusion layer, typically hundreds of micrometers in size), electrical double layer (typically nanometers in size), followed by the adsorption and entrapment of solid particles. The five steps in order are outlined below:

1. Adsorption of ionic species onto the particle surface
2. Forced convection displaces the particle towards the cathode's hydrodynamic boundary layer (δ_0). δ_0 represents the distance from an object to the fluid where the velocity remains relatively constant.
3. Diffusion of the solid particle through the double diffusion layer (δ)
4. adsorption of the solid particle, together with its ionic cloud onto the cathode substrate surface
5. Some adsorbed ionic species are reduced, resulting in the irreversible incorporation of the solid particles onto the metal matrix

Solid particles dispersed in the electrolytic bath are constantly transferring due to Brownian motion. The interaction that exists between these solid particles determines whether they remain separate or agglomerate. When the attraction energy between solid particles exceeds the repulsive energy between them, agglomeration occurs. Conversely, when the repulsive energy is higher, separation of solid particles occurs. The overall condition and characteristics of the system largely dictate the net force that leads to the formation of agglomerated structures. Therefore, understanding the structure of the interfacial region is crucial for assessing the stability of particle dispersion in the electrolyte.

This model applies under steady-state conditions, assuming no variations in concentration, pressure, temperature, or over-voltage throughout the process. Additionally, the cathode surface must be accessible to the plating solution and its particles. Lastly, a uniform suspension of particles in the plating solution must be maintained.

1.9 Common types of composite coatings and their functional properties

Functional properties of metal and alloy-based composition coatings including mechanical properties (hardness, adhesion and wear resistance properties), corrosion resistance properties, as well as thermal and electrical conductivity are affected by many factors. These factors include composition, microstructure, and surface morphology. Research efforts and progress have been directed towards customizing these to fulfill particular application purposes.

Metal coatings based on chromium have long been valued for their high hardness and corrosion resistance properties. Incorporation of graphene or graphene oxide into chromium electrodeposits help further enhance these desirable functional properties by refining grain size and providing a barrier against corrosion. For example, graphene additives tend to eliminate microcracks and produce a dense hillock-rich Cr microstructure. Specifically, one report found that adding GO and ZnO nanoparticles to a Cr(III) plating bath yielded a crack free, hillock covered Cr-graphene surface,

markedly improving corrosion resistance relative to pure Cr deposits. In general, graphene incorporation impedes Cr grain growth and blocks defect paths, leading to finer grains and higher microhardness. In Ni-Cr-GO coatings, for instance, adding GO raised Vickers hardness from ~4.4-5.5 GPa (pure Ni-Cr) up to ~6.1-7.3 GPa, depending on coating current. Similarly, Cr-graphene deposits are consistently harder than Cr alone.

Cobalt-vanadium alloy coatings are robust, catalytic coatings for hydrogen electrodes and wear-resistant surfaces. Vanadium, when co-deposited with Co, significantly alters the deposit morphology and properties. Recent studies have investigated electrodeposited Co-V coatings, often prepared form citrate-based baths. Typical Co-V electrolytes contain $CoSO_4$ and a vanadium source (mainly V_2O_5 or $VOSO_4$) in citrate complexant (pH ~3-4). Both constant and pulse currents have been used. Vanadium co-deposition is challenging due to its tendency for oxide formation, but pulsed coating (or chemical reduction during pauses) helps in such a way that during a pulse pause, adsorbed hydrogen atoms can reduce adsorbed vanadium ions, increasing vanadium in the deposit. Co-V coatings are reported as uniform and microcrystalline. SEM analysis revealed that a nodular cobalt matrix whose grain size decreases slightly with higher V. In fact, higher V content tends to refine the cobalt grains, since some V oxides may pin grain boundaries. All reports agree that adding V drastically increased hardness over pure Co. this improvement is attributed to formation of Co-V intermetallic phases and the fine grain structure. Moreover, hardness tended to increase with increasing vanadium content; the harder coatings corresponded to higher V wt.%.

Incorporating V also improves corrosion performance relative to pure Co. In alkaline (NaOH) and neutral salt tests, Co-V electrodes showed lower corrosion currents and more noble potentials. This is likely due to V raising the overpotential for hydrogen evolution (cathodic reaction) and making the coating more passive. The exact mechanism may involve a thin V-oxide at the surface. Crucially, an increase in vanadium content correlated with better corrosion resistance.

Co-V alloy coatings are also excellent for hydrogen evolution. The overpotential for H_2 evolution on Co-V was reported to be 0.1-0.2 V lower than Co alone, and exchange current densities were higher. Hence, Co-V functions as a better catalytic cathode (and might be chosen for electrolyzers). In effect, the same factors (fine grains, V presence) that increase hardness also enhance catalytic sites. Vanadium co-deposition is sensitive to current density. General electrodeposition theory and some data suggest that raising cathode current density tends to decrease V content (because higher currents produce more H_2, which competes for charge). Practically, it is possible to tune current density and use of pulses to trap as much V as possible without stifling deposition. Higher currents might thicken the coating but at the expense of V incorporation and uniformity.

A wide variety of composition coatings can be obtained via reinforcing different nanoparticles into the metal matrix such as Al_2O_3, SiC, CNTs, ZrO_2, Si_3N_4, and WC. Pulse electrodeposited Ni-SiC and Ni-Al_2O_3 composite coatings [46] were widely studied for their tribological behaviors. These composite coatings demonstrated

superior hardness and wear resistance compared to other composite coatings, primarily attributed to the high hardness of alumina nanoparticles. It was also indicated in [47] that an adequate amount of nanoparticles is crucial for enhancing the microhardness and anticorrosion properties of the coatings. Another study [48] conducted to study preparation, characterization, wear and corrosion behavior, inhibitory effects Ni-Cu matrix composite reinforced with CNTs showed that the presence of CNT particles improved the hardness, tribological performance, and electrochemical behavior of the coating. Furthermore, in a study conducted to examine the influence of Si_3N_4 nanoparticles on morphology, hardness and corrosion resistance properties of electrodeposited Ni-Co-Si_3N_4 coatings [49], it was revealed that the corrosion resistance of nanocomposite coatings was more than that of electrodeposited Ni-Co coating.

Ni-Al_2O_3 composite coatings

Nickel composite coatings containing ceramic materials like Al_2O_3 obtained by electrodeposition have been extensively researched due to their enhanced mechanical, corrosion and wear resistance properties over pure nickel coatings on various substrates. Ni-Al_2O_3 composite coatings, consisting of nickel (Ni) and alumina (Al_2O_3), have emerged as a powerful technology for enhancing the properties of underlying substrate materials. These coatings offer a unique blend of properties derived from their individual constituents. Nickel provides excellent ductility, strength, and electrical conductivity, while alumina contributes superior wear resistance, high-temperature stability, and outstanding corrosion resistance [50]. Consequently, this synergy makes Ni-Al_2O_3 coatings ideal for various applications demanding protection against harsh environments. It was observed in [51] that the effect of current density on electrodeposited Ni-P- Al_2O_3 composite coatings was tremendous. Microhardness, corrosion and wear resistance of this composite coating showed a remarkable enhancement at a current density of 7 A/dm^2. These significant improvements in the functional properties were mainly due to the combined influences dispersion strengthening as well as refined gran sizes. The microhardness values of the coatings were found to be 669.2 HV. By varying the content of alumina, in the electrolyte bath, it was possible to achieve improved corrosion and wear resistance properties [52]. Here, the wear rate of the coatings has decreased from 5.96×10^{-5} to 3.16×10^{-5} mm^3/Nm with the increase of Al_2O_3 particles in the composite coating which indicates approximately two times improvement in the wear resistance. The corrosion resistance was also increased and an improvement in corrosion rate was achieved from 392 value to 063 μm/year value with increasing particle concentration. It was found that, using pulse electrodeposition method, roughness properties of Ni-Al_2O_3 composite coatings were improved with varying duty cycles from 20% - 100%. Results demonstrated that with decrease in duty cycle, there was an enhancement in surface roughness properties from 0.779 to 0.245 μm. This change in surface roughness was due to variation of grain size which resulted from the varying time intervals during pulse coatings.

Moreover, microhardness and wear resistance properties of composite coatings are immensely influenced by current density as well [53]. Microhardness values of composite coatings tend to increase with increasing current density. This phenomena

of higher microhardness values may be because of the larger magnitudes of incorporated alumina particles. Upon increasing current density from 3 A/dm^2 to 5 A/dm^2, the polarization resistance value improved, and corrosion current density decreased. Moreover, the corrosion potential of these samples has shifted toward more positive side, indicating improved corrosion resistance. It was found out that the coating deposited at 5 A/dm^2 was characterized by homogeneous distribution of the ceramic phase, relatively small values of the residual stresses as well as showing the smallest corrosion current density and the highest polarization resistance.

In Ni-Al_2O_3 composite coatings, it is the Al_2O_3 that plays a decisive role in improving corrosion resistance properties, so that the corrosion rate of the coating decreases with increasing Al_2O_3 content [54]. Increasing the current above 50 mA decreases the influence of the current on the corrosion rate, and the degradation potential becomes higher for the coating developed at a current of 60 mA than for the other composite coatings. Increasing the bath temperature up to 40 °C the corrosion current density has decreased. However, an increase in temperature above 40 °C caused an increase in the corrosion current density and consequently a decrease in the corrosion resistance of the composite coatings. Additionally, microstructure and wear resistance of Ni-Al_2O_3 composite coatings are highly influenced by pulse frequency. Better hardness and wear resistance properties were exhibited at lower frequencies that at higher frequencies. Because of the presence of adhesive wear, wear resistance of composite coatings is largely influenced by microstructure and less influenced by reinforcing alumina particles [55].

Ni-SiC composite coatings

Ni-SiC composite coatings have emerged as a promising material for surface engineering applications due to their ability to combine the desirable properties of nickel (Ni) with the exceptional hardness and wear resistance of silicon carbide (SiC). Electrodeposition is a widely used technique for creating Ni-SiC coatings. Recent studies have explored optimizing this process to achieve better control over SiC particle distribution and content within the nickel matrix. For instance, research by [56] investigated the use of binary non-ionic surfactants to improve the incorporation of SiC nanoparticles during electrodeposition. Their findings demonstrated that surfactants improved the dispersion of SiC nanoparticles, leading to more uniform and higher hardness coatings compared to pure nickel coatings.

The primary motivation for incorporating SiC nanoparticles into nickel is to improve its mechanical properties. Studies have shown that Ni-SiC composites exhibit enhanced micro-hardness, wear resistance, and corrosion resistance compared to pure nickel coatings. This makes them suitable for applications in various tribological environments, such as cutting tools, gears, and bearings. For instance, a study by investigated the effect of SiC nanoparticle concentration on the properties of Ni-SiC coatings fabricated via high-frequency inductive cladding [57]. They observed that increasing the SiC content resulted in a significant improvement in wear and corrosion resistance, making these coatings ideal for protecting carbon steel components. This method offers rapid deposition rates but requires further investigation into optimizing parameters for achieving uniform and well-distributed SiC particles.

The microstructure of Ni-SiC composites plays a crucial role in determining their performance. The size, distribution, and interfacial bonding between Ni and SiC particles significantly impact the mechanical properties. Studies by [57] employed electrodeposition to fabricate Ni-SiC coatings with varying SiC particle concentrations. They observed that increasing the SiC content led to grain refinement and enhanced corrosion resistance in the composite coating. The incorporation of SiC nanoparticles into the nickel matrix generally improves the micro-hardness and wear resistance of the coating. Research by [56] showed a significant increase in micro-hardness compared to pure nickel coatings. This improvement can be attributed to the presence of hard SiC particles that act as load-bearing reinforcements within the nickel matrix.

Recent research efforts in Ni-SiC composites focus on improving the control over deposition processes and understanding the effect of SiC particle characteristics (size, morphology) on the final properties of the coating. Additionally, researchers are exploring novel fabrication techniques like laser cladding to achieve superior properties and address limitations associated with conventional methods.

Ni-ZrO_2 composite coatings

Nickel and zirconia (zirconium dioxide, ZrO_2) have good compatibility because of their similar coefficient of thermal expansion and elastic modulus. Several techniques have been employed to produce Ni-ZrO_2 composite coatings and electrodeposition is a widely used method, allowing for the incorporation of ZrO_2 particles within the nickel metal matrix [58,59].

Studies have explored optimizing the ZrO_2 content in the plating bath to achieve a balance between particle incorporation and distribution within the coating [60]. Sol-enhanced electroplating has also been investigated, demonstrating improved dispersion of ZrO_2 nanoparticles compared to traditional powder addition methods [61].

Recent research highlights the importance of achieving a uniform distribution of ZrO_2 particles within the nickel matrix [61–63]. This distribution is influenced by the ZrO_2 concentration in the fabrication process and can significantly impact properties like hardness and wear resistance. The incorporation of ZrO_2 into nickel coatings leads to substantial improvements in various properties. A key area of focus is enhanced wear resistance, achieved through the dispersion of hard ZrO_2 particles within the softer nickel matrix [61,64]. Additionally, Ni-ZrO_2 composites demonstrate improved corrosion resistance compared to pure nickel coatings [65]. This study explores the impact of ZrO_2 concentration in the electrolytic bath on the particle distribution and corrosion resistance of the coatings. Their findings suggest an optimal ZrO_2 concentration for achieving the best combination of these properties. This enhancement is attributed to the barrier effect of ZrO_2 particles, hindering the diffusion of corrosive species towards the substrate. It was also found out that the microhardness and tribo-corrosion properties of these composite coatings were significantly improved due to reinforcement of uniformly dispersed ZrO_2 particles in the nickel matrix followed by combined effect of dispersion strengthening and structural modification.

Current research efforts in Ni-ZrO_2 composites are directed towards optimizing fabrication techniques for superior control over microstructure and achieving the

desired balance between different properties. Sol-enhanced electroplating is a promising approach for achieving better dispersion of ZrO_2 nanoparticles [61]. It has investigated a sol-enhanced electroplating method, demonstrating superior improvements in mechanical properties compared to traditional ZrO_2 powder incorporation. Furthermore, studies are exploring the influence of ZrO_2 particle size and morphology on the overall performance of the composite coatings.

Ni-ZrO_2 composite coatings hold immense potential for various industrial applications due to their combined advantages of good mechanical properties, corrosion resistance, and compatibility with different substrates. Further research focused on optimizing fabrication techniques, exploring alternative ZrO_2 dopants, and investigating the tribological behavior of these coatings will pave the way for their wider adoption in fields like automotive, aerospace, and machine tools.

The microstructure of Ni-ZrO_2 composite coatings plays a crucial role in determining their performance. Studies [61,64] utilize Scanning Electron Microscopy (SEM) and X-ray Diffraction (XRD) to analyze the distribution and crystallographic phases within the coatings These studies emphasize the importance of achieving a uniform dispersion of ZrO_2 nanoparticles within the Ni matrix for optimal properties.

The primary advantage of Ni-ZrO_2 composite coatings lies in their enhanced functionalities compared to individual materials. A study by [66] demonstrates a significant improvement in wear resistance with increasing ZrO_2 content in the coatings. Similarly, other research highlights the enhanced corrosion resistance achieved through Ni-ZrO_2 composite coatings.

Ni-TiO_2 Composite Coatings

Ni-TiO_2 composite coatings have gained significant attention in recent years due to their potential applications in various industrial sectors. These coatings consist of a mixture of nickel (Ni) and titanium dioxide (TiO_2) nanoparticles, which are deposited onto a substrate surface using techniques such as electrodeposition or chemical vapor deposition. The unique combination of properties offered by both Ni and TiO_2, such as corrosion resistance, mechanical strength, and photocatalytic activity, makes these composite coatings highly versatile and suitable for a wide range of applications.

One of the key advantages of Ni-TiO_2 composite coatings is their enhanced corrosion resistance compared to traditional coatings. The addition of TiO_2 nanoparticles improves the overall chemical stability of the coating, making it more resistant to harsh environments and corrosive substances [67]. This property is particularly beneficial in industries such as aerospace, automotive, and marine, where components are constantly exposed to corrosive elements. Additionally, the photocatalytic activity of TiO_2 nanoparticles can also provide self-cleaning properties to the coating, making it easier to maintain and prolonging its lifespan. In a study carried out to investigate the electrochemical corrosion behavior of Ni–TiO_2 composite coatings electrodeposited from a deep eutectic solvent-based electrolyte [26]. It has been determined that incorporating titania particles into the Ni matrix and increasing their concentration in the coating results in a shift of corrosion potential towards more positive values, a reduction in corrosion current density, and an increase in polarization resistance. The results indicate that in the series of coatings Ni, Ni–TiO_2(5%), and Ni–

TiO_2(10%) deposited from a DES-assisted plating bath, there is an enhanced resistance to electrochemical corrosion in aggressive environments of a 3% aqueous solution of NaCl. These observed improvements in the corrosion resistance of the coatings are attributed to the barrier effect provided by the dispersed phase particles and the formation of corrosion microcells, which contribute to inhibiting local corrosion. Furthermore, the mechanical strength of Ni-TiO_2 composite coatings makes them suitable for applications where wear and abrasion resistance are crucial. The Ni component provides excellent adhesion to the substrate surface, while the TiO_2 nanoparticles act as reinforcements, improving the overall hardness and durability of the coating [68]. This makes them ideal for use in components subjected to high levels of mechanical stress, such as cutting tools, bearings, and medical implants. Overall, the unique combination of properties offered by Ni-TiO_2 composite coatings makes them a promising material for various industrial applications.

Ni-WC Composite Coatings

Ni-WC composite coatings have gained significant attention in recent years due to their exceptional mechanical and tribological properties. These coatings are formed by incorporating tungsten carbide (WC) particles into a nickel (Ni) matrix, resulting in a material that combines the hardness of WC with the ductility of Ni. The unique combination of properties exhibited by Ni-WC composite coatings makes them ideal for a wide range of industrial applications, including cutting tools, wear-resistant surfaces, and protective coatings.

One of the key advantages of Ni-WC composite coatings is their exceptional hardness and wear resistance. Tungsten carbide is one of the hardest materials known, with a Mohs hardness of 9, while nickel provides the necessary toughness and ductility to prevent cracking and delamination. This combination of hardness and toughness makes Ni-WC composite coatings highly resistant to wear, abrasion, and erosion, making them ideal for applications in which components are subjected to severe mechanical stresses. In addition to their outstanding mechanical properties, Ni-WC composite coatings also exhibit excellent corrosion resistance [69,70]. The nickel matrix in these coatings acts as a barrier to prevent corrosive elements from reaching the substrate material, while the tungsten carbide particles provide additional protection against chemical attack. As a result, components coated with Ni-WC composites are able to withstand harsh operating environments, such as those found in the aerospace, automotive, and oil and gas industries.

Another key advantage of Ni-WC composite coatings is their versatility and ease of application. These coatings can be deposited using a variety of techniques, including thermal spray, electroplating, and chemical vapor deposition, allowing for customization based on the specific requirements of the application. Additionally, the composition and microstructure of Ni-WC coatings can be tailored to optimize properties such as hardness, wear resistance, and corrosion resistance, making them highly versatile and adaptable to a wide range of applications. Despite their many advantages, Ni-WC composite coatings do have some limitations that must be considered. For example, the high hardness of tungsten carbide particles can result in increased tool wear during machining and grinding processes, which may require

specialized equipment and techniques for processing. Additionally, the high cost of tungsten carbide can make Ni-WC coatings more expensive than alternative coating materials, which may limit their use in cost-sensitive applications [71].

Generally, Ni-WC composite coatings offer a unique combination of mechanical, tribological, and corrosion-resistant properties that make them ideal for a wide range of industrial applications. Their exceptional hardness, wear resistance, and corrosion resistance, coupled with their versatility and ease of application, make Ni-WC coatings a highly attractive option for components subjected to severe mechanical and environmental stresses. While they do have some limitations, the many advantages of Ni-WC composite coatings make them valuable and promising material for future research and development in the field of surface engineering.

Overall, nickel electrodeposition is a widely used technique for producing thin films with a variety of desirable properties. In recent years, there has been a growing interest in the development of nickel-based composite coatings, which incorporate additional elements or particles into the nickel matrix for the purpose of achieving enhanced functional properties of different substrates. These composite coatings can offer improved corrosion and wear resistance, hardness, and other functional properties compared to pure nickel coatings. Some of the recent advancements in electrodeposited nickel composite coatings include:

• Improved wear resistance: researchers have found that incorporating Al, Si, Zr, C, W and Ti particles into nickel coatings can significantly improve wear resistance. The uniform distribution of the particles within the nickel matrix acts as a barrier to wear and tear.

• Enhanced mechanical properties: studies have shown that electrodeposited nickel composite coatings with Al, Si, Zr, C, W and Ti particles exhibit superior mechanical properties, including increased hardness. The presence of these particles refines the grain size of the nickel matrix and hinders the movement of defects, leading to enhanced mechanical strength.

• Better corrosion resistance: nickel based composite coatings offer improved protection against corrosion when compared to pure nickel metal coatings.

1.10 Electrodeposition process parameters for composite coatings and their effect

The quality of coatings is influenced by several parameters during electrodeposition, including the type and concentration of electrolyte, the nature of the cathode, the temperature of the electrolyte, electrolyte pH, the method of electrolyte stirring, pulse frequency, duty cycle, the electrodeposition time (which determines coating thickness), and the current density used in the electrodeposition process. In this section, effects of these parameters on different functional properties of composite coatings is reviewed in detail.

Electrodeposited Ni, Co, Cu, Al, Ti, Fe and their alloys are widely used in industry for corrosion protection, wear resistance and electronic applications. Electrodeposition offers dense, low porosity coatings; for instance, electrodeposited Ni films exhibit superior dense and lower porosity, while pure Ni is prized for its superior corrosion and wear resistance. Alloying (e.g. Ni-Co) further enhances properties: Ni-

Co deposits have roughly double the microhardness of pure Ni and much better wear resistance [72]. Controlling deposition parameters, therefore is critical. The key variable in direct current electrodeposition – current density, bath composition, bath temperature, pH and deposition time – strongly affect coating microstructure, hardness, corrosion resistance and wear behavior.

Effects on microstructure and surface morphology

Current density

Higher cathodic current density generally increases the nucleation rate of metal grains, producing finer-grained and smoother deposits up to an optimum. For example, electrodeposited Al (from an ionic liquid bath) showed large dendritic crystals at low current but uniformly fine grains at higher current density [73]. Similarly, Ni and Ni-Co coatings become finer and denser as current density rises [72,74]. In one study of Ni-Au/Ni plating on Al, elevated current density resulted in reduced grain size and improved surface morphology, ensuring superior anti-corrosion performance [74]. Excessive current, however, can cause concentration polarization and hydrogen evolution, leading to dendritic growth or burrs. For instance, Ni-Co deposits, at very high current densities, develop a rough, colony-like surface. In practice, electrodeposition is often done at moderate current densities (e.g. <200A/dm^2 for Ni-Co) to balance grain refinement and deposit uniformity [72].

Bath composition and additives

The metal-ion chemistry and additives in the deposition bath critically shape deposit structure. Alloy composition (e.g. Ni:Co ratio) dictates crystal structure and grain size. In Ni-Co baths, adding $NiBr_2$ and organic brightener yielded nanocrystalline Ni-Co with ~14 nm grains (versus ~21 nm without additives) [75]. Alloying usually refines grain structures; for example, Ni-Co alloys (solid solution of two metals) inherently have finer grains and higher defect density than pure Ni. Co-depositing hard ceramic particles (Al_2O_3, ZrO_2, SiC, etc.) with Ni or Co produces a nodular, composite morphology. These particles appear as embedded nodules in the metal matrix, giving a rougher surface than pure metal but dramatically altering properties. For example, incorporation of nanoscale Al_2O_3 or ZrO_2 into Ni films creates a composite with nodular uniform morphology [72].

Organic additives, like saccharin in Ni baths, and complexing agents also affect structure: citrate-complexed Ni-Co baths allow electrodeposition over a wide pH range [76], and agents like boric acid buffer pH and refine grains. In Cu deposition, additives like PEG, SPS, etc. are known to control grain orientation and brightness, indicating a general effect that bath chemistry sets nucleation conditions and grain growth directions.

Bath pH

Solution pH can alter deposit composition and crystallography. Especially in anomalous systems like Ni-Co. Recent works show that Ni-Co electrodeposition in citrate baths is extremely pH sensitive. At low (acidic) pH, cobalt tends to deposit preferentially (anomalous co-deposition), yielding Co-rich Ni-Co films with fine, uniform grains. At higher (alkaline) pH, Ni is favored, producing Ni-rich, nodular

deposits. For example, coating at pH ~8.8 contained 89-95 at.% Ni and had a nodular (fcc) structure, whereas pH 2-3 yielded 43-81 at.% Co with mixed (fcc+hcp) phases [76]. Thus, raising pH tends to enlarge grains by enhancing Ni deposition (Ni grows more slowly and forms coarser nodules), whereas acidic pH promotes many nucleation sites of Co.

Temperature

Increasing the bath temperature generally accelerates electrochemical kinetics and diffusivity, which can increase deposition rate and grain growth. In nickel sulfamate and Watt's baths, typical depositing temperatures (40-60 ^{o}C) are chosen to balance deposition speed and film quality. Higher temperature often reduces internal stress and yields coarser, more equiaxed grains (lower hardness) due to faster surface diffusion. However, temperature effects are bath-specific and often secondary to current density and chemistry. For Al deposition in ionic liquids, higher temperatures (up to decomposition limits) greatly increase growth rate [73]. In general, moderate temperature is kept to maintain smooth deposits; too high a temperature can lead to roughness and unwanted side reactions (e.g. hydrolysis).

Agitation (stirring) and deposition time

Mechanical agitation (magnetic stirring or solution flow) enhances mass transport of metal ions and any suspended particles. Agitation tends to produce more uniform deposits and can reduce the formation of dendrites. For example, high speed deposition often causes edge burrs, but vigorous stirring causes a distinct reduction of burrs and improves uniformity. In composites, stirring increases the concentration of particles at the cathode: moderate agitation helps embed more nanoparticles into the growing film (up to a concentration limit) [72]. Too little agitation can cause localized depletion and large grains; too much can dislodge loosely bound nodules. Overall, agitation generally smooths morphology and improves thickness uniformity but has little direct impact on intrinsic grain size once depositing conditions are steady.

The main effect of depositing time is film thickness. Longer plating time produces thicker coatings, given fixed current density. Thickness does not directly change grain size (beyond the initial nucleation layer), but thicker coatings can develop columnar growth or evolve texture. Notably, coating thickness strongly affects functional properties: e.g. extending Ni deposit thickness provides a second physical barrier for the dense and thick Ni layer to resist invasion of corrosive media [74]. In many studies, longer deposition times simply raised properties related to thickness (wear life, corrosion impedance) until a point; very long depositing can introduce stress cracks. In nanocomposite baths, time can also influence particle incorporation: some reports note that thinner or shorter deposits embed a larger fraction of nanoparticles which then plateaus as thickness grows [72]. Table 3 below summarizes these trends.

Table 3 - Summary of how electrodeposition parameters affect coating microstructure, hardness, corrosion and wear

Parameter	**Microstructure/ Morphology**	**Hardness**	**Corrosion resistance**	**Wear resistance**
Increased current density	Finer grains (less nodular) up to an optimum, excessive current causes dendritic growth [73,74]	Generally increases (finer grains, more alloying) [77,78]	Often increases (denser, smoother deposits) [74]	Generally increases (via higher hardness) [77]
Bath composition (alloying, additives, particles)	Alloying/additives modify crystal structure, refine grains; co-deposited ceramics create nodular composite morphology [72, 77]	Alloying/particles greatly increase hardness [72,77]	Composition alters stability: alkaline bath Ni rich deposits are more corrosion resistant, [76]	Particles and alloying raise hardness and thus dramatically improve wear resistance [72, 77]
Bath pH (esp. Ni-Co baths)	Alters alloy composition in anomalous systems, e.g. Acidic pH → uniform Co-rich Ni-Co films; alkaline pH → nodular Ni-rich films [76]	(Ni-Co) Ni rich (higher pH) alloys tend to softer (less Co) that Co-rich alloys.	Ni-Co alkaline (Ni-rich) films showed highest polarization resistance vs acidic [76]	-
Increased Agitation/stirring	Smoother, more uniform coatings; reduced edge "burrs" and dendrites [72]	Minimal direct effect [79]	Produces denser films (fewer defects), likely improving corrosion resistance	Enhances particle dispersion (increases hardness and wear in composites [72]
Increased Deposition time	Increase thickness (no intrinsic microstructural change beyond initial grain structure)	Longer time yields thicker coatings; in composites allows more uniform particle incorporation [79]	Thicker layers act as better diffusion barriers (corrosion protection)	Thicker coatings generally improve wear life (more material to abrade

Microhardness

Microhardness of electrodeposited coatings is largely governed by grain size (Hall-Petch strengthening), alloying content, and inclusion of hard phases. In most cases, conditions that refine grains or add stiff phases raise hardness.

• Current density: as in microstructure, raising current density usually hardens the deposit by creating finer grains. For Ni-P/CeO2 composite coatings, hardness rose from ~596 to 689 HV when current increased from 20 to 40 A/dm2 [77]. Similarly, in Ni-Co deposits (in sulfamate bath), hardness increased with applied current density [78] (correlated with grain refinement and composition shifts). Very high currents can eventually reduce hardness, however, if deposits become porous or lose alloying elements. In Ni-Co alloys, above ~200 A/dm2 the Co content drops, reducing solid solution strengthening even as grains shrink [72]. Overall, moderate current increases strengthen coatings (microhardness up), consistent with the Hall-Petch trend.

• Bath composition and alloying: alloying metals and co-deposited particles dramatically boost hardness. Ni-Co alloys routinely outperform pure Ni: one study found nanocrystalline Ni-Co films with ~60 at. % Co and ~14 nm grains reached 862 HV [75], whereas pure Ni under similar conditions is typically ~200-300 HV. Indeed, Ni-Co alloy coatings exhibited approximately double the microhardness of pure Ni films [72]. Electrodeposited Ni-P or Ni-B (from chemical bath) can exceed 500-900 HV, though these are electroless rather than DC processes. Adding hard particles further raises hardness: embedding Al_2O_3 or ZrO_2 into Ni causes dispersive hardening. For example, Ni-P with embedded ZrO_2/CeO_2 particles showed hardness ~12% higher than a Ni-P film. The particulate act as barriers to dislocation motion, which effectively prevent grain boundary slip thereby improving the hardness [77]. A Taguchi optimization study of Ni-Al_2O_3 composites confirmed that current density, particle concentration and plating time were the dominant factors in maximizing hardness, whereas agitation had little effect [79].

• Temperature: higher bath temperature tends to coarsen grain size (through enhanced diffusion and reduced hydrogen evolution), which usually lowers hardness. Depositing baths are often optimized around 40-60 ºC to balance deposition rate and structural refinement. Rapid deposition at very high temperatures can introduce stresses or defects that decrease hardness.

• pH, agitation and deposition time: pH alters alloy composition in some systems. For Ni-Co, higher pH (more Ni deposition) tends to reduce hardness (less Co) [76]. In neutral or basic Ni-Cu-Co baths, pH effects also shift alloy ratios via complexation. In pure metal deposition (e.g. Cu in acid, Ni in mildly acidic), pH is usually fixed near the optimal. No major direct effect on hardness is reported beyond its effect on composition. Varying agitation has little direct effect on the crystal grain or hardness of a given deposit. Experimental studies (Ni-Al_2O_3 composites) find that changes in stirring rate have very little effect on the coatings microhardness [79]. Agitation mainly affects deposit uniformity and particle loading, not intrinsic strength. Longer depositing (thicker fildeposits) can increase measured hardness if the coating becomes denser or if initial substrate effects are reduced. In composites, longer time can allow more even particle distribution, raising hardness. The cited Taguchi analysis ranked deposition time as the most influential factor for Ni-Al_2O_3 hardness. This likely reflects achieving full thickness of dense composite. In summary, hardness follows the trends of microstructure and composition: fine-grained, alloyed particle-containing deposits are hardest. Typical hardness values span wide ranges: pure Cu deposits (~50

- 100 HV), pure Ni (coarse ~150 - 250 HV), Ni-Co alloys (400 - 800 HV), Ni-P or Ni-B (600 - 1000 HV), composites (often >800 HV). The cited studies show how adjusting deposition conditions can push hardness to extreme values (e.g. 862 HV for Ni-Co [75]).

Corrosion resistance

Corrosion behavior depends on coating density, composition and defect level. Dense, adherent deposits resist penetration of corrosive species, so parameters promoting compact microstructure improve corrosion protection.

• Current density: increased current density can enhance corrosion resistance by producing finer, less porous deposit - up to a point. In Ni-Au protective deposits on Al, elevated current density resulted in reduced grain size and improved surface morphology, ensuring superior anti corrosion performance [74]. The smoother, defect-free surface hinders localized attack. However, if current is too high, the resulting roughness or microcracks can degrade corrosion resistance.

• Bath composition and alloying: alloy chemistry is critical. Nickel-rich deposits generally corrode slower than cobalt-rich ones in neutral/alkaline media. In the Ni-Co example above, alkaline baths (Ni - rich deposits) had much higher polarization resistance (66.1 $k\Omega.cm^{-2}$) than acidic (Co-rich) ones [76]. Thus, deposition parameters that favor Ni in the alloy (higher pH, higher current density as noted in some reports [76]) yield more corrosion-stable coatings. Pure Ni, Ni-Co, and Ni-Cu alloys are often chosen for corrosion protection, e.g. ~85 to 95 at. % Ni coatings exhibit excellent chloride resistance. Composite coatings (Ni with ceramic particles) can also improve corrosion by sealing defects; dense Ni-P+Al_2O_3 has shown lower porosity.

• pH, agitation and deposition time: as above, bath pH influences alloy content and thus corrosion: alkaline Ni-Co baths produce Ni-rich (less reactive deposits), whereas acidic baths yield more reactive Co-rich films [76]. For pure metal depositing, pH is normally controlled at the optimal point (e.g. ~4 for nickel sulphate, ~1 for Cu acid) to minimize hydrogen evolution and porosity. By improving bath transport, agitation tends to make deposits more uniform and freer of iron-depleted zones, enhancing corrosion resistance indirectly. Uniform stirring reduces formation of channel-like porosity, so higher agitation (within reason) can improve the barrier quality. As noted, longer deposition time yields thicker coatings, which serve as better corrosion barriers. The Ni-Au study explicitly noted that extended Ni deposition provided a second physical barrier in the coating, greatly delaying penetration of corrosives [74]. Thicker layers (up to an optimal thickness) thus typically raise charge-transfer resistance in corrosion tests. Copper coatings typically have modest corrosion resistance; Cu forms stable oxides but is less noble than Ni. In aggressive environments (e.g. acids, salts), Ni or Ni-alloy layers are preferred.

Wear resistance

Where resistance in electrodeposited films correlates strongly with hardness and toughness. Hard, dense coatings resist abrasion and adhesion damage, whereas soft or porous films were quickly.

• Current density: wear resistance generally improves with current density up to the point of maximum hardness. In the Ni-P+ZrO_2-CeO_2 composite coatings, wear-scar measurements showed the best wear performance at the dame optimal current of 40 mA/dm^2 that gave peak hardness. As the authors note, higher hardness makes the composite coating more wear resistant. Too low a current yielded a soft nanoparticle-deficient coating that deformed easily, too high a current produced roughness and weaker cohesion, worsening wear [77].

• Bath composition and particles: hard particles or alloying phases greatly enhance wear performance by raising hardness. Ni-Co alloys (harder than Ni) resist wear better, and Ni-Co-SiC or Ni-Co-Al_2O_3 nanocomposites show much lower volume loss. The cited Ni-P composite found that the embedded ZrO_2/CeO_2 (and Ni_2O) inclusions acted as barriers to dislocation motion, improving wear via dispersion strengthening [77]. Review literature notes that dispersing hard Al_2O_3 in a Ni matrix improves microhardness and wear resistance [72]. In contrast, Cu and pure Ni (low hardness) make poor wear surfaces unless reinforced.

• Agitation and other parameters: better agitation (up to an optimum) leads to more uniform particle co-deposition, which can improve wear. In Ni-Co nanocomposite coating, stirring was found to increase the fraction of embedded nanoparticles up to a saturation point [72]. Moe hard second-phased content means tougher, wear resistant coatings. Moreover, bath pH and temperature mainly affect wear indirectly via structure hardness. Longer deposition times (thicker, denser coatings) also prolong wear life, as the volume of hard material increases.

In summary, electrodeposited coatings optimized for wear combine high hardness with integrity. For example, nanocrystalline Ni-Co (with ~60% Co, 14 nm grain) achieved ultra-high hardness (862 HV) and would be expected to show exceptionally low wear. Likewise, Ni-P or Ni-B coatings (often deposited with additives) can reach >600-900 HV and exhibit superior tribological properties. Each parameter above can be tuned to approach these extremes by producing the finest, hardest deposit possible.

1.11 Formulation of research objectives

Electrochemical deposition has long been recognized as a versatile, cost effective, and scalable technique for producing metallic, alloy and composition coatings with tailored functional properties. Compared to physical vapor deposition or thermal spraying methods, it offers fine control over coating deposition, microstructure, thickness, and surface morphology through relatively simple adjustment of process parameters such as electrolyte composition, temperature, pH, current density and agitation. Consequently, electrodeposited coatings are widely applied in corrosion protection, wear resistance, microelectronics, energy devices, and surface engineering of structural components.

In recent years, increasing industrial demand for coatings with multi-functional performance, combining high mechanical strength, enhanced corrosion resistance, and controlled surface characteristics, has driven research toward alloy and composition coatings rather than single metal coatings. Metal alloys, such as Ni-Cu and Co-V as well as metal-carbon based compositions, such as Cr-graphene, have emerged as

promising systems due to synergetic effects between their constituents. These combined effects may result in grain refinement, enhanced mechanical and corrosion properties, and modified electrochemical behavior in corrosive environments.

Despite significant progress, electrodeposition of such advanced coatings remains highly sensitive to processing conditions. Minor variations in process parameters such as deposition temperature on current density can dramatically alter nucleation kinetics, growth mechanisms, hydrogen evolution behavior and incorporation efficiency of secondary phases. Therefore, many previously reported studies focus on limited parameter windows or emphasize either microstructural or functional properties in isolation, leaving critical optimization gaps unaddressed.

This dissertation is motivated by the need for a systematic and comparative investigation of three technologically relevant coating systems, Cr-graphene, Ni-Cu, and Co-V, prepared via electrodeposition. Special attention is given to identifying and addressing specific gaps in literature related to temperature-controlled graphene incorporation in chromium coatings and current-density driven optimization of alloy coatings, particularly with respect to hydrogen evolution, microhardness and corrosion performance.

Chromium based coatings are widely used for their high hardness, wear resistance, and chemical stability. Traditional hard chromium coatings, however, are associated with environmental and health concerns, as well as microcrack formation and limited corrosion resistance in aggressive media. To overcome these limitations, composite chromium coatings incorporating carbon-based reinforcements such as graphene have attracted increasing research interest. Graphene, owing to its exceptional mechanical strength, high surface area, chemical inertness, and barrier properties is considered an ideal reinforcement for metal matrices. Numerous studies have reported that the incorporation of graphene or carbon into metal coatings can lead to grain refinement, increase microhardness, reduce porosity, and improved corrosion resistance in chromium -graphene systems, graphene sheets can act as physical barriers against corrosive species while simultaneously hindering dislocation motion within the chromium matrix. However, electrodeposition of chromium-graphene composite coatings is particularly challenging due to the complex reduction behavior of chromium ions, low current efficiency, and the tendency of graphene to agglomerate in aqueous electrolytes. Previous research has primarily focused on electrolyte composition, surfactant use, and graphing concentration, while the role of deposition temperature has often been treated as a secondary parameter or maintained constant. Deposition temperature directly influences electrolyte conductivity, ion mobility, nucleation rate, grows kinetics, and hydrogen evolution in composite systems temperature additionally affects the dispersion ability of graphene and its incorporation efficiency into the growing metal matrix. Yet systematic studies evaluating a wide temperature range and correlating it with surface morphology, Carbon content, grain size evolution, micro hardness enhancement, and corrosion resistance of chromium-graphene coatings remain limited thus a clear research gap exists in understanding how controlled variation of deposition temperature specifically within the range of 15 to 60° C affects the structural and functional performance of chromium graphene composite

coatings and in identifying temperature that balances graphene incorporation with coating integrity.

Nickel-copper alloy coatings are well known for their excellent corrosion resistance particularly in marine and alkaline environments as well as four their good electrical conductivity and mechanical stability the complete solid solubility of nickel and copper across a wide composition range allows for continuous tuning of cutting properties by adjusting the alloy composition. Electrodeposition of nickel copper alloys has been extensively studied, with prior research focusing on bath composition, pH, complexing agents, and agitation. It's well established that current density plays a decisive role in determining alloy composition, grain size, surface roughness, and internal stress. At low current densities deposition is often controlled by activation kinetics, while at higher current densities, mass transport limitations and hydrogen evolution become increasingly significant. Hydrogen revolution during electrodeposition not only reduces current efficiency but also leads to porosity, surface defects, and embrittlement of the coating. Also, many studies report the effect of current density on either alloy composition or corrosion behavior, fewer works provide a comprehensive correlation between current density, hydrogen evolution tendency, surface morphology, microhardness, and corrosion resistance within a unified experimental framework. Furthermore, inconsistencies in reported optimal current density ranges adjust that system specific optimization is required, particularly when targeting multifunctional performance rather than a single property this highlights the need for a systematic investigation of current density as a primary control parameter in nickel copper without position with emphasis on minimizing hydrogen pollution while maximizing mechanical and corrosion performance.

Cobalt based alloy coatings are valued for their high hardness, wear resistance, magnetic properties, and thermal stability. Allowing cobalt with vanadium offers additional benefits, including solid solution strengthening grain refinement, and potential improvement in corrosion resistance. Co-V coatings are therefore of interest for applications in protective coatings, microelectromechanical systems, and energy related devices. Despite these advantages, electrodeposition of Co-V alloys is less extensively studied than that of more conventional systems such as Ni-Cu. The co-deposition of cobalt and vanadium is complicated by their different reduction potential and the tendency of vanadium to form complex ionic species in aqueous solutions. As a result, deposition parameters must be carefully controlled to achieve uniform alloy composition and defect free coatings. Existing studies indicate that current density strongly influences vanadium incorporation, phase structure, surface morphology, and hydrogen evolution behavior. High current densities may promote vanadium co-position but often at the expense of increased hydrogen evolution and surface roughening. Conversely, low current densities may build smooth coatings with limited vanadium content. A notable research gap lies in the lack of systematic optimization studies that simultaneously evaluate current density effects on hydrogen evolution, microstructure, mechanical properties, and corrosion resistance of Co–V coatings. Addressing this gap is essential for establishing reliable processing–structure–property relationships for this alloy system.

Based on these justifications, the following research tasks were formulated and solved in the dissertation.

• To develop and optimize electrochemical deposition parameters (bath temperature and current density) for the formation of uniform and adherent Cr–graphene composite and Ni–Cu and Co–V alloy coatings on metallic substrates, and to investigate the influence of synthesis conditions on nucleation, growth, microstructural evolution, and functional properties of the coatings.

• To study the morphological, structural, and compositional characteristics of the electrodeposited coatings using scanning electron microscopy, energy-dispersive spectroscopy, X-ray diffraction, atomic force microscopy, and related surface analytical techniques.

• To evaluate the functional properties of the coatings, including microhardness and corrosion resistance, and to analyze their correlation with electrochemical synthesis parameters and microstructural features.

• To establish structure–property relationships that determine the effect of electrochemical synthesis routes on coating quality and functional performance.

• To formulate optimized electrochemical deposition strategies for obtaining high-performance protective and functional coatings suitable for practical and industrial applications.

1.12 Conclusions and trends

Over the past decade, research has clarified how electrode position parameters tune coating performance for Ni, Cu, Co, Al, and related systems. The overarching patterns are: increasing current density refines grain structure (higher hardness, better wear and often better corrosion), provided the bath can sustain the increased demand. Bath chemistry (metal ratios, complexes additives, particles) often has equal or greater influence: alloying (Ni-Co, Ni-Cu, etc.) and nanoparticle co-position can double hardiness and dramatically alter corrosion behavior compared to pure metals. Control of pH and complexing agents is especially important in anomalous systems like Ni-Co. Ni-based coatings have been studied most extensively; they form the baseline (as in many cited studies) and serve as host matrices for alloys and composites. Coatings of copper are mainly used for electrical connectivity, so their wear and corrosion aspects are less often optimized by process tweaking (Cu is soft, but additives in coating baths can make it harder or brighter). Aluminum electrodeposition is still emerging (often in ionic liquids) and tends to yield very fine grains at elevated currents but is limited by electrolyte stability. Titanium metal coatings remain niche (requiring ionic-liquid or molten-salt processes) and were not widely featured in recent literature; instead, Ti is more often used as a deposited ceramic (TiN, TiO_2) in composite coatings. Overall, state-of-the-art electrodeposited Ni and Co coatings (particularly with composite reinforcements) can achieve microhardness well above 800 HV and provide wear resistance comparable to or exceeding that of heart chromium. Corrosion resistance likewise can be tailored: Ni-rich (high pH) deposits excel in corrosion tests, and thick, fine-grained deposits from high current and long coating times form very effective barriers. Current research trends focus on combining these effects – e.g. pulse coating, forced electrolyte flow, and novel additives - to further refine microstructure. In

designing a coating process for a given functional requirement, one therefore must balance parameters. For example, to maximize hardness and wear resistance one would use high current density, nickel-cobalt annoying, hard particle co-position, and moderate agitation; to maximize corrosion resistance one might favor a more nickel-rich bath, smooth brighteners, and a slightly lower current for a defect-free finish. Literature consistently shows these parameter-property relationships across nickel cobalt, copper, and aluminum systems, providing a guide for optimizing industrial electrodepositing processes.

2 RESEARCH METHODS

To comprehensively evaluate the structure, morphology, mechanical integrity, and functional performance of electrodeposited Cr-graphene coatings, Ni-Cu alloy coatings and Co-V alloy coatings, a multi-technique methodological approach was employed. The selection of methods was designed to provide complementary insights at different length scales and property domains. Comprehensive microscopic analysis techniques such scanning electron microscopy and energy dispersive spectroscopy, (SEM, EDS), optical microscopy, and atomic force microscopy (AFM) were utilized to assess, study and investigate surface morphology, microstructural features, and topography. Raman spectroscopy and XRD (X-ray diffraction) enabled to analyses structural and phase analysis, correlating vibrational and crystallographic information with processing conditions. To establish practical performance, mechanical testing (microhardness, nanoindentation, adhesion) and tribological evaluation (pin-on-disk and wear scar analysis) were performed, while electrochemical corrosion measurements in a three-electrode configuration provided insights into coating stability in aggressive environments. Together, these methods form a systematic framework to link synthesis conditions with the resulting structural, mechanical, and functional properties of the coatings.

The research methodology was structured as a sequential workflow (Figure 8), where each technique contributed unique but complementary information about the coatings. After electrodeposition synthesis, the samples were first examined by structural and morphological characterization (SEM/EDS), AFM, optical microscopy, XRD, Raman spectroscopy) to establish phase composition, crystallinity, and microstructural features. Next, mechanical property measurements (microhardness, nanoindentation, adhesion) were conducted to evaluate load-bearing capacity and coating-substrate integrity. These results were correlated with tribological testing (pin-on-disk, wear scar analysis) to determine wear resistance under simulated contact conditions. Finally, electrochemical corrosion studies in a three-electrode cell provided a measure of environmental durability. Together, this workflow ensured a systematic evaluation of the relationship between synthesis conditions, microstructure, and functional performance.

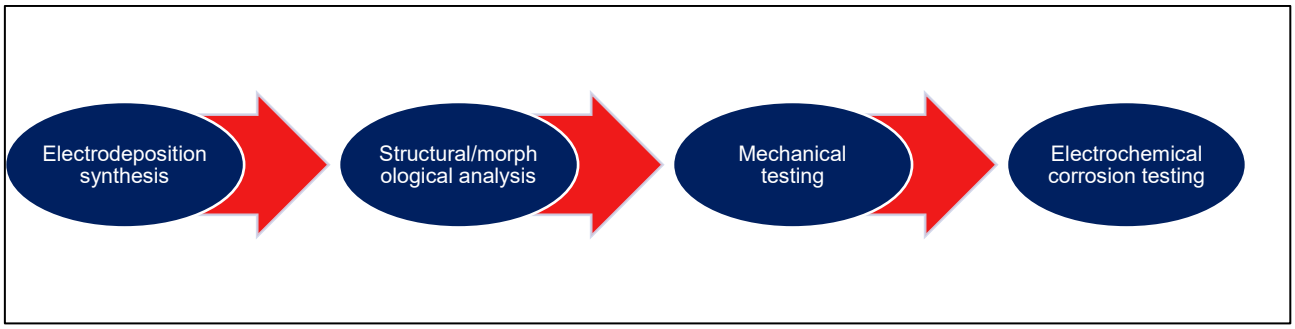


Figure 8 - Workflow of research methodology

The schematic illustrates the stepwise experimental approach adopted in this study. The process begins with electrodeposition of chromium, nickel and cobalt-based composition coatings on copper and steel substrates under controlled electrochemical

conditions. The synthesized coatings then undergo structural and morphological characterization, including SEM/EDS (surface morphology and composition), AFM (nanoscale topography), Raman spectroscopy (vibrational and phase analysis), optical microscopy (surface features at the micron scale), and XRD (crystallographic phase identification). Following structural analysis, mechanical property testing is performed via microhardness, nanoindentation, and adhesion measurements to determine load-bearing capability and coating-substrate bonding. Subsequently, tribological evaluation is carried out using pin-on-disk and ball-on-disk setups, where wear scars are later analyzed microscopically. The final stage involves electrochemical corrosion testing using a three-electrode cell (working, reference, and counter electrode) in NaCl solution, providing insight into corrosion resistance and coating stability. The integrated workflow ensures that each dataset builds upon the previous stage, allowing comprehensive correlation between synthesis parameters, microstructure, and functional performance.

2.1. Scanning Electron Microscopy (SEM) and Energy Dispersive X-ray Spectroscopy (EDS)

Scanning Electron Microscopy (SEM), often integrated with EDS, is an essential technique for the characterization of solid (and liquid) samples across numerous scientific disciplines, including metallurgy, coatings technology, materials science, and nanotechnology. In the present study, SEM and EDS were employed to analyze the morphology and chemical composition of electrodeposited nickel coatings on copper substrates. These techniques enable both high-resolution surface imaging and localized compositional analysis, which are essential for correlating microstructural features with the mechanical and tribological performance of the coatings.

The principle of SEM fundamentally relies on the intricate interactions between a finely focused electron beam and the constituent atoms of a sample, leading to the generation of various signals that provide comprehensive information about the sample's surface morphology, elemental composition, and crystallographic properties [80–82]. This technique is indispensable for unraveling the complex relationships between material structure and properties across scales, from mesoscale morphology to atomic arrangements [83]. When the primary electron beam strikes the specimen surface, a variety of signals are generated, including secondary electrons, backscattered electrons, and characteristic X-rays. Secondary electrons, which originate from near-surface regions (a few nanometers), provide high-resolution topographical information [84, 85]. Backscattered electrons, which penetrate deeper, carry information about compositional contrast due to differences in atomic number. Meanwhile, characteristic X-rays emitted because of electron-atom interactions form the basis for EDS analysis, enabling qualitative and quantitative determination of the elemental composition present in the sample [82,85].

Compared with optical microscopy, SEM offers several advantages, including higher spatial resolution (down to 0.4 nm), superior depth of field, and the ability to generate three-dimensional-like surface images. These capabilities make SEM particularly suitable for examining the fine-scale morphology of electrodeposited

nickel layers, such as grain size, surface roughness, porosity, crack formation, and tribological wear features after mechanical testing.

In this work, a FEI quanta 200i 3D SEM (Figure 9) equipped with an EDS detector was used for morphological and compositional analysis. SEM imaging was performed under high-vacuum conditions with an accelerating voltage in the range of 10-20 KV, optimized depending on the surface characteristics of the coating. Lower accelerating voltages (≈10 KV) were used to minimize charging and beam damage while providing surface-sensitive imaging, whereas higher voltages (≈20 KV) were applied to obtain deeper penetration and enhanced x-ray generation for EDS.

EDS analysis complements SEM by providing localized chemical information about the coating and substrate. The technique allows identification of elemental composition across different regions of the coating and at the coating-substrate interface, which is critical for evaluating adhesion quality and elemental distribution [86–88]. In the case of nickel coatings on copper, EDS enables verification of coating purity, detection of impurities, and possible diffusion or incorporation of copper into the nickel layer. Both qualitative analysis (element identification) and semi-quantitative analysis (relative concentration of detected elements) were carried out.

Sample preparation prior to SEM/EDS involved cutting the coated specimens into small sections, followed by cleaning in ethanol to remove surface contaminants. Since the studied samples (nickel coatings on metallic copper) are inherently conductive, no additional conductive coating was necessary. However, care was taken to ensure proper grounding to avoid charging effects.



Figure 9 - SEM Quanta 3D 200i

Thus, the combined use of SEM and EDS provided essential insights into the surface morphology, structural features, and chemical homogeneity of electrodeposited coatings, serving as a foundation for correlating microstructural characteristics with their measured mechanical and tribological properties. Furthermore, elemental maps and point analyses from the eds spectra confirm the distribution and incorporation of

elements or reinforcing particles within the coating layer [89, 90]. A schematic diagram of the Quanta 200i SEM used in this research is shown in Figure 10.

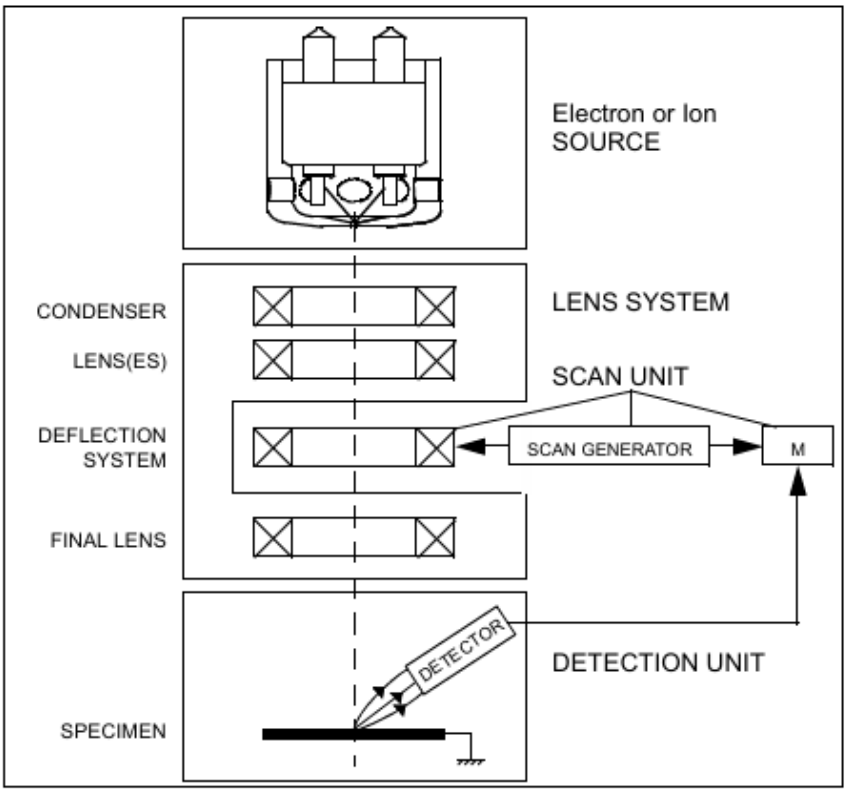


Figure 10 - Schematic diagram of Quanta 200i SEM (adapted from manufacturer's schematic)

In this system, electrons are emitted from the electron source (usually a tungsten filament or LaB_6 crystal) and accelerated toward the specimen by a high-voltage electric field. The emitted electron beam passes through a series of electromagnetic lenses and apertures that concentrate and control the beam into a fine probe with a diameter of several nanometers. The lens system (condenser and objective lenses) and deflection coils are used to focus and raster-scan the beam across the specimen surface, as illustrated in the schematic.

Thus, the SEM-EDS investigation provides essential insight into the relationship between surface morphology, composition, and functional performance of the synthesized coatings.

2.2 Raman Spectroscopy

Raman spectroscopy is a powerful analytical technique used to investigate vibrational, rotational and other low frequency modes of molecules providing detailed insights into their chemical bonds, molecular structure, and interactions [91, 92]. It provides detailed information on the structural, chemical, and physical states of materials in both solid and liquid phases. The method is based on the inelastic scattering of monochromatic light, known as the Raman effect, which occurs when photons from an excitation source interact with molecular vibrations or lattice phonons. This leads to a shift in the energy (frequency) of the scattered light relative to the incident laser,

allowing identification of specific molecular bonds, crystallographic phases, and structural defects [93].

In the present work, Raman spectroscopy was employed to complement SEM/EDS analysis by probing the structural features and phase composition of electrodeposited nickel coatings on copper substrates. Raman analysis is particularly useful for detecting the presence of nickel oxides, hydroxides, or other secondary phases that may form during electrodeposition or post-treatment, as well as for evaluating microstructural changes associated with mechanical and tribological testing.

A modern Raman spectrometer integrates several key components to facilitate the detection and analysis of Raman Scattering, providing molecular and structural information about a sample. The fundamental architecture typically comprises an excitation laser source, an optical system for both illuminating the sample and collecting scattered light, a wavelength selector, and a detector. These elements work synergistically to overcome the inherent weakness of the Raman Effect and enable precise spectroscopic measurements [94–99]. In this study, a confocal micro-Raman spectrometer equipped with a high-resolution spectrograph with a confocal optical microscope was used (Figure 11). The choice of excitation wavelength was made to balance penetration depth, fluorescence minimization, and signal intensity for metallic coatings.



Figure 11 - Horiba LabRam HR Evolution Raman Spectrometer

During measurement, the sample is irradiated with a focused laser beam in the visible or near-infrared range. The majority of photons are elastically scattered (Rayleigh scattering), but a small fraction undergoes inelastic scattering (Raman scattering). This consequences in either energy loss (stokes scattering) or energy gain (anti-stokes scattering), which corresponds to molecular vibrational transitions. The resulting Raman spectra provides unique fingerprints of the vibrational modes of the material, enabling identification of different structural phases.

For nickel coatings, Raman analysis can reveal signals corresponding to NiO, $Ni(OH)_2$, and other nickel-based compounds that may form at the surface or grain

boundaries. These phases can strongly influence the corrosion resistance, wear resistance, and adhesion of the coatings. Furthermore, Raman spectroscopy allows detection of carbon-based phases (graphitic or amorphous carbon) if present in composite coatings, as well as stress-induced structural changes after tribological testing [100]. The Horiba LabRam HR Evolution Raman Spectrometer operates based on the principle of inelastic light scattering, where monochromatic laser radiation interacts with the molecular vibrations of a material, resulting in energy shifts in the scattered photons known as the Raman effect. The system uses a confocal optical microscope to focus the incident laser beam-typically in the visible range-onto a microscopic region of the sample surface. The scattered light is collected by the same objective lens and directed through an edge or notch filter that removes the intense Rayleigh (elastically scattered) light, allowing only the weaker Raman-shifted light to pass. The schematic diagram is presented in Figure 12.

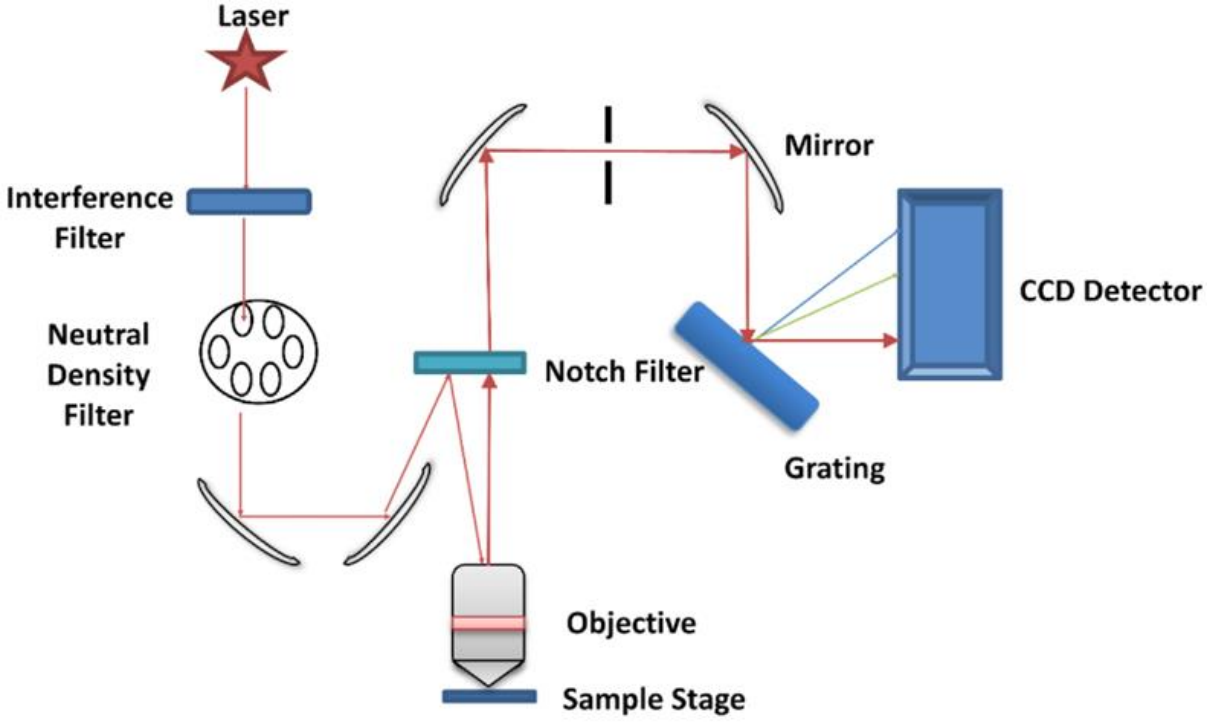


Figure 12 - A schematic of Horiba LabRam HR Evolution Raman Spectrometer [101, p 10]

The transmitted light is then dispersed by a high-resolution diffraction grating housed in the spectrograph and detected by a cooled charge-coupled device (CCD) detector, which records the Raman spectrum as intensity versus Raman shift (cm^{-1}). The confocal configuration of the LabRam HR system allows spatial filtering through a variable pinhole, thereby improving depth discrimination and enabling three-dimensional Raman mapping of the coating structure. This optical design minimizes background interference and enhances signal quality from localized micro-regions.

For the present study, this spectrometer was used to analyze nickel-based composite coatings deposited on copper substrates. The system's high spatial resolution (~1 μm) and spectral accuracy (<1 cm^{-1}) make it particularly suitable for detecting vibrational modes associated with Ni, NiO, and incorporated second-phase

particles, as well as identifying structural defects, phase transformations, and stress-induced spectral shifts that arise from the electrodeposition process.

During Raman scattering, three types of signals are generated [94, 102]: Rayleigh scattering, corresponding to elastic scattering with no change in photon energy; stokes scattering, where photons lose energy due to excitement of vibrational modes; and anti-stokes scattering, where photons gain energy from already excited vibrational states. For electrodeposited nickel coatings, stokes scattering is typically more intense and is therefore the primary source of spectral information. It provides vibrational fingerprints of nickel-oxygen, nickel-hydroxide, or other structural bonds that may form in the coating. Anti-stokes scattering, while weaker, can be useful for probing surface heating effects and vibrational population levels, which may become relevant under tribological loading when coatings are subjected to frictional heating.

Figure 13 schematically illustrates these processes: in stokes scattering, incident photons excite the coating material from its ground vibrational state to a virtual energy level, and re-emission occurs at a lower frequency (longer wavelength). In contrast, anti-stokes scattering occurs when the material is already in an excited vibrational state (due to thermal effects or external stress), leading to re-emission at a higher frequency (shorter wavelength). This distinction is particularly important in the present study, as it allows correlation between the Raman-active vibrational modes of nickel-based coatings and the influence of microstructural defects, oxides, or thermally induced transformations that directly affect their mechanical and tribological performance.

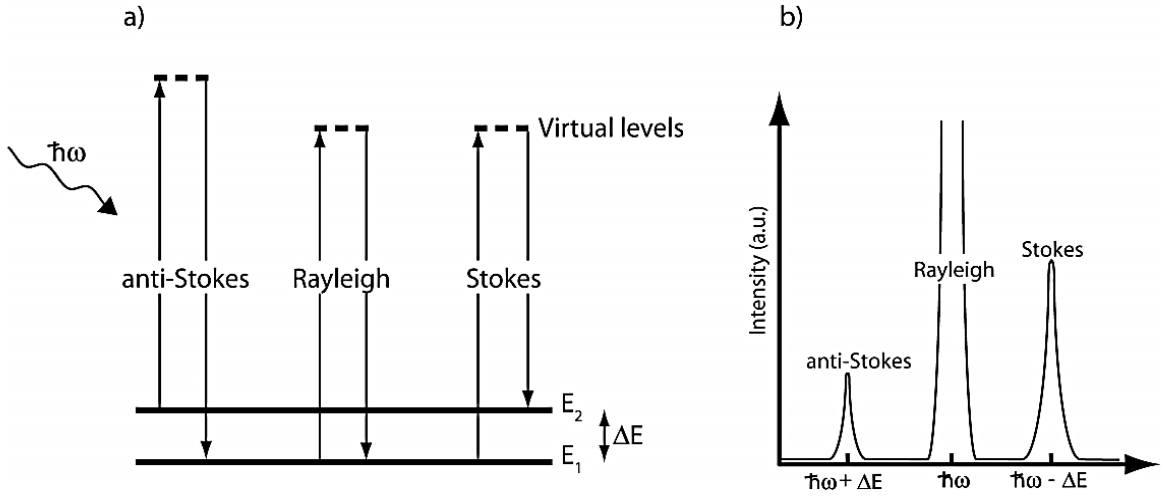


Figure 13 - Stokes scattering of Raman spectroscopy [103, P 5]

Sample preparation for Raman analysis was minimal since the nickel-coated copper substrates provided a reflective and stable surface. Care was taken to minimize laser-induced heating during measurement, which can lead to local oxidation or structural modification of the coatings. Spectra were recorded in the wavenumber range of [state range, e.g., 200-2000 cm^{-1}], and multiple points across each sample were analyzed to ensure representative data.

In summary, Raman spectroscopy was employed in this study to provide phase- and structure-sensitive characterization of electrodeposited nickel coatings, complementing SEM/EDS analysis. This method enabled identification of oxide and

hydroxide phases, evaluation of structural integrity, and detection of microstructural changes relevant to the functional properties of the coatings.

2.3 Mechanical properties testing

Mechanical properties testing is essential for evaluating the performance and reliability of electrodeposited composite coatings, as it provides direct evidence of their ability to withstand service conditions. These coatings are primarily developed to enhance properties such as hardness, wear resistance, and load-bearing capacity; however, such improvements cannot be assumed solely based on composition or microstructural observations. Techniques such as microhardness testing, scratch adhesion testing, and wear analysis enable a quantitative assessment of the coating's resistance to deformation, fracture, and material loss under applied stresses. Hardness measurements reflect the strengthening effect of incorporated reinforcement particles, while adhesion tests determine the integrity of the coating-substrate interface, which is critical for preventing delamination during operation. [104–106]. Furthermore, mechanical testing plays a crucial role in establishing the relationship between processing parameters, microstructure, and resulting properties. Variations in electrodeposition conditions, such as current density, bath composition, and deposition mode, directly influence grain size, particle distribution, and internal stresses within the coating. By correlating these factors with measured mechanical properties, it becomes possible to optimize the deposition process for improved performance. Additionally, mechanical characterization helps identify potential defects, such as microcracks or weak interfacial bonding, which may not be fully evident from structural analyses alone. Therefore, mechanical properties testing not only validates the effectiveness of the coating design but also ensures its suitability for practical engineering applications.

Particularly in this dissertation, microhardness testing was performed using a Vickers microhardness tester in accordance with ASTM E384 standards [107,110]. Indentations were made with a diamond pyramid indenter under a load of 25 - 100 grams for a dwell time of 10 – 15 seconds. The applied load was chosen to ensure penetration within the coating thickness while minimizing substrate effects. At least five indentations were made at different regions on each substrate to obtain representative values. The hardness values (HV) were averaged and compared across samples with different electrodeposition conditions. This method provided a baseline measure of coting hardness, which is directly linked to grain size, microstructural density, and defect content. Moreover, microhardness testing can reveal variations in structural uniformity and deposition quality, providing valuable information about process stability. Higher hardness values generally indicate improved wear resistance and durability, making microhardness a key parameter for predicting coating performance in tribological investigations and applications. However, it is also important to interpret hardness results in connection with other mechanical properties. Therefore, microhardness testing not only serves as a fundamental tool for characterizing electrodeposited composition coatings but also aids in optimizing the balance between strength and toughness for enhanced functional coating performance.

2.4 Scanning Probe Microscopy (SPM) and Atomic Force Microscopy (AFM)

Scanning Probe Microscopy (SPM), in particular Atomic Force Microscopy (AFM), is one of the most essential and versatile tools in the field of materials science for characterizing surface topography at the nanometer scale. By combining AFM with complementary optical methods (e.g., confocal and Raman modules), the Integra Spectra platform provides simultaneous structural, morphological, and spectroscopic characterization. This integration enables detailed mapping of the surface properties of coatings with high spatial resolution [111–113].

The working principle of AFM is based on scanning the sample surface by utilizing an ultrasharp probe (typically <10 nm tip radius). The probe is situated above the surface of the sample and approaches till short-range interactions happen between the sample and the tip. The characteristic tip-surface distance in probe-based microscopes is usually in the order of 0.1-10 nm. As the probe scans across the surface of the sample, deflections of the cantilever are measured via a laser beam reflected onto a photodetector, providing quantitative topographic information. This allows nanoscale visualization of grain structure, nodularity, roughness, and defects in the nickel coatings deposited on copper substrates.

In the Integra Spectra system, the AFM module can be integrated with optical spectroscopy. The probe tip is positioned at the laser focus, enhancing local electromagnetic fields and significantly amplifying Raman scattering signals from the surface (tip-enhanced Raman scattering, TERS). This makes it possible to correlate nanoscale topography with local spectroscopic features, providing insights into structure-property relationships in composite coatings.

Movement of the probe with sub-nanometer precision is achieved using piezoelectric ceramic manipulators, ensuring stable imaging and accurate surface mapping. Figure 14 below shows the configuration of the Integra Spectra Scanning Probe Microscope, illustrating both the Atomic Force Microscope integration and the architecture of the modular device.

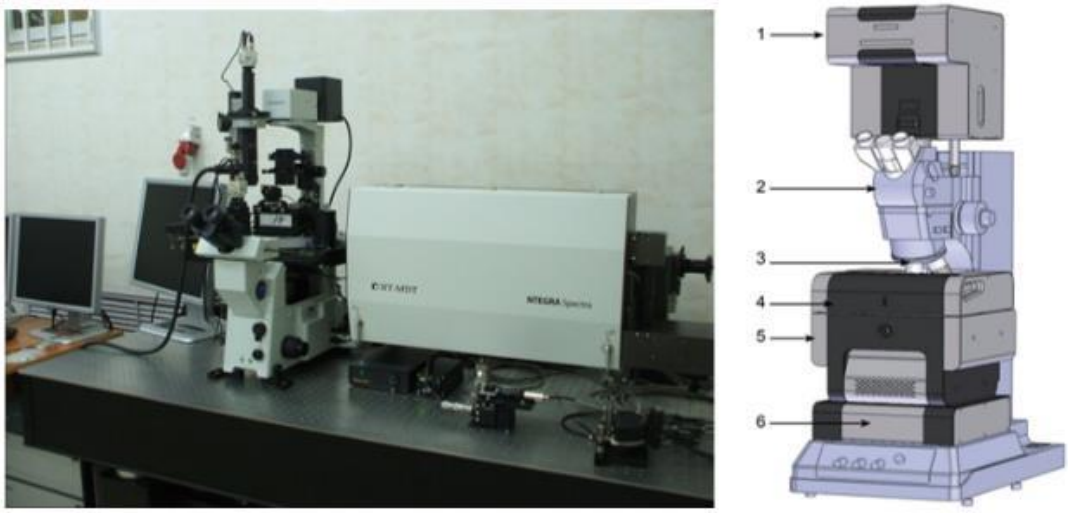


Figure 14 – Scanning Probe Microscope (Integra Spectra): a) SPM and AFM integration, b) system device

Based on Figure 14b, the Integra Spectra AFM comprises of lots of main components. These components are confocal module with a scanning mirror, direct microscope for optical inspection purposes, four position lens turret for multiple objectives, AFM module with interchangeable probe heads, and measuring stage. During measurement, AFM scans generate a nanoscale sized topographic map of the coating surface. In combination with detection of Raman scattering, the system produces correlative maps of surface morphology and spectral properties, reflecting both the physical topology and chemical distribution across the coating. In the context of nickel-based composite coatings, this method provides critical insights into grain structure evolution, surface roughness, nodularity, and localized compositional variations, all of which directly influence mechanical performance and tribological behavior.

2.5 X-ray Diffraction (XRD)

X-ray diffraction (XRD) is a widely used, non-destructive technique for structural analysis of crystalline materials. Its principle is based on the constructive interference of X-rays scattered by the periodic arrangement of atoms within a crystal, as first demonstrated by Laue in 1912 and theoretically developed by W. and L. Bragg in 1913. Since then, XRD has become a cornerstone technique in materials science for identifying crystalline phases, evaluating grain size, detecting structural defects, and analyzing residual stresses [114–116].

In this study, XRD was employed to investigate the crystallographic structure and phase composition of nickel-based composite coatings deposited on copper substrates. Measurements were performed using a Rigaku SmartLab X-ray Diffractometer SOP (Figure 15), equipped with a Cu Kα radiation source (λ = 1.5406 Å). The diffractometer was operated at 40 kV and 30 mA, with a scanning range of 20–90° (2θ), a step size of 0.02°, and a counting time of 1s per step, ensuring high resolution and reliable peak intensity measurements.



Figure 15 – Rigaku SmartLab X-ray Diffractometer

To minimize substrate interference and preferentially probe the coating, grazing incidence XRD (GIXRD) was applied at low incidence angles (1-2°). This allowed detailed structural characterization of the thin coatings while suppressing background diffraction from the copper substrate. Diffraction patterns were analyzed with reference to the ICDD PDF-4+ database for phase identification. Crystallite size was estimated using the Scherrer equation, while lattice strain and dislocation density were evaluated through Williamson-Hall analysis. Texture measurements (pole figures) were also carried out to assess preferred crystallographic orientations, which are directly linked to coating hardness, adhesion, and tribological properties. Thus, XRD provides essential insights into the phase stability, grain size distribution, and structural stress states of the electrodeposited nickel coatings, complementing scanning electron microscopy/energy dispersive spectrometer, Raman spectroscopy, and atomic force microscopy analyses.

X-ray diffraction is a fundamental and essential tool for analyzing crystallographic structure, phase composition, and preferred orientation (texture) of metal and alloy-based composition coatings. This method is based on the principle of the elastic scattering of monochromatic X-rays by the periodic arrangement of atoms in a crystal lattice, which produces constructive interference at specific angles according to Braggs's law.

$$n\lambda = 2d \sin\theta$$

Where n is the order of reflection, λ is the X-ray wavelength, d is the interplanar spacing, and θ is the angle of diffraction.

In the context of chromium-graphene, nickel and nickel-alloy composite coatings, and Co-V alloy coatings, XRD is particularly useful for:

• Identifying crystalline phases (e.g., fcc-Ni, NiO, Ni-P, or reinforcing second phases).

• Evaluating crystallite size and microstrain via line broadening analysis (Scherrer equation, Williamson-Hall plots).

• Determining coating texture (preferred crystallographic orientation), which strongly influences hardness, adhesion, and wear resistance.

• Detecting lattice distortions or residual stresses arising from electrodeposition parameters.

Instrument setup: The measurements will be performed using a powder X-ray diffractometer equipped with a Cu Kα radiation source (λ=1.5406 Å) operated at 40 kV and 30 mA. A monochromator will be used to reduce fluorescence, and the diffracted beam will be recorded with a high-resolution scintillation detector. Typical scanning parameters will include a 2θ range of 20°-90°, step size of 0.02°, and a counting time of 1-2 s per step, ensuring both adequate angular resolution and sufficient signal-to-noise ratio.

For thin nickel coatings on copper substrates, grazing incidence X-ray diffraction (GIXRD) may be employed to minimize substrate interference. By setting a small incidence angle (e.g., 1-2°), the penetration depth of the X-ray beam is reduced, allowing preferential collection of diffracted signals from the coating layer rather than the underlying Cu substrate.

Data analysis: The obtained diffraction patterns will be processed using standard software packages (e.g., HighScore Plus, JADE) with reference to the International Centre for Diffraction Data (ICDD) PDF-4+ database. Phase identification will be performed by matching experimental peaks with standard reference files. The average size of crystallite (D) is estimated using Scherrer's equation.

$$D = \frac{K\lambda}{\beta \cos \theta}$$

Where K is the shape factor, (typically a value of 0.9), β is the full width at half maximum (FWHM) of the diffraction peak, measured in radians, and θ is the Bragg angle.

Williamson-Hall analysis will be applied to separate contributions from size and lattice strain broadening. Pole figure measurements may also be carried out to analyze coating texture and preferred orientation. By correlating XRD results with SEM/EDS, AFM, and Raman data, a comprehensive picture of the structural–morphological evolution of the nickel-based composite coatings will be established. For example, the presence of nanocrystalline fcc-Ni grains, secondary reinforcing phases, or residual stresses can be linked to mechanical hardness and tribological behavior, providing insight into the effect of electrodeposition parameters on coating performance.

2.6 Optical Microscopy

Optical microscopy remains an important tool for characterizing materials at the micro- and sub-micron scale, complementing higher-resolution techniques such as SEM and AFM. In this work, a Leica DM 6000 M optical microscope (Figure 16) was used to evaluate the surface morphology and cross-sectional features of nickel coatings deposited on copper substrates. The microscope is equipped with high-resolution digital cameras and automated imaging software for capturing and analyzing surface features. It operates in both incident light (reflection) and transmitted light modes, supporting bright-field and dark-field imaging. This versatility enables the examination of transparent, translucent, and opaque samples with a lateral resolution of up to ~200 nm.



Figure 16 - Leica DM6000M Optical Microscope

The Leica DM 6000 M system is also equipped with a motorized, coded turret accommodating six objective lenses with magnifications of 5x, 10x, 20x, 50x, 100x, and 150x. Automated aperture and diaphragm controls, motorized stage movement in x-y-z, and a memory function for lens/contrast switching allow precise imaging of both surface features and cross-sections.

In the context of this research, optical microscopy was primarily applied for:

• Preliminary inspection of coating uniformity and surface quality before SEM/AFM characterization.

• Thickness measurements from polished cross-sections.

• Detection of cracks, pores, or delamination zones in the coatings.

In combination with high-resolution methods, optical microscope provides a fast and effective way to investigate coating integrity and surface morphology at the nanoscale, which ensures reliable interpretation of subsequent structural and mechanical properties characterization.

2.7 Electrochemical testing

A key method for evaluating the corrosion resistance properties of metal and alloy-based composition coatings, electrochemical testing provides detailed insights into coatings' stability, passivation behavior and electrochemical kinetics in aggressive environments. In this study, the corrosion resistance properties of electrodeposited chromium-graphene, nickel-copper, and cobalt-vanadium were investigated using potentiodynamic polarization and electrochemical impedance spectroscopy (EIS).

Experimental setup: all electrochemical tests were conducted in a conventional three-electrode electrochemical cell connected to an AUTOLAB PGSTAT302N potentiostat/galvanostat. The working electrode was the nickel-coated copper specimen with an exposed surface area of 1 cm^2. A saturated calomel electrode (SCE) served as the reference, and a platinum wire was used as the counter electrode.

The electrolyte solution was a 3.5 wt.% NaCl aqueous solution, simulating a chloride-rich corrosive medium relevant to structural and industrial applications. Prior

to testing, the solution was de-aerated with high-purity nitrogen for 30 minutes to minimize dissolved oxygen interference, while open-circuit potential (OCP) was monitored for 30 minutes to allow system stabilization.

Potentiodynamic Polarization (PDP): Potentiodynamic polarization measurements were performed by sweeping the potential from -250 mV below OCP to +1000 mV vs. SCE at a scan rate of 1 mV/s. The resulting polarization curves were analyzed to determine key corrosion parameters, including:

• Corrosion potential (E_{corr}) – indicative of thermodynamic stability.

• Corrosion current density (i_{corr}) – calculated via Tafel extrapolation, providing a measure of corrosion rate.

• Passivation behavior – detection of passive film formation and its stability across applied potentials.

The comparison of polarization parameters among coatings with different deposition conditions provided insights into the role of microstructure and phase composition on corrosion resistance.

Electrochemical Impedance Spectroscopy (EIS): EIS measurements were carried out at OCP over a frequency range of 100 kHz to 0.01 Hz with a sinusoidal perturbation amplitude of 10 mV. The Nyquist and Bode plots obtained were analyzed using equivalent electrical circuit (EEC) models to extract electrochemical parameters such as:

• Charge transfer resistance (Rct) – reflecting the barrier properties of the coating.

• Double-layer capacitance (Cdl) – related to surface roughness and porosity.

• Coating resistance (Rc) and coating capacitance (Cc) – characterizing dielectric and protective properties of the film.

Higher Rct and Rc values, along with reduced Cdl, indicated superior corrosion resistance, often linked to denser microstructure and uniform phase distribution within the nickel coatings.

2.8 Relevance to chromium, nickel and vanadium-based coatings

By combining potentiodynamic polarization and EIS techniques, a comprehensive assessment of the coatings' electrochemical stability, passivation capacity, and degradation mechanisms was achieved. These findings provide crucial correlations between the morphological, structural, and tribo-mechanical properties of nickel coatings and their resistance to corrosive attack, strengthening the overall functional evaluation.

3 SYNTHESIS AND FUNCTIONAL PROPERTIES OF METAL AND ALLOY-BASED COMPOSITION COATINGS

3.1 Morphology and corrosion resistance of electrodeposited chromium-graphene composite coatings under varying temperatures

Composite coatings have gained significant attention in various fields due to their multifunctional and unique properties as well as diverse applications [117–119]. The combination of different materials in a composite coating allows for the enhancement of specific characteristics such as wear resistance, anticorrosion properties, thermal conductivity, and tribological performance [120–122].

Studies show that highly sophisticated material surface properties including mechanical, electrochemical, tribological, optical, electronic, and magnetic properties can be obtained by creating new nanocomposite coating materials [123–125). Consequently, these nanocomposite coatings are found to be greatly attractive for different applications in engineering such as high-speed machining, tooling, environmental and optical applications, and magnetic storage devices due to their unique mechanical, electronic, optical, magnetic and electrochemical properties [126–128]. To produce these nanocomposite coatings, several kinds of methods can be employed, such as physical and chemical vapor depositions, laser cladding, lase melt injection, electrodeposition, sputtering, and plasma electrolytic oxidation [129–136]. Among all these applicable methods to produce nanocomposite coatings, electrodeposition stands out as a simple, scalable, and economical electrochemical method with minimal waste production [137–139].

Composite coatings are synthesized and applied to the surface of various kinds of substrates mainly to enhance desired surface properties and protect the substrates form corrosion under demanding working environments. When using electrodeposition method to produce coatings, micro and nano sized particles or fibers are incorporated into a metal matrix through the process. These composite coatings typically combine the properties of both the reinforcing material and the metal matrix, which enables the substrate materials to find special industrial applications. It has been extensively researched and explored the co-deposition of Al_2O_3, TiO_2, SiC, SiO_2, and carbon nano tubes into different metal matrices, for the purpose of revealing composite coatings posses enhanced hardness and better wear and corrosion resistance properties compared to pure chromium metal coatings [140, 141]. More recent studies have aimed to expand investigating and demonstrating the effectiveness of graphene based composite coatings for enhanced functional properties [142].

Graphene, a single layered and incredibly strong carbon atoms, possesses all the known vital properties for obtaining corrosion resistance coatings, including atomic thinness, extreme tensile strength, wear resistance, lightweight ness, impermeability, and chemical inertness. Because of these unique and exceptional properties, composite coatings based on graphene are widely utilized for the purpose of enhancing desired surface and mechanical, as well as corrosion resistance properties of various substrates. Researches successfully synthesized the chromium-graphene oxide (GO) nanocomposite coating using the electrodeposition method [143, 144]. These studies investigated the influence of adding graphene oxide on surface topography,

microhardness, and corrosion resistance behavior of chromium coatings. The results of the studies revealed that the addition of graphene oxide particles had a significant impact on the surface microhardness of the coatings. The maximum surface microhardness value was observed in samples with 10 wt.% of graphene oxide particles. The combination of graphene oxide particle addition and coating thickness was found to have a more pronounced effect on surface microhardness than the grain size of topographies. Additionally, the corrosion resistance of the chromium coating was found to decrease with the addition of graphene oxide particles. However, the layer with 5 wt.% of graphene oxide particles exhibited better corrosion resistance compared to other composite coatings. The study also highlighted the meaningful relationship between corrosion resistance and roughness measurement, explained as the ratio of arithmetic mean height (Sa) to maximum peak height (Sp). This suggests that incorporating graphene into composite coatings can improve their corrosion resistance properties.

The use of graphene in composite coatings has also been explored in other studies. For example, composite electrochemical coatings based on nickel-chromium alloy modified with multilayer graphene oxide were obtained by and electrodeposition of composite coatings modified with graphene oxide [145–147]. These investigations proved the potential of graphene-based composition coatings to improve corrosion and wear resistance properties. Overall, existing literature highlights the growing interest in chromium-graphene composition coatings along with their potential applications in improving surface, mechanical, corrosion and wear resistance properties. The incorporation of graphene particles to chromium metal coatings showed to have significant influence in enhancing surface microhardness and corrosion and the findings of this study offer a new strategy for tuning the structural and protective properties of Cr-graphene coatings through precise thermal control during electrodeposition. Further research in this area could lead to the development of advanced composite coatings with enhanced performance characteristics.

3.1.1 Experimental

Natural graphite flakes (with 325 mesh) was procured from QR graphite manufacturing company, China. All other chemicals for analytical were procured from Beijing chemical works company. The substrate material to be coated was Q235 low-carbon structural steel widely used for construction and machinery parts. The elemental composition of the substrate is outlined in Table 4 below.

Tabel 4 – Elemental composition (in wt.%) of low-carbon steel substrate (Q235)

Elements	C (≤)	Si (≤)	Mn (≤)	S (≤)	P (≤)
Wt.%	0.17	0.35	1.4	0.035	0.035

3.1.2 Synthesis of graphene

Graphene oxide was prepared using improved Hummer's method, a widely applied technique of chemical exfoliation for synthesizing graphene oxide [148]. The

synthesis procedure begins with mixing together 1 gram of graphene flakes and 6 gram of potassium permanganate ($KMnO_4$) to another chemical mixture containing concentrated strong acids of 180 mL sulfuric acid and 20 mL phosphoric acid. The mixture results in an exothermic reaction of mild magnitude at 35-40 ^oC. Next to this, the mixture reaction temperature was raised to 50 ^oC and maintained at this level while stirring for a period of 12 hours. Upon completion, the mixture was brought to cool down to room temperature, and addition of 400 mL ice water with 3 mL of 30% concentration of hydrogen peroxide followed. This resulting mixture was then allowed to stand for 24 hours followed by removal of the supernatant by 8000 rpm for 5 hours of centrifuge, and the remaining mixture was washed repeatedly before being transferred onto a glass plate and dried under vacuum at 60 ^oC for 24 hours, yielding solid graphene oxide. Subsequently, graphene oxide was reduced to graphene via chemical reduction by treating it with hydrazine hydrate, which acts as a reducing agent to remove oxygen-containing functional groups and restore the sp^2 carbon network [149].

3.1.3 Electrodeposition process

The Cr-graphene composite coatings were prepared using an electrodeposition process. Q235 carbon steel samples with dimension 10 × 20 × 2 mm were used as the substrate (cathode) for the coatings, with their chemical composition detailed in Table 4 above. This sample dimension was chosen for various subsequent surface, mechanical, and electrochemical properties tests of the composite coatings. The composition of the electrolyte bath is presented in Table 5 below. The electrodeposition process, carried out in a conventional Watt's bath, parameters are a current density of 5 A/dm^2, 0.2 g/L concentration of graphene, and a pH of 3-4. For the purpose of enhancing the dispersion of graphene nanosheets in electrolyte bath, ultrasonication was done for one hour. The electrodeposition process was carried out, with four distinct deposition temperatures, for one hour under constant stirring at 400 rpm. Surface, mechanical and electrochemical properties of the electrodeposits were evaluated at those varying deposition temperatures of 15 ^oC, 30 ^oC, 45 ^oC, and 60 ^oC (±2 ^oC at each temperature).

Table 5 – Electrolyte bath composition for electrodeposition

Chemicals	**gL^{-1}**
$CrSO_4.6H_2O$	95-110
$CrCl_2.6H_2O$	15-20
H_3BO_3	30-40
Surfactant (SDS)	0.4
Graphene	0.2

Before the electrodeposition process was carried out, the low-carbon steel samples were prepared for the process by grinding them with emery papers of varying grit sizes, #240, #320, #600, and #1200, in order to get uniform, smooth and bright

substrate surfaces. Subsequently, chemical cleaning with 10% concentrated hydrochloric acid 5% sulfuric acid to get rid of surface impurities, oil, dust, and oxide layers.

The setup of the experimental process comprises of two chromium anode plates, with dimensions 70 × 40 × 1 mm situated at both ends of the bath electrolyte solution. The carbon steel substrate cathode was positioned between these two anodes. To improve the dispersion of graphene sheets in the electrolyte bath during electrodeposition, a surfactant, sodium dodecyl sulfate (SDS) was added. The adsorption of sodium dodecyl sulfate onto graphene sheets induced electrostatic repulsion between the layers, which resulted in enhanced dispersion of graphene.

3.1.4 Characterization methods

Once the electrodeposition was completed, rinsing with deionized water and subsequent drying was carried out of the coatings. The microhardness values of the four composite coatings were measured by using HSX-1000A microhardness testing equipment, applying a weight of 200 grams for a duration of 12 seconds. For each coating, measurements were taken for a frequency of five uniformly distributed areas, and the average microhardness values were recorded for analysis.

The surface morphology of each coating was examined using a scanning electron microscope (SEM), while elemental composition analysis was conducted using an energy dispersive X-ray spectroscopy (EDAX spectrometer), while thickness was measured using a TT230 coating thickness gauge. Grain sizes and structural phase analysis measurements of the composition coatings were performed using a Rigaku Miniflex 600 X-ray diffractometer. The test conditions for this measurement were Cu Kα radiation, tube voltage of 40 kV, tube current of 200 mA, sampling width of 0.02^0, scanning range of 20-90^o, with a scanning speed of 10^o per minute. Surface roughness was analyzed using INTEGRA Therma atomic force microscope (AFM).

Electrochemical tests were carried out using a CS350 electrochemical workstation in a conventional three-electrode setup. The composite coated low carbon steel, with an exposed surface are of approximately 1 centimeters squared, was the working electrode while a saturated calomel electrode and platinum electrode served as the reference electrode and auxiliary electrodes respectively. Measurements of polarization curves for corrosion resistance properties were carried out in a standard 3.5% sodium chloride solution, with parameters 0.3 V scanning start potential, relative to the open circuit potential (OCP), 0.5 V end scanning potential with a scan rate of 1 mV/s. EIS measurements were also conducted by immersing the composite coated samples in a 3.5% sodium chloride solution for stabilizing the OCP, over a frequency range of 0.01 Hz-100 kHz with a 10 mV alternate current potential signal relative to the OCP.

3.1.5 Characterization of graphene

Figures 17 and 18 below present the scanning electron microscopy images of the prepared graphene sheets and the X-ray diffraction patterns of graphene oxide and reduced graphene oxide, respectively. Graphene oxide sheet's characteristic carbon peak (001) appears at 10^o, corresponding to d-spacing (interlayer spacing) of 0.8 nm.

After reducing graphene oxide into graphene, the characteristic peak (001) is no longer, and a new peak (002) appears at 2θ = 25.4°, with a corresponding d-spacing of approximately 0.4 nm. This observation aligns with previous investigations and confirms the expected structural arrangement of graphene layers [150, 151].

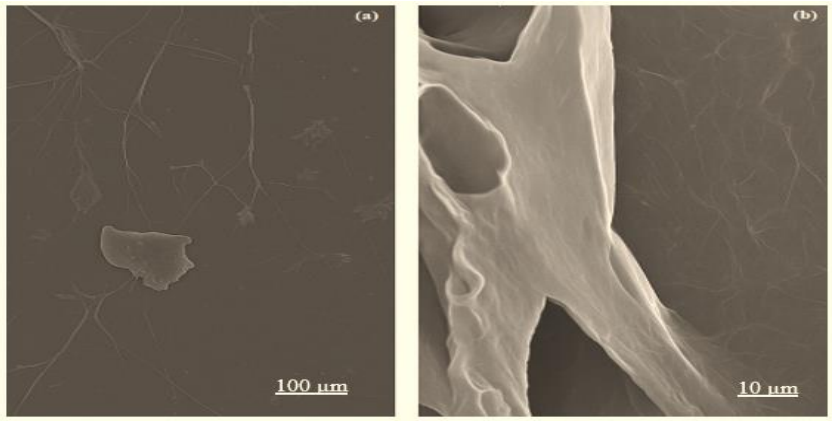


Figure 17 – SEM images of graphene oxide sheets

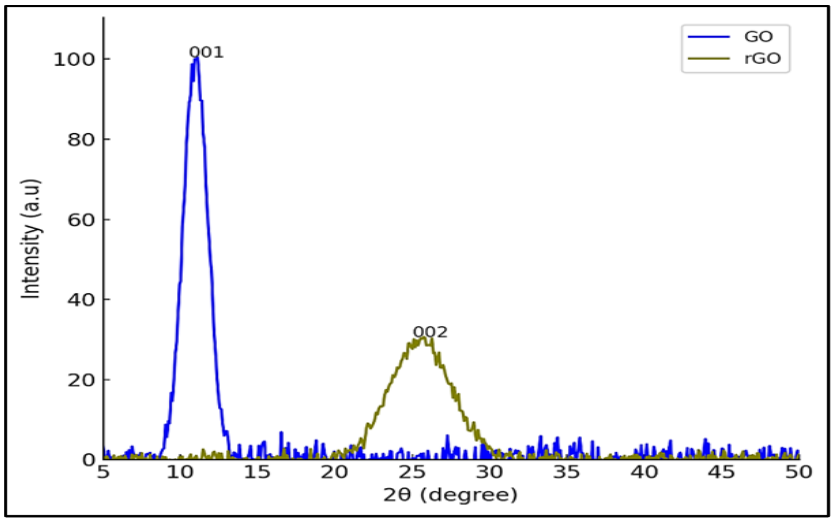


Figure 18 – X-ray diffraction patters of synthesized graphene oxide and graphene

Figure 19 further outlines the structural transformation of graphene oxide to graphene during the chemical reduction process. It is revealed by Raman spectroscopy analysis that graphene shows the presence of a D peak at approximately 1350/cm and a G peak at approximately 1590/cm. This confirms distortions of lattice [152]. The intensity ratio (ID/IG) is ~0.8 for graphene oxide and ~0.9 for graphene, which indicates a reduction in the average sizes of sp^2 domains, and an increase in the edge defects because of the partial reduction of carbon-carbon double bonds in graphene oxide [153].

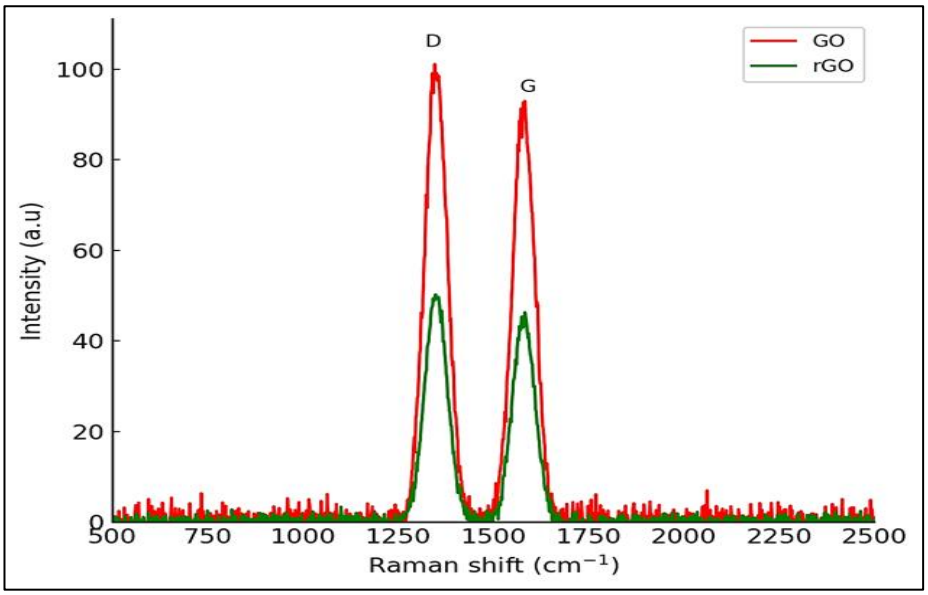


Figure 19 – Raman spectras of graphene oxide and graphene for electrochemical deposition process

3.1.6 Effect of varying deposition temperature on surface morphology and carbon content of coatings

The electrochemically deposited chromium-graphene composite coatings showed strong adhesion and stability towards the substrate surface. Figure 20 below presents the coating surface morphologies prepared at four different deposition temperatures with the electrolyte bath presented in Table 5.

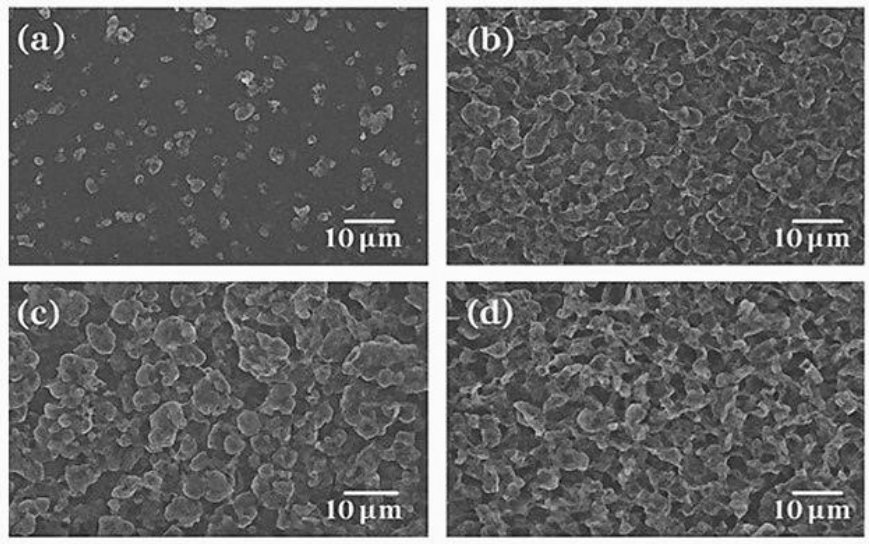


Figure 20 – SEM images of chromium-graphene composition coatings prepared at varying deposition temperatures: a) 15 ± 2 ºC, b) 30 ± 2 ºC, c) 45 ± 2 ºC, and d) 60 ± 2 ºC

From the SEM images, it is revealed that deposition bath temperature has a significant effect on the surface morphology of chromium-graphene composite coatings on low-carbon steel. When the deposition temperature rises from 15 ºC to 45

ºC (±2 ºC), the coatings became progressively coarser, more compact, and established a spherical morphology, as shown in Figures 20a-c. But, at a deposition temperature of 60 ºC, the compactness of the composite coatings diminished, and degradation started to occur. This phenomenon is probably attributed to the formation of cracks and voids on the coating at elevated temperatures, which could compromise the structural integrity of the deposited composite coatings.

The SEM images showed that the coarseness of the composite coatings increase as the deposition temperature increases, reaching its peak at 45 ± 2 ºC. But, increasing the deposition temperature beyond this level to 60 ± 2 ºC didn't result in any significant change in surface roughness. Scanning electron micrographs showed an increasing trend in terms of uniform distribution of graphene sheets, with the substrate being fully covered and well deposited by the composite coatings, with absence of surface cracks at a deposition temperature of 45 ± 2 ºC. This effect is likely because of grain growth and evolution of phase structure of the coatings. The composite coatings showed to be comprised of two morphological structures of distinct nature: spherical and flakelike structures, both of which increased upon increment of deposition temperature to 45 ± 2 ºC. On the other hand, at a deposition temperature of higher magnitude, 60 ± 2 ºC, the composite coatings showed predominant flakelike structures.

Atomic force microscopy was used to investigate the surface-roughness of the composite chromium-graphene coatings. Figure 21 and Table 6 show the AFM images and the corresponding surface-roughness values, respectively. Table 6 indicates that surface-roughness increases as the deposition temperature increases up to 45 ± 2 ºC, and remains nearly intact beyond this temperature. This plateau in surface-roughness is highly likely because of the stabilization of incorporated carbon content in the composite coating beyond the peak depositing temperature of 45 ± 2 ºC.

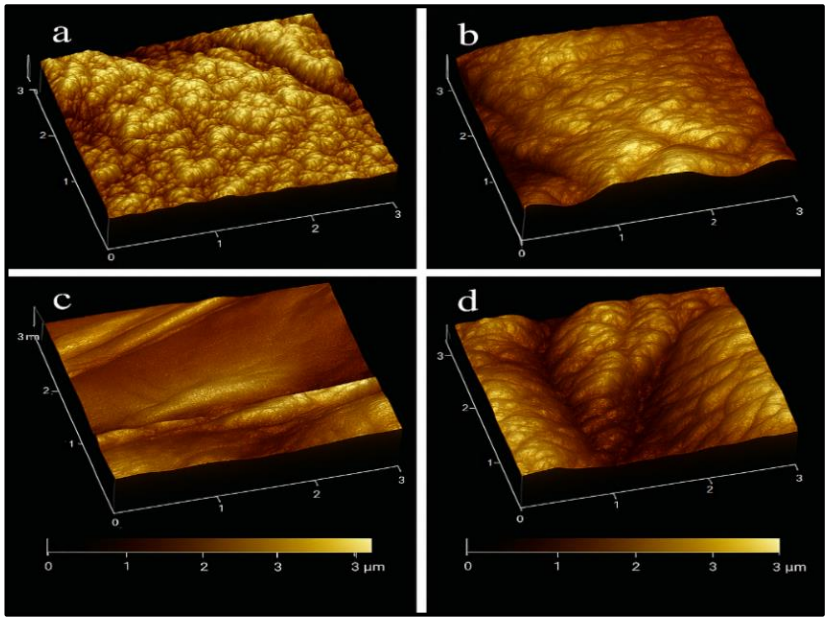


Figure 21 – AFM images chromium-graphene composite coatings prepared at varying deposition temperatures: a) 15 ± 2 ºC, b) 30 ± 2 ºC, c) 45 ± 2 ºC, d) 60 ± 2 ºC

Table 6 – Surface-roughness values of chromium-graphene composite coatings prepared at varying deposition temperatures

Deposition temp., °C	Average roughness (R_a), nm	Root mean square roughness (R_q), nm
15 ± 2	34.2	47.7
30 ± 2	91.1	113
45 ± 2	128	199
60 ± 2	151	184

Analysis using EDS (Energy Dispersive Spectroscopy) was carried out to confirm the elemental composition of the electrochemically deposited chromium-graphene composite coatings, presented in Figure 22, showing composition analysis and EDS spectra of the composite coatings obtained at varying deposition temperatures. The results revealed the presence of both elemental chromium and carbon (graphene) which confirms the successful incorporation of graphene sheets during the electrodeposition process into the chromium metal matrix. Furthermore, the analysis showed that the content of graphene in the composite coatings increased with increasing bath deposition temperature, reaching its peak amount of 19.06 wt.% at a deposition temperature of 45 ± 2 °C. This increasing trend is highly likely because of enhanced reduction of chromium metal ions, which in turn facilitates the incorporation of graphene sheets within the chromium metal matrix.

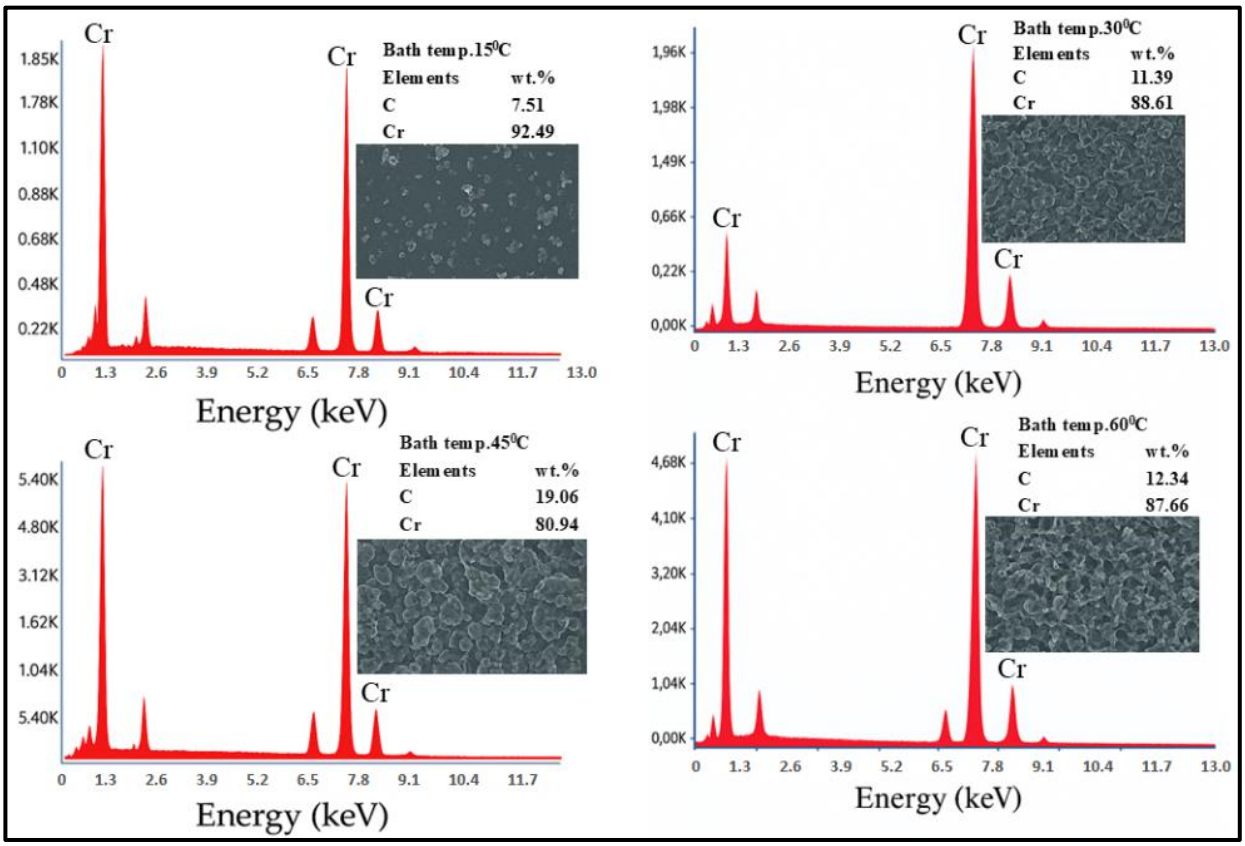


Figure 22 – EDS results of chromium-graphene composite coatings prepared at varying deposition temperatures

Due to the fact that graphene is highly conductive in nature, chromium metal ions are more likely to adsorb onto its surface. This results in the formation of graphene-rich bulges on the surface of the coating. Conversely, when the deposition temperature was increased to 60 ± 2 °C, the content of carbon decreased to 12.34 wt.%. This decline in carbon content is highly probably because of the rapid movement of chromium metal ions dissolved at the anode, leaving not enough duration for their adsorption onto the surface of the graphene sheets. Furthermore, at higher temperatures, graphene nanosheets are known to tend to agglomerate, resulting in further hindrance of their incorporation onto the composite coatings.

Investigation of the cross-section of the chromium-graphene composite coatings was conducted using SEM, as shown in Figure 23. Figure 24 presents the effect of deposition temperature on coating thickness. The results showed that when the deposition temperature increases, so does coating thickness.

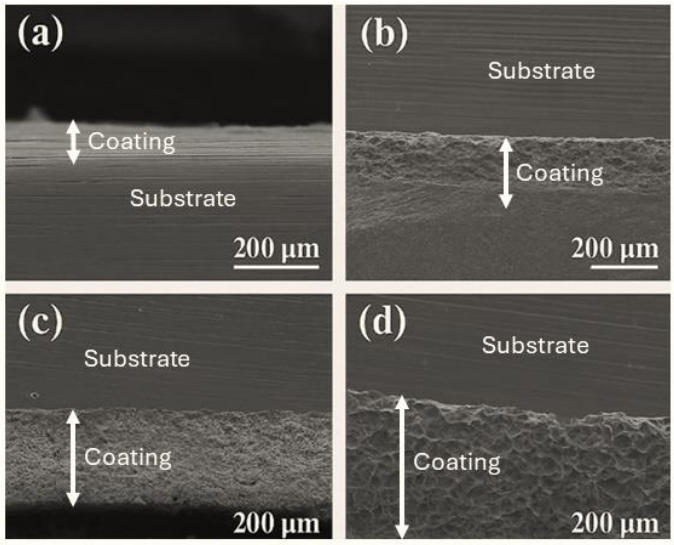


Figure 23 – SEM cross-sectional micrographs of chromium-graphene composite coatings prepared at varying deposition temperatures: a) 15 ± 2 °C, b) 30 ± 2 °C, c) 45 ± 2 °C, d) 60 ± 2 °C

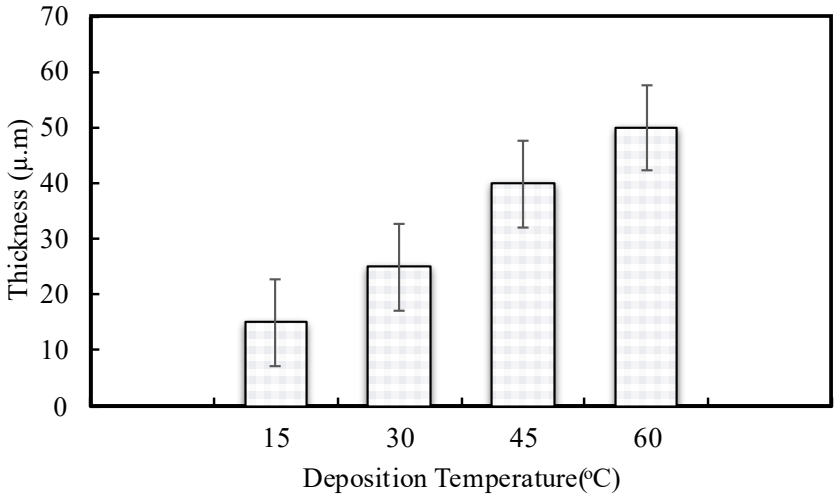


Figure 24 – Effect of varying deposition temperature on the coating thickness of chromium-graphene composite coatings

3.1.7 Gran sizes and microhardness

The X-ray diffraction patterns of chromium-graphene composite coatings prepared at varying deposition temperatures are presented in Figure 25 below. It is evident that the peak width of the coatings obtained at a temperature of 45 ± 2 ºC is found to be broader than those obtained at lower deposition temperatures of 15 ± 2 ºC and 30 ± 2 ºC and higher deposition temperature of 60 ± 2 ºC. Generally, the successful incorporation of graphene nanosheets improves the preferred orientation at (200) with increasing deposition temperature. This is because of the higher carbon (graphene) content in the composite coatings, which intensifies the (200) peak. But, as the deposition temperature increases to 60 ± 2 ºC, the (200) peak further increases. This is because of the rapid reduction of chromium metal ions at elevated deposition temperatures and improved crystal growth along both of the (111) and (200) planes. Though nucleation predominantly happens around graphene nanosheets, not all grains in the composite coatings are affected by graphene sheets at higher temperatures. This can be explained by the fact that there exists a higher peak intensity of (200) compared to (111). These results show that the incorporation of graphene into chromium metal matrix deposition significantly changes the crystal structure, preferred orientation, and growth behavior which is consistent with previous investigations [154-156].

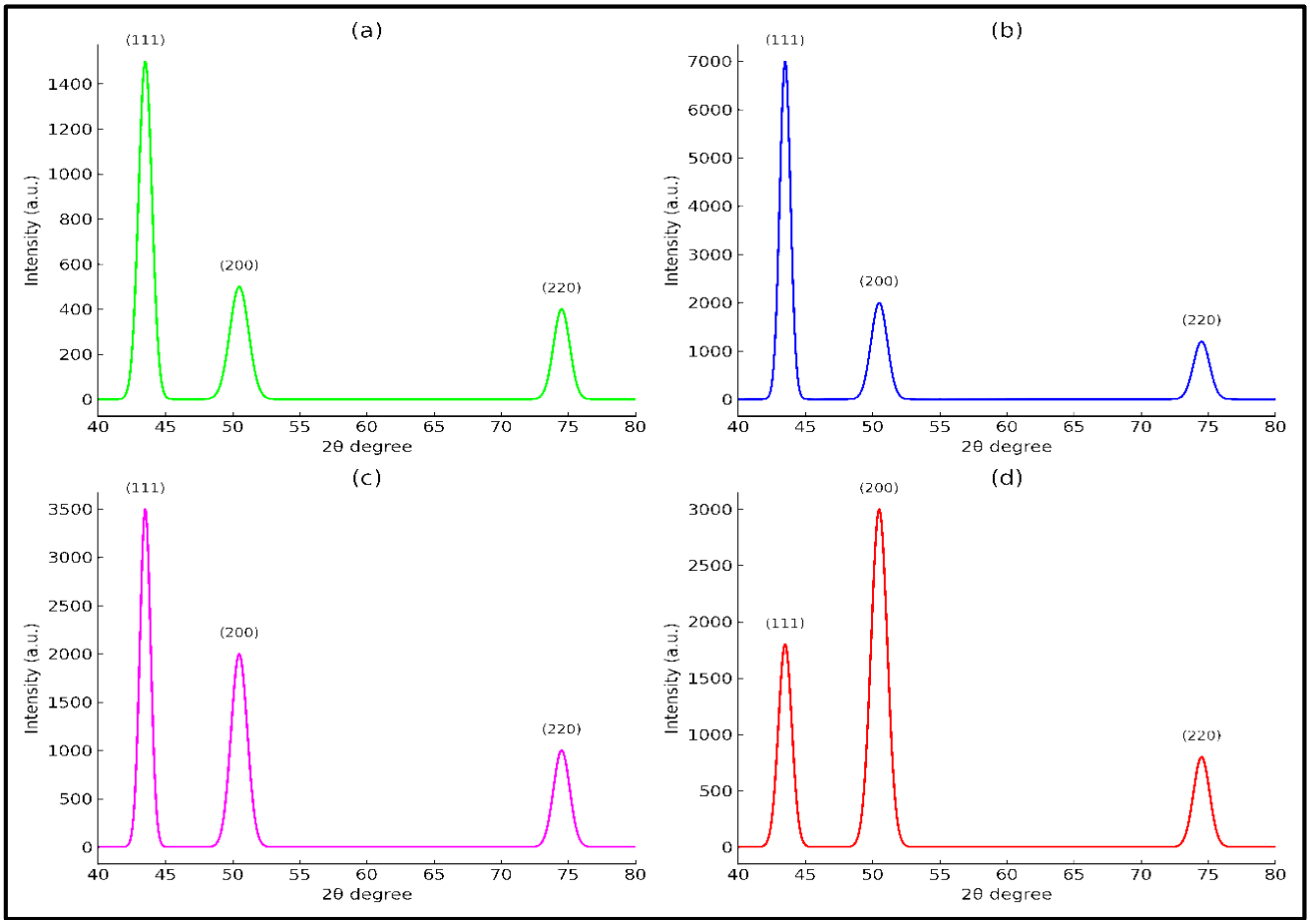


Figure 25 – X-ray diffraction patterns of chromium-graphene composite coatings prepared at varying deposition temperatures: a) 15 ± 2 ºC, b) 30 ± 2 ºC, c) 45 ± 2 ºC, d) 60 ± 2 ºC

This phenomenon is attributed to the reduction in grain sizes of the chromium metal matrix, as the capture of graphene sheets into the metal matrix deters chromium crystal growth. The average grain sizes of the four deposited composite coatings were calculated by using Scherrer's equation. The corresponding equation parameters are provided in Table 7.

$$D = K\lambda/\beta \cos\theta$$

Where D is the average crystallite size, K is the Scherrer constant, λ is the wavelength, β is the full width half maxima (FWHM), and θ is the diffraction angle.

Table 7 – Scherrer's equation parameters for chromium-graphene composite coatings obtained at varying deposition temperatures

Bath temperature, °C	2θ	hkl plane	FWHM	Average D, nm
15 ± 2	21.93	(111)	0.2197	26
	25.95	(200)	0.3271	
	37.89	(220)	0.1987	
30 ± 2	21.95	(111)	0.2879	25
	25.98	(200)	0.3468	
	38.26	(220)	0.4758	
45 ± 2	22.17	(111)	0.2298	19
	25.74	(200)	0.3973	
	38.32	(220)	0.5246	
60 ± 2	22.35	(111)	0.2938	28
	26.43	(200)	0.3832	
	38.52	(220)	0.4265	

Effect of deposition temperature on the grain sizes of the four deposited chromium-graphene composite coatings is presented in Figure 26. The incorporation of graphene sheets into the chromium metal matrix facilitated grain refinement because graphene hinders chromium crystal growth and increases nucleation sites [143]. It was found that grain sizes decreased as the deposition temperature increases, reaching a minimum grain size at a deposition temperature of 45 ± 2 °C, before increasing as the temperature rose to 60 ± 2 °C.

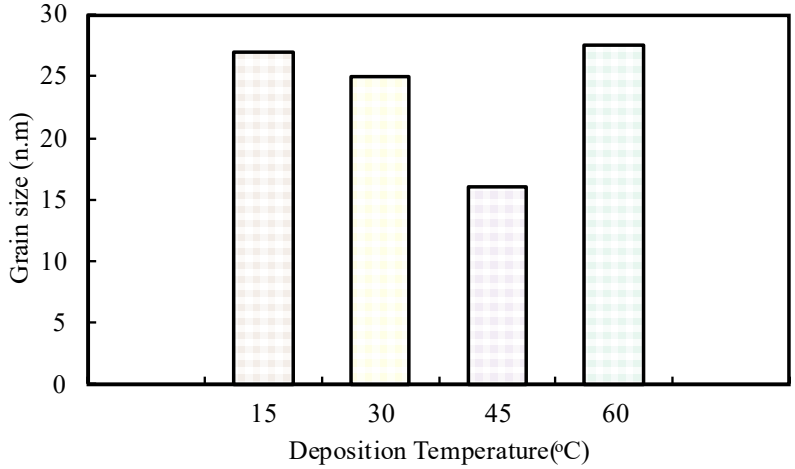


Figure 26 – Effect of varying deposition temperature on the grain sizes of chromium-graphene composite coatings

For this trend, two possible explanations can be presented. Firstly, the nucleation process tends to be slow at lower deposition temperatures which provides fewer chromium metal matrix nucleation sites for the incorporation of graphene. Secondly, at an elevated temperature of 60 ± 2 °C, the chromium reduction reaction occurs rapidly, resulting in less graphene being incorporated into the chromium metal matrix and increased graphene agglomeration, as discussed earlier. These findings show that reduction in grain size is associated with the maximum amount of graphene incorporation (carbon content) at the optimal deposition temperature. It is necessary to do further investigations to find out the optimal deposition temperature that allows for the maximum graphene incorporation (that produces the highest carbon content in terms of wt.%). Here, the bath deposition temperature of 45 ± 2 °C was identified as the optimal one, because it yielded the highest carbon concentration in the chromium-graphene composite coatings.

Figure 27 below illustrates the influence of varying deposition temperature on the microhardness values of the four chromium-graphene composite coatings. Vickers microhardness of these composite coatings was found to increase linearly with the deposition temperature up to 45 ± 2 °C, then happens to decrease when the temperature was increased to 60 ± 2 °C. The peak microhardness values were recorded at 45 ± 2 °C. This observed variation in microhardness values follows an exactly similar trend to that of graphene content as a function of deposition temperature. Previous reports noted that when graphene nanosheets are present within metal matrix, they result in inhibition of dislocation motion and restrict plastic deformation, which contributes to improved hardness values [143]. Moreover, graphene sheets act as a reinforcing phase because of their fine size and characteristically excellent mechanical properties further help strengthen the composites [147]. This enhancement in microhardness is primarily attributed to the reinforcing and strengthening effect of fine graphene nanosheets incorporated in the composite coatings.

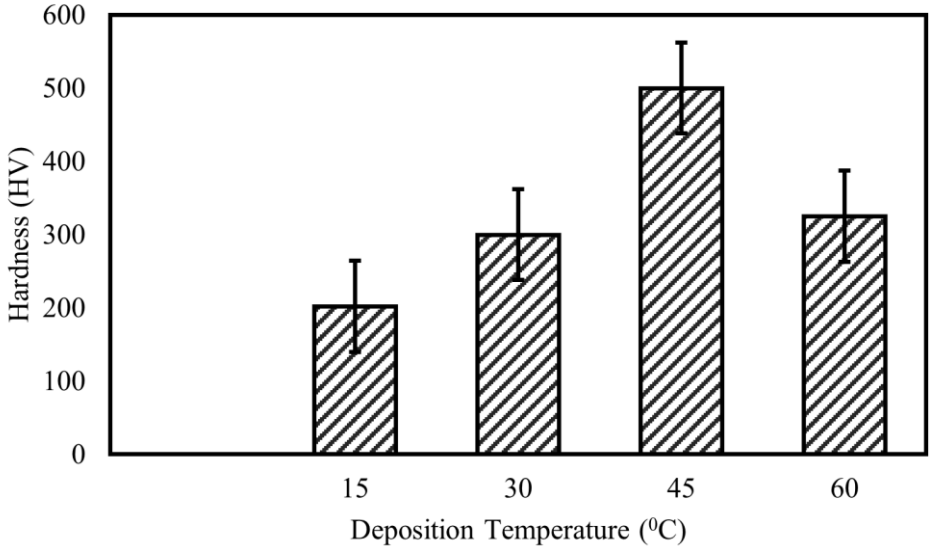


Figure 27 – Vickers microhardness values of chromium-graphene composite coating prepared under varying deposition temperatures

3.1.8. Effect of varying deposition temperature on the corrosion resistance properties

Presented in Figure 28 and Table 8 below are the polarization curves of the four chromium-graphene composite coating prepared at varying deposition temperatures of 15 ºC, 30 ºC, 45 ºC, and 60 ºC (± 2 ºC), and the corresponding current densities (I_{corr}) and corrosion potentials (E_{corr}) (which are determined and summarized from the polarization curves), respectively.

The results reveal that the chromium-graphene composite coatings deposited at 45 ± 2 ºC show lower corrosion current densities and higher corrosion potentials when compared to those coatings prepared at lower deposition temperatures of 15 ± 2 ºC and 30 ± 2 ºC. On the other hand, corrosion resistance happens to diminish significantly when the deposition temperature is set at 60 ± 2 ºC. This suggests that excessive (higher) deposition temperature negatively influences the corrosion protective properties of the chromium-graphene composite coatings.

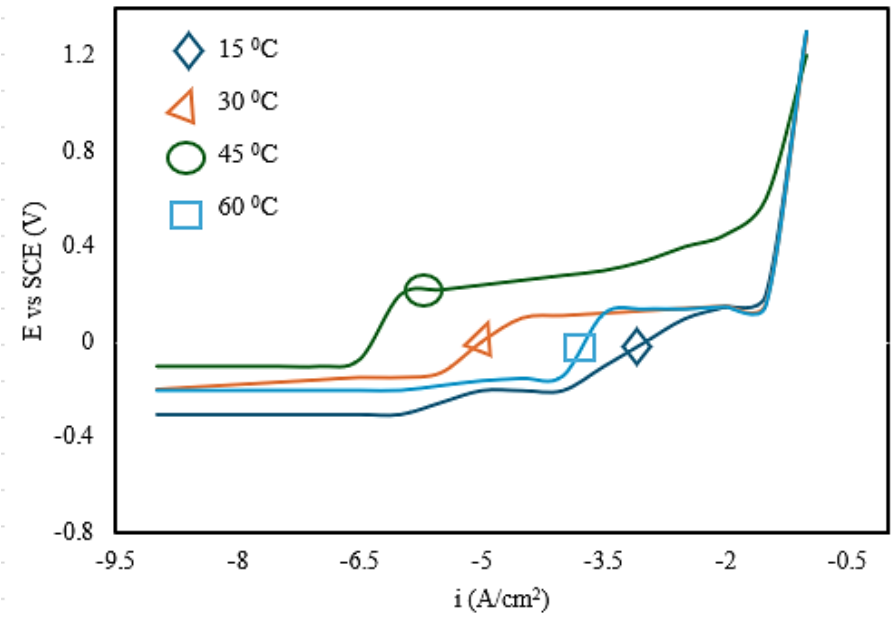


Figure 28 – Effect of varying deposition temperature on the corrosion polarization curves of chromium-graphene composite coatings in 3.5% NaCl solution

Table 8 - Effect of varying deposition temperature on the corrosion current densities and corrosion potentials of chromium-graphene composite coatings

Deposition temperature, (±2 ºC)	**15**	**30**	**45**	**60**
I_{corr} (A/cm$^{2)}$	3.87×10^{-6}	1.474×10^{-6}	2.766×10^{-7}	1.692×10^{-6}
E_{corr} (V)	-0.253	-0.193	-0.119	-0.198

This variation in corrosion resistance at different deposition temperatures is a result of several factors. The enhanced corrosion resistance properties of the composite coatings at the optimal temperature of 45 ± 2 ºC is mainly because of the uniform dispersion of graphene sheets. This again efficiently fills micro-sized pores, crevices, and gaps in the chromium metal matrix. Moreover, the homogeneous distribution

graphene sheets during electrodeposition process and its characteristic inert physical barrier properties help further improve corrosion resistance properties. Nevertheless, when the deposition temperature is set at 60 ºC, corrosion resistance values diminish because of the formation of fine cracks on the surface of the coating. Additionally, hydrogen atoms adsorbed on the surface of the coating tend to diffuse into the deposited coating, which results in residual stress buildup, which in turn adversely influences corrosion resistance property [157-160].

For the purpose of further investigation of corrosion resistance properties, EIS (electrochemical impedance spectroscopy) tests were carried out in a 3.5% NaCl solution. Presented in Figure 29 below is the Nyquist plots of chromium-graphene composite coatings prepared at varying deposition temperatures of 15 ºC, 30 ºC, 45 ºC, and 60 ºC (± 2 ºC). The composite coatings obtained at a deposition temperature of 45 ± 2 ºC showed the highest impedance, which indicates the highest corrosion resistance. In contrast, chromium-graphene composite coatings prepared at lower of higher deposition temperatures showed narrower semi-circles in the Nyquist plots. Since the diameter of the semi-circle determines the corrosion resistance performance, in such a way that larger diameter indicates better corrosion resistance, the results approve that chromium-graphene composite coatings deposited at 45 ± 2 ºC possess the highest of all impedances which aligns with the best corrosion protection.

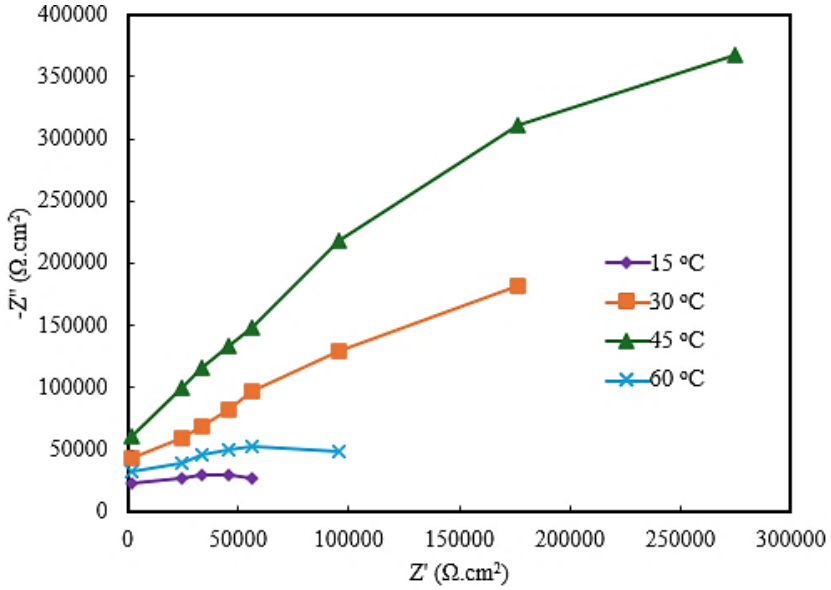


Figure 29 – Effect of varying deposition temperature on the impedance spectra of chromium-graphene composite coatings

Furthermore, for comparison purposes, pure graphene and pure chromium metal coatings were prepared using the same electrodeposition method at 45 ºC, presented in Figure 30. The results revealed that both pure graphene and pure chromium metal electrodeposited coatings showed inferior corrosion resistance properties when compared to chromium-graphene composite coatings. In order to investigate the long-term performance, further EIS tests were also carried out for the chromium-graphene composite coatings obtained at the optimal deposition temperature of 45 ± 2 ºC, with impedance test results illustrated in Figure 31.

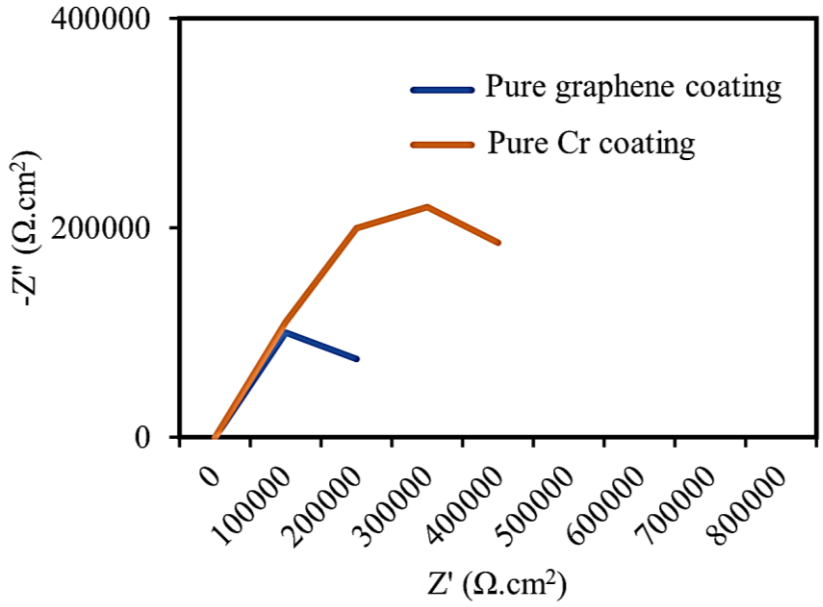


Figure 30 – Impedance spectra of pure chromium and pure graphene coatings obtained at 45 ºC in 3.5% NaCl solution

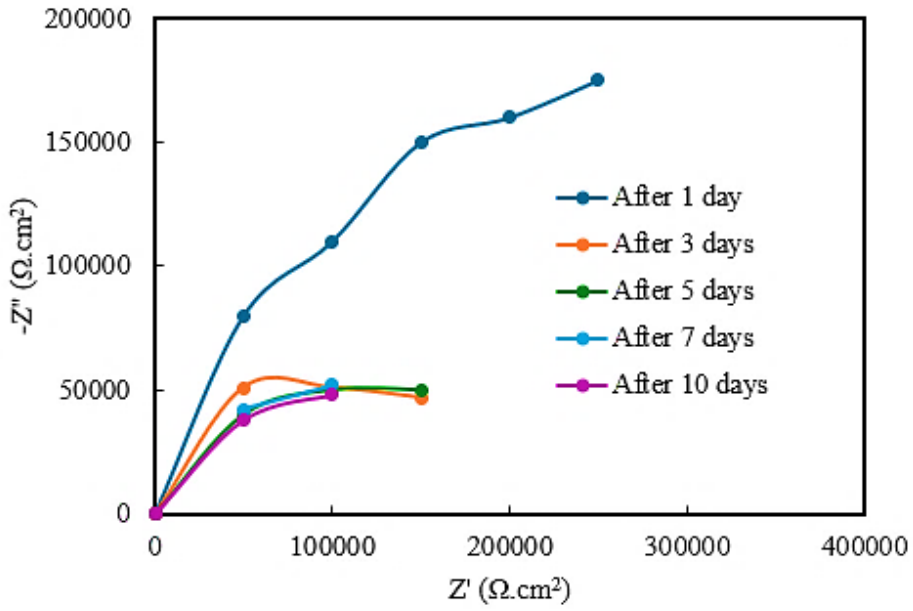


Figure 31 – Impedance spectra of chromium-graphene composite coatings obtained at 45 ± 2 ºC deposition temperature with different immersion times in 3.5% NaCl solution

3.1.9 Summary

In this part of the dissertation, chromium-graphene composite coatings were electrodeposited on low-carbon steel at varying deposition temperatures of 15 ºC, 30 ºC, 45 ºC and 60 ºC (±2 ºC) and the result morphological, mechanical and corrosion resistance properties were investigated. The results revealed that electrodeposition temperature has a significant influence on the surface morphology, coating thickness and elemental composition of the composite coatings. Surface roughness and carbon

content were found to increase when the deposition temperature increases, reaching their peak values at 45 ± 2 °C. Beyond this temperature, carbon content in the coatings diminished while surface roughness remains nearly unchanged. Moreover, it was revealed that thickness of the composite coatings increased linearly with increasing deposition temperature. X-ray diffraction analysis also showed that the incorporation of graphene sheets into chromium metal matrix improved the preferred orientation along the (200) plane while contributing grain refinement. Grain sizes, Vickers microhardness values, and corrosion resistance properties of the composite coatings followed the exact same trend as the carbon content, reaching their peak measurements at the optimal deposition temperature of 45 ± 2 °C. These results altogether illustrate that incorporation of graphene sheets into chromium composite coatings help enhance desired functional surface properties such as roughness, and results in a significant improvement in mechanical and corrosion resistance properties. These findings make chromium-graphene composite coatings more durable and functional.

3.2 Characterization of microstructural and surface properties of nickel-copper coatings electrodeposited at high current density on AISI304 substrate

Electrodeposition is a versatile method for producing metal coatings at ambient temperature and pressure, with benefits of low cost and high rate of deposition using the mechanism of electrolysis [137–139]. By adjusting bath chemistry and operating chemistry, it is possible to tailor deposit characteristics, such as grain size, morphology, roughness, hardness, thickness, etc. [161]. Nickel is one of the most widely used plating metals, and electrodeposited nickel exhibits unique combination of properties such as high corrosion resistance, good wear resistance and enhanced hardness properties [135,162–165]. As a result, Ni coatings are employed in diverse industries of automotive, aerospace, electronics, oil, and gas, etc. to enhance component durability and appearance [166–170]. Key benefits of nickel electrodeposition include improving corrosion durability by forming protective nickel layers [171,172], increased surface hardness and wear life of substrates [173], and bright and lustrous finish which adhere to the substrate often serving as an undercoat for further plating [174,175].

AISI304 steel is the most widely used austenitic stainless steel, which its popularity arises from good balance of corrosion resistance, mechanical strength and formability, making it common in food processing chemical, and structural applications [176,177]. However, as a soft stainless alloy, it has moderate hardness, typically ~200-215 HV in annealed form and only fair wear resistance. In demanding conditions, this can lead to surface wear or galling. Consequently, applying hard coatings, such as Ni onto 304 steel is industrially relevant, as nickel layers can impart additional hardness and wear protection to extend component life. Electrodeposition parameters strongly influence deposit structure. Current density particularly governs nucleation and growth rates, altering surface morphology. Studies consistently report that Ni deposit morphologies change with electrodeposition current in such a way that at lower current densities, coarse nodular grains and deep surface crevices form, whereas higher currents produce finer, pyramidal grains. For example, Banovic et al. found that Ni deposits from a Watts bath plated below ~0.01 A/cm^2 showed a laminar morphology with large, deep crevices, while above this threshold the surface consisted of truncated pyramidal crystals whose planar size increased with current [178]. In other words, as current density increases, columnar grain widths and terrace sizes tend to grow. More recent work [179] confirms that varying the deposition current density significantly alters the Ni grain size and orientation. In practice, this means that higher currents generally yield denser, more uniform Ni coatings, up to a point, whereas too low current densities can lead to very rough, porous deposits. These microstructural changes affect coating thickness uniformity and defect levels on the 304 substrates.

The variations in morphology translate into changes in mechanical performance. In terms of hardness, electrodeposited Ni hardness typically increases with current density because finer grains impede dislocation motion (Hall-Petch effect) [178]. In other words, faster plating tends to refine the microstructure and harden the deposit. However, multiple studies indicate an optimal current range. For example, Ni-TiO_2 composite coatings showed increased hardness values as current density increased from 2 to 5 A/dm^2, but hardness declined at higher currents [137]. Similarly, another

study noted that a current density of 5 A/dm^2 produces higher microhardness values [165]. Thus, there is a typical peak in hardness, and related wear resistance, at some intermediate current density. Higher hardness from Ni electrodeposits usually yields better wear performance. Wear tests of Ni-based coatings often show that optimally plated samples, with fine microstructure, have significantly lower wear rates than poorly plated ones. For instance, Ni composite coatings investigated under varying current densities exhibited maximum resistance to wear at the same current density that yielded maximum hardness. In general, thicker, defect-free Ni layers resist abrasion much more effectively than uncoated 304 substrate. Furthermore, a critical requirement for any coating is adhesion to the substrate. In this regard, Ni bonds especially well to stainless steel. Recent mesoscale mechanical testing showed that electrodeposited Ni on 304 stainless steel can achieve an interfacial strength close to the yield strength of the substrate material. In fact, for a standard Watts Ni plating bath, the Ni/304 interface was so strong that failure occurred in the nickel layer rather than at the interface [180]. This demonstrates that, under proper plating conditions, Ni coatings adhere robustly to AISI 304, ensuring that enhancements in hardness and wear resistance are not compromised by delamination.

Despite extensive studies of Ni electrodeposition, the specific case of Ni electrodeposited on AISI 304 steel under different current densities remains under-explored. Most literature on current density effects deals with Ni on generic substrates or Ni-composite coatings on hard substrates. For instance, recent work has examined Ni-WC-TiC composite coatings on 304 stainless steel, finding that a 40 mA/cm^2 deposition current produced the densest microstructure [181]. However, analogous systematic data for pure Ni coatings on 304 stainless steel are scarce. In particular, the interplay between current density, coating morphology, hardness, and wear on austenitic stainless steel has not been fully established. To address these gaps, this study focuses on DC electrodeposition of pure Ni on AISI 304 stainless steel and investigates outcomes on microstructural and surface morphology (grain structure, roughness) changes. The findings will guide the tailoring of Ni electrodeposition processes for stainless steel components in applications demanding enhanced surface durability.

3.2.1 Substrate preparation

AISI 304 stainless steel sheets were cut into specimens of 30 x 15 x 4 mm dimensions. The surfaces were ground sequentially with silicon carbide papers up to 1200 grit and then polished to a mirror finish. The samples were ultrasonically degreased in acetone, rinsed thoroughly in deionized water and dried. Prior to plating, the polished sample substrates were acid-etched to remove the passive oxide film, using an HCl based pickling system, with a mixture of HCl and H_2SO_4 to activate stainless steel. In practice, chromic/sulfuric/HCl mixtures (~60g/L each of CrO_3, H_2SO_4, and HCl) or nitric/HF solutions have been reported for pickling austenitic stainless steel [182].

3.2.2 Electrolyte, deposition conditions and characterization methods

The nickel-copper electrodeposition electrolyte bath was a Watt's type solution. The composition is presented in Table 9 below.

Table 9 – Electrolyte bath composition for electrodeposition

Chemicals	**gL^{-1}**
$NiSO_4.6H_2O$	240-250
$NiCl_2.6H_2O$	45
$CuSO_4.5H_2O$	2-10
H_3BO_3	35-40

During electrodeposition, nickel and copper were simultaneously reduced at the cathode according to $Ni^{2+} + 2e^- \rightarrow Ni$ and $Cu^{2+} + 2e^- \rightarrow Cu$, resulting in the formation of a substitutional Ni-Cu solid solution. Hydrogen evolution ($2H^+ + 2e^- \rightarrow H_2$) occurred as a competing cathodic reaction under acidic conditions. A pure nickel anode was employed, where anodic dissolution ($Ni \rightarrow Ni^{2+} + 2e^-$) maintained the Ni^{2+} concentration in the electrolyte. Boric acid acted as a buffering agent, stabilizing the local pH near the cathode surface and promoting uniform alloy deposition. The bath temperature was maintained at 45 ^oC and the pH was adjusted to 4 using ammonium sulfuric acid. Electrodeposition was carried out under constant direct current. Three different current densities were applied: 20, 30, 40, and 50 mA/cm^2. Each coating was deposited for a fixed duration of 30 min to achieve comparable thicknesses across conditions. The electrodeposition cell was a standard two-electrode configuration. High purity nickel plates served as the soluble anodes and the AISI 304 substrates were cathodes. A DC power supply and coulometer were used to control the current. The anode-to-cathode spacing was on the order of a few centimeters, and the solution was mildly agitated by magnetic stirring to ensure uniform ion distribution. Nickel anodes dissolve to replenish Ni2+ in the bath, while nickel ions are reduced onto the steel cathode [181,183]. All coated samples were rinsed with deionized water and ethanol after electrodeposition and dried.

The surface morphology of the Ni coatings was examined by SEM (JEOL JSM-IT810) at various magnifications. The chemical composition (Ni content and any impurities) was studied by energy-dispersive X-ray spectroscopy (EDS) attached to the SEM. SEM imaging and EDS mapping allowed visualization of grain structure, nodules and any defects on the coating. Crystallographic phases and texture were determined by Rigaku SmartLab XRD using Cu Kα radiation 40 kV, 30 mA. Data were collected over a suitable 2θ range at a step of ~0.02^o. The diffraction patterns were analyzed to identify the Ni crystal planes and any preferred orientations or secondary phases. Crystallite size and lattice parameters were evaluated using the Scherrer equation and standard XRD software. Surface roughness was analyzed using Atomic Force Microscope (AFM) and measurements were carried out on a Solver Spectrum (NT-MDT) instrument in a semi- contact (tapping) mode using NSG10 silicon tip. The scanning area for all samples was 50 × 50 μm^2. Height variation ranges from ~1 to ~2.2 μm within this area.

3.2.3 Surface morphology and elemental composition of Ni-Cu coating at 40 mA/cm^2

The surface morphology of the nickel coating electrodeposited at 40 mA/cm^2 is shown in Figure 32 below.

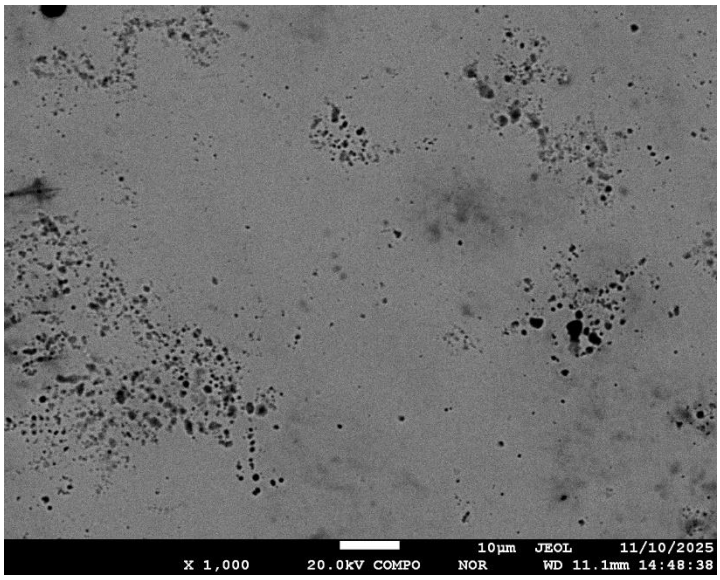


Figure 32 – Surface micrograph of nickel coating electrodeposited at 40 mA/cm^2

The SEM micrograph reveals a predominantly dense and continuous surface, characteristic of uniform nickel nucleation and growth under sufficiently high current density. This phenomenon arises from the interplay between electrochemical driving forces and mass transport dynamics during the electrodeposition process. At elevated current densities, the rate of electron transfer at the cathode interface increases, promoting a higher supersaturation of nickel ions near the substrate surface. This enhanced supersaturation significantly accelerates the nucleation rate, leading to a greater number of initial nuclei forming simultaneously across the substrate. As a result, the spatial distribution of these nuclei becomes more homogeneous, minimizing the formation of isolated growth centers that could lead to non-uniform or dendritic structures [184]. Although small clusters of fine particles and occasional darker pores are visible across the surface, these features are relatively sparse and do not disrupt overall coating continuity. Such isolated porosity is commonly observed in nickel electrodeposition, particularly when deposition proceeds rapidly and localized hydrogen evolution occurs. This phenomenon is intrinsically linked to the concurrent hydrogen evolution reaction (HER), which becomes particularly pronounced under conditions of rapid deposition. During electrodeposition, especially at high current densities, the reduction of water or H^+ ions compete with the reduction of Ni^{2+} ions at the cathode surface. This dependent HER generates gaseous hydrogen bubbles that can become entrapped within the growing metallic deposit if they do not desorb or diffuse away before being encapsulated by subsequent layers of nickel [185,186]. Nonetheless, the coating produced at 40 mA/cm2 exhibits substantially fewer defects and a more compact morphology compared to coatings obtained at lower or higher current

densities, demonstrating a more favorable balance between nucleation rate and growth kinetics.

The corresponding EDS elemental mapping (Figure 33) further confirms the homogeneity of the coating. The Ni-K map shows a uniformly distributed nickel signal across the entire scanned region, aligning with the visually compact SEM morphology. Only trace amounts of oxygen are detected, appearing in isolated clusters that may correspond to surface oxidation or adsorbed contamination, which is an expected occurrence during post deposition air exposure. Upon removal from the electrolytic bath, nickel surfaces are inherently reactive and can rapidly react with atmospheric oxygen. This reaction results in the formation of nickel oxide (NiO) or nickel hydroxide ($Ni(OH)_2$), which depends on humidity and ambient conditions. This forms a thin passive layer, which may be uneven in density due to factors like surface energy differences, grain boundaries, or surface defects, leading to isolated oxygen-rich clusters [187,188].

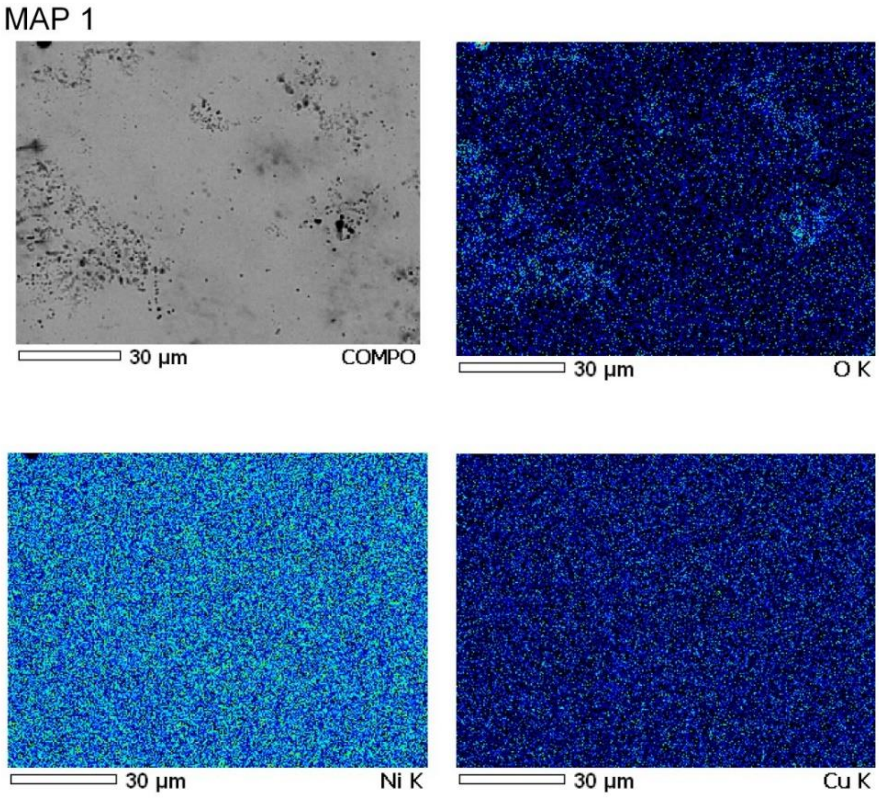


Figure 33 - EDS elemental mapping

A low but detectable Cu signal is also observed; this may originate from the underlying sample holder, minor bath impurities or scattered substrate exposure at micro-defect sites. However, the copper distribution is extremely sparse and does not indicate any significant incorporation within the coating.

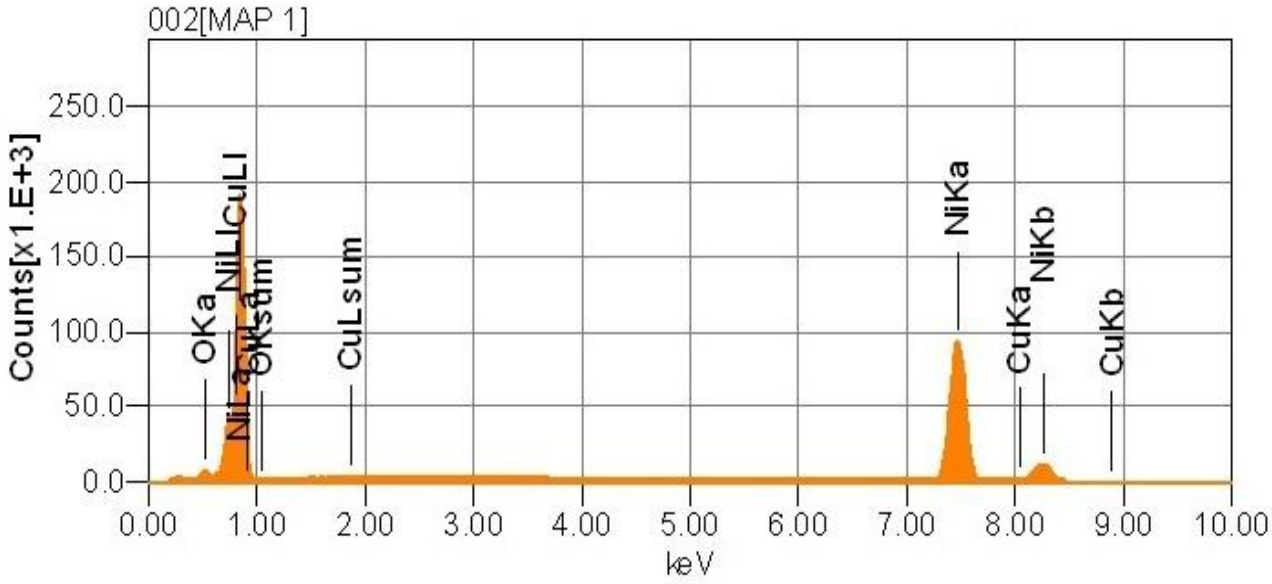


Figure 34 - EDS quantitative analysis of nickel electrodeposited coating

Quantitative EDS analysis (Figure 34) reveals that the coating consists of approximately 94.9 wt.% Ni, with only 1.6 wt.% O and 3.5wt.% Cu. The high nickel fraction supports successful deposition, while the low oxygen content confirms the coating remains largely metallic, with minimal oxide formation. The minor Cu signal (3-4 wt.%) is small enough to be attributed to superficial contamination rather than alloying, as no-copper rich clusters appear in the morphological image (Figure 32).

Overall, the SEM and EDS analyses demonstrate that the electrodeposited coating produced at 40 mA/cm^2 is both compositionally pure and morphologically compact. These characteristics suggest that this current density improves an optimal deposition environment, sufficiently high to ensure rapid nucleation and dense film growth, yet not so high as to cause severe hydrogen-induced porosity or coarse, columnar structures. In the next section, how this improved microstructural quality correlates strongly with mechanical properties and crystallographic features studied by hardness testing and XRD/AFM analyses will be discussed.

3.2.4 XRD Analysis: Phase identification and texture analysis

The XRD pattern of the Ni-Cu alloy coated AISI 304 steel is presented in Figure 35. It shows the characteristic face-centered cubic (FCC) Ni peaks, the (111) reflection near 2θ≈44.5o, the (200) near 51.8o, and the (220) near 76.4o (with the (311) reflection expected just above 90o outside the scan range). These match well with the standard Ni powder [189]. In the coating, the Ni(111) peak is by far the most intense, with the (200) and (220) peaks significantly weaker. The absence of any detectable oxide (NiO) peaks indicates that the deposit is essentially oxide free, reflecting a high purity metallic Ni layer, consistent with SEM/EDS analysis showing negligible oxygen. Comparing intensities reveals that the Ni(200)/(111) intensity ratio in the sample (~0.35 by integrated intensity) is smaller than that in the powder standard (≈0.42). This implies no strong (200) texture; instead, the (111) orientation dominates, as is common in Ni electroplating.

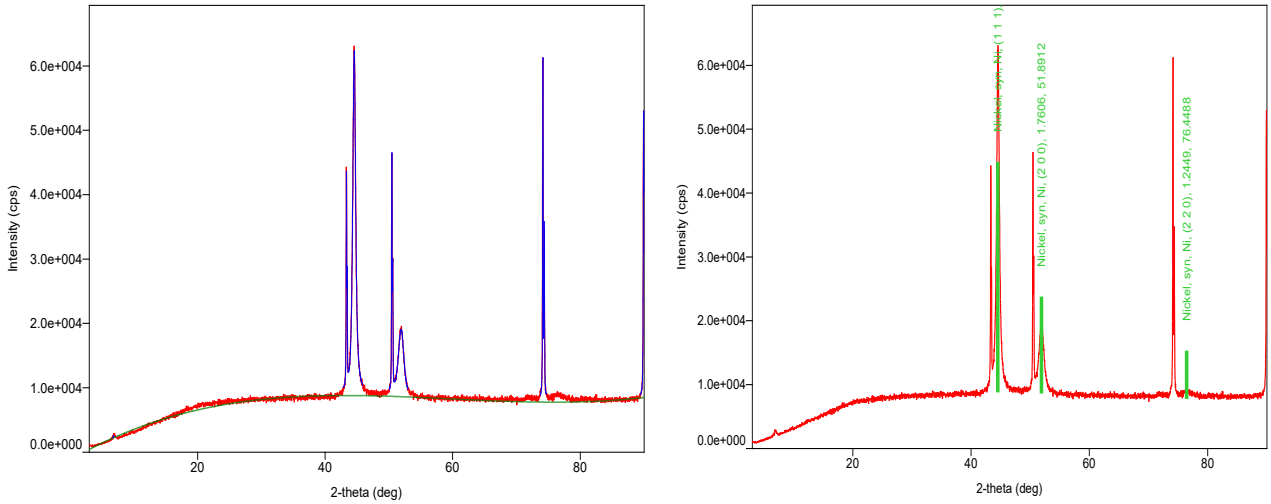


Figure 35 - XRD pattern of the Ni-Cu alloy coating

The pronounced Ni(111) orientation is consistent with the nodular densely packed grain morphology seen in SEM. Besides Ni, clear diffraction lines at 2θ≈43.35°, 50.47°, 74.14° and 89.94° were observed, matching the (111), (200), (220) and (311) reflections of fcc Cu (Figure 36), suggesting the presence of Cu arising from extrinsic sources (for example, substrate holder). Similar Cu substrate peaks have been reported at 43.7°, 50.8°, and 74.4° [190]. In contrast, no peaks of Ni oxides, which would appear around 37°, 43-47°, etc., are present, underscoring the metallic nature of the Ni coating [191].

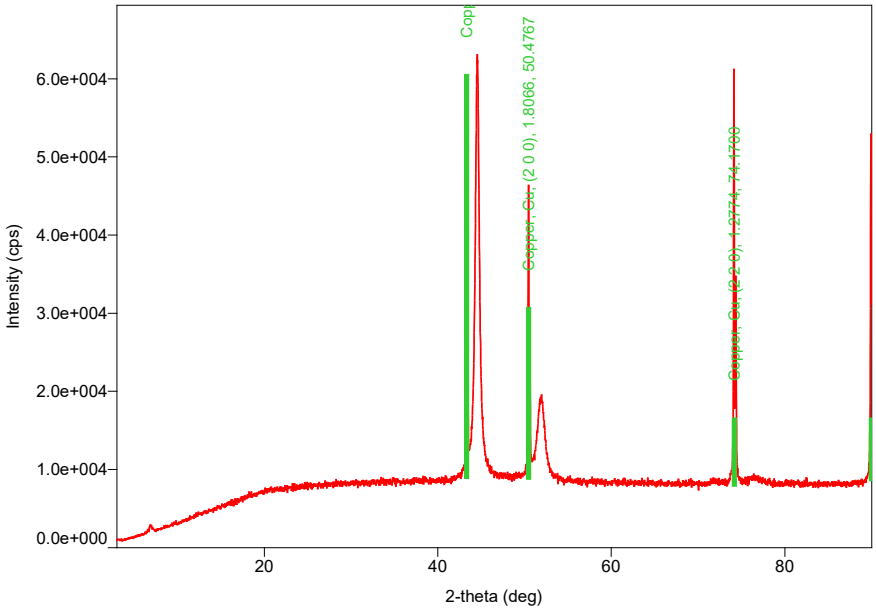


Figure 36 - XRD pattern of Cu phase

Crystallite size (Scherer analysis)

Using the most intense Ni(111) peak to estimate the average coherent diffraction domain (crystallite size), the Scherrer equation was applied [192].

$$D = \frac{K\lambda}{\beta \cos\theta}$$

Where K = 0.9 (shape factor), λ = 0.15406 nm (Cu Kα), β is the peak FWHM in radians, and θ is the Bragg angle. Substituting the measure values for Ni(111):
θ = 22.2655°

FWHM β = 0.507° = 0.00885 rad.

K = 0.90, λ = 0.15406 nm

$$D = \frac{K\lambda}{\beta\, cos\theta} = \frac{0.90 \times 0.15406}{0.00885 \times \cos\,(22.2655)} \approx 16.9\, nm$$

Therefore, the mean crystalline size estimated from the Ni(111) peak reflection is 17 nm.

The XRD results, a pure fcc Ni phase with dominant Ni(111) intensity and an estimated crystallite size of ~17 nm, align with the earlier SEM/EDS observations for the coating. SEM showed a continuous, compact nickel layer with fine nodular/columnar features and only sparse surface porosity; EDS confirmed high Ni content and negligible oxygen. A dominant (111) texture commonly correlates with compact, closely packed grain facets and tends to produce dense deposits with relatively smooth morphology at the microscale. The XRD data show no peaks corresponding to NiO, $Ni(OH)_2$, Ni_2O_3 or other oxide or hydroxide phases. In fact, past studies of freshly electrodeposited Ni find essentially no detectable NiO in XRD or XPS [191]. This pattern likewise contains only metal Ni metal reflections. This confirms that the as-deposited layer is purely metallic Ni (apart from the minor Cu), with no oxide crystalline impurities.

The small ~17 nm grain size implies an extremely high-volume fraction of grain boundaries. According to Hall- Petch strengthening, such nanocrystalline Ni should exhibit high hardness. Indeed, it is well established that hardness increases with decreasing grain size in electrodeposited Ni. The measured nanometer-scale grains therefore suggest that the coating should be significantly harder than a coarse-grained Ni film. In addition, the (111) texture tends to produce faceted pyramidal grains with flat facets; this is consistent with the observed SEM morphology. In summary, the pronounced (200) texture and nanocrystalline grain size (D = ~17 nm) correlate with a fine-grained, columnar microstructure and the expected high hardness of the Ni coating [193,194].

3.2.5 AFM surface topography analysis

Figure 37 shows the 2D height map and 3D AFM topography of the nickel-copper coating electrodeposited at 40 mA/cm^2. AFM was performed using a solver spectrum (NT-MDT) instrument in semi-contact (tapping) mode with an NSG10 silicon tip. All AFM scans were acquired over an area of 50 × 50 μm^2. The height (Z) scale across the mapped area varied from approximately 1.0 μm to 2.2 μm.

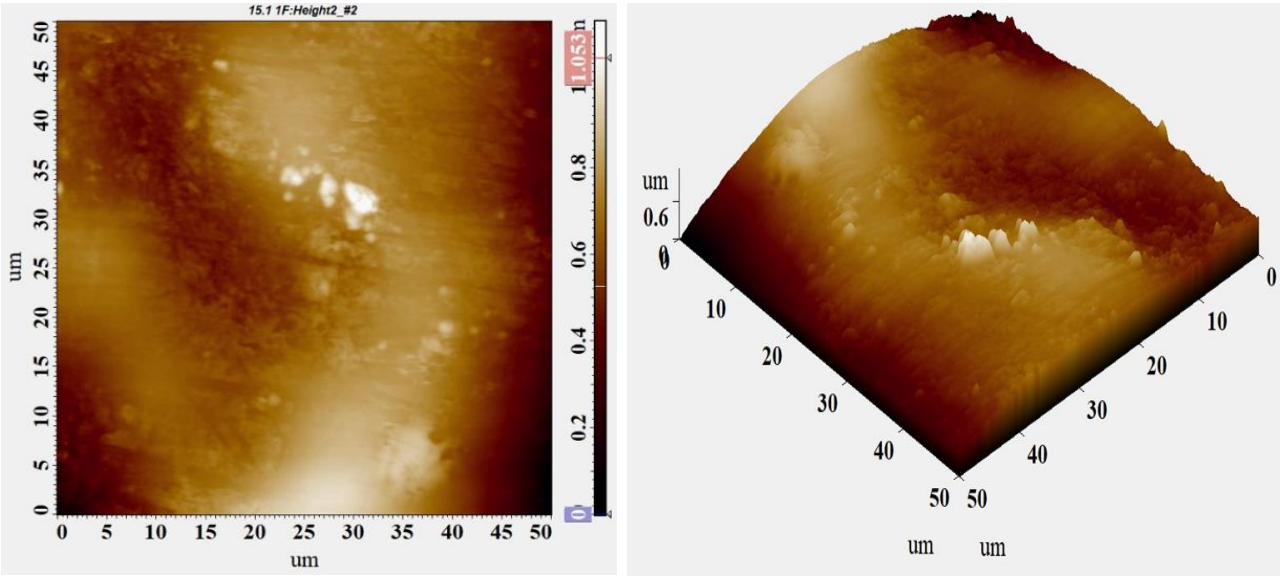


Figure 37 - AFM images a) 2D height map, and b) 3D AFM topography

The 2D height map, Figure 37a, shows an irregular, nodular texture with many densely packed submicron granules and several larger, raised aggregates (visible between ~20–35 µm positions). The peak to valley height, Sz = 1.20 µm demonstrates that the topography is dominated by micron-scale height variation superimposed on nanoscale granularity, consistent with SEM images that displayed dense nodules and only isolated surface porosity. The scanned area of 50 µm x 50 µm reveals (Figure 37b) a surface composed of densely packed nanoscale feature forming a continuous, hill-and-valley structure typical of electrodeposited Ni films with high nucleation rates. The "hill-and-valley" topography observed in such Ni films is primarily driven by rapid nucleation events during the electrodeposition process. High nucleation rates lead to the formation of numerous small nuclei that eventually grow and coalesce, creating an interconnected surface structure with localized variations in height and surface roughness. This process can be explained through the following mechanisms:

a) Electrochemical Conditions: The use of high overpotential or current densities accelerates the nucleation of nickel atoms on the substrate. These rapid nucleation events reduce the average grain size and produce nanoscale features [195-197].
b) Hydrogen evolution during electrodeposition can also impact morphology. Hydrogen bubbles may interact with the forming nickel film, inducing changes in the local growth dynamics and contributing to the formation of microscopic pores or irregularities in the surface texture [198, 199].

The overall height variation across the scan is approximately 0.6 µm, indicating a moderately developed micro/nanostructured surface. The coating exhibits fine granular morphology with no large voids, pits, or discontinuities, which agrees with SEM observations showing a compact deposit [200-202]. Numerous small protrusions and rounded clusters are distributed uniformly across the surface, suggesting stable nucleation and growth behavior under the chosen current density. The presence of a few taller asperities near the central region reflects localized accelerated growth zones,

which are commonly encountered in high-current electrodeposition due to spatial differences in ion concentration or micro-turbulence near the cathode [203-205].

From a structural standpoint, the AFM texture is consistent with the (111)-oriented nanocrystalline structure identified by XRD. Nickel films dominated by the (111) orientation often develop closely packed, pyramid or nodule-type surface features, producing the smooth undulating topography seen here. The fine, clustered feature also correlates with the ~17 nm crystalline size estimated from the Scherrer analysis, indicating that the nanoscale grain architecture directly influences the topographic relief observed at the microscale. In summary, AFM reveals that the Ni coating produced at 40 mA/cm^2 possesses a uniform, densely packed nanostructured surface with moderate roughness and no significant defects. These topographic characteristics complement the SEM and XRD findings, confirming that this current density produces a high-quality, structurally coherent nickel coating.

3.2.6 Microhardness analysis

The microhardness of the electrodeposited Ni-Cu alloy coatings was evaluated using Vickers hardness tester in order to assess the influence of high deposition current density on mechanical performance. The coating deposited at 40 mA/cm^2, identified as the optimal condition, exhibited the highest hardness among the investigated samples, shown in Figure 38.

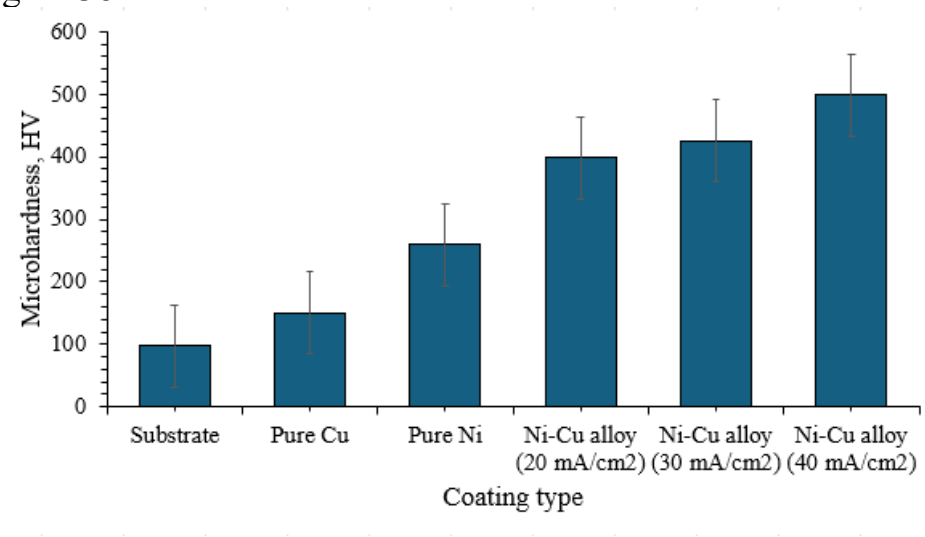


Figure 38 - Hardness values

The enhanced hardness can be primarily attributed to the nanocrystalline microstructure revealed by XRD analysis. The Scherrer-based crystallite size of approximately 17 nm indicates a high density of grain boundaries, which act as effective barrier to dislocation motion. The grain refinement leads to significant strengthening in accordance with the Hall-Petch relationship, which is well established for electrodeposited nickel coatings. Surface morphology also plays an important role in determining hardness. SEM observations showed that the coating deposited at 40 mA/cm^2 possessed a dense and compact microstructure with minimal porosity, while AFM analysis revealed a moderately rough but uniform surface topography (Sa ≈ 0.31 μm). Such morphological features reduce stress concentration sites and enable more uniform distribution during indentation, contributing to improved hardness values.

Furthermore, the string Ni(111) preferred orientation observed in XRD patterns may also contribute to the mechanical response. The (111) plane in fcc nickel is closely packed and has been reported to exhibit higher resistance to plastic deformation compared to other crystallographic orientations. The combination of preferred orientation, grain refinement, and dense morphology explains the superior hardness of the coating deposited at 40 mA/cm^2.

Overall, the microhardness results demonstrate a clear correlation between deposition current density, microstructural evolution, and mechanical strengthening, confirming that controlled electrochemical parameters are crucial for tailoring the mechanical performance of nickel-copper coatings.

3.2.7 Corrosion resistance properties

The corrosion behavior of the electrodeposited Ni-Cu coatings is closely related to their microstructural integrity, surface morphology, and crystallographic characteristics. Based on SEM, XRD, and AFM analyses, the coating deposited at 40 mA/cm^2 is expected to exhibit enhanced corrosion resistance compared to coatings produced at lower or higher current densities. SEM examinations revealed a continuous and compact surface with only sparse isolated pores, which is critical for corrosion protection. Dense coatings act as effective physical barriers, limiting the penetration of aggressive electrolyte species toward the AISI 304 substrate. In contrast, coatings with higher porosity or microcracks typically provide pathways for localized corrosion initiation.

The nanocrystalline structure identified by XRD further contributes to corrosion resistance. Although nanocrystalline materials possess a high grain-boundary density, the absence of secondary phases or oxide inclusions, as confirmed by XRD and EDS, ensures chemical homogeneity. The dominant Ni(111) texture has been reported to exhibit superior corrosion resistance in aqueous environments due to its lower surface energy and higher atomic packing density, which reduces active dissolution sites. The polarization curves for comparing corrosion resistance values for the various coatings in 3.5% NaCl is shown in Figure 39.

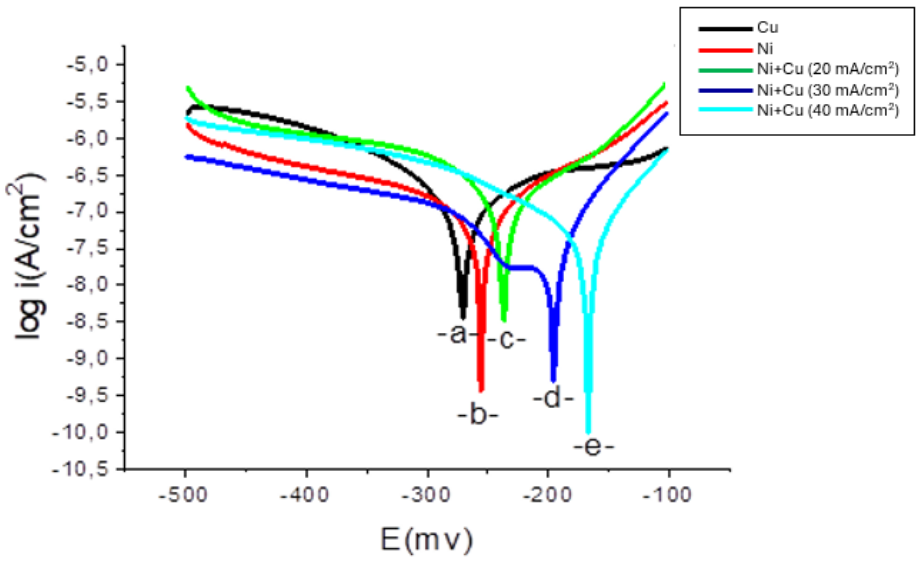


Figure 39 - Polarization curves for comparing corrosion resistance in 3.5% NaCl

The different electrochemical parameters deduced from the polarization curves are grouped together in Table 10.

Table 10 - Corrosion characteristic obtained from potentiodynamic polarization measurement for pure Ni-Cu alloy coatings

Coating	E_{corr} (mV)	i_{corr} (µA/cm²)	R_p (KΩ.cm²)	r_{corr} (µm/an)
Cu	-274.8	0.14568	168.35	1.704
Ni	-259.6	0.1379	225.32	1.612
Ni-Cu (20 mA/cm²)	-240.7	0.1235	122.39	1.444
Ni-Cu (30 mA/cm²)	-200.1	0.0783	247.2	0.845
Ni-Cu (40 mA/cm²)	-171.7	0.0505	309.51	0.591

Figure 39 shows the cathodic and anodic polarization curves of Ni-Cu alloy coatings. It is important to note that as the current density increases in the deposit, the E_{corr} potential shifts to more positive values and the i_{corr} density decreases, indicating that the polarization resistance in the medium studied increases significantly with the increase in current density. The Ni-Cu (40mA/cm^2) deposit therefore has the best polarization resistance. Note also that the values of Rp (Table 10.) increase as the values of i_{corr} decrease. These results are in good agreement because the resistance Rp is inversely proportional to i_{corr} and can be obtained through the Stern-Geary relationship. Moreover, AFM analysis showed a moderate surface roughness with no sharp asperities or deep pits. Such a surface morphology is benefited from a corrosion standpoint, as excessively rough surfaces can promote localized corrosion by increasing the effective surface area and creating micro-galvanic cells. The measured roughness parameters (Sa and Sz) suggest a balanced topography that doesn't compromise protective performance. Additionally, the low oxygen content detected by EDS indicates minimal surface oxidation during deposition, further supporting the formation of a stable metallic Ni-Cu surface. Together, these characteristics suggest that the coating deposited at 40 mA/cm^2 would exhibit lower corrosion current density and more noble corrosion potential in electrochemical testing.

In summary, the improved corrosion behavior of the optimal Ni-Cu coating can be attributed to its dense microstructure, nanocrystalline grain size, favorable crystallographic orientation, and uniform surface topography [200-202]. These results highlight the importance of current density control in producing Ni-Cu coatings with enhanced protective performance on AISI 304 stainless steel.

3.2.8 Summary

This study examined the microstructural and surface property consequences of DC electrodeposition of nickel onto AISI 304 steel using a Watts bath. The main findings and implications are: the coating deposited exhibited favorable combination of structural and surface properties. SEM micrographs show a compact, continuous Ni layer with only isolated pores; EDS indicates the deposit is largely metallic Ni (≈94.9 wt.%) with negligible oxygen and only trace Cu contamination. These observations

indicate good bath chemistry control and effective substrate coverage. Moreover, XRD confirms a single-phase fcc Ni deposit with a dominant Ni(111) reflection and no detectable crystalline oxide phases. Scherrer analysis on the Ni(111) peak yields an average crystallite (coherent domain) size of ≈17 nm, indicating a nanocrystalline structure. AFM mapping (50 μm x 50 μm) shows hierarchical surface in which nanocrystalline grains assemble into a micron-sized nodules. Collectively, these results demonstrate that careful control of current density and bath concentration during Watts bath electrodeposition is effective for producing high-quality nanocrystalline Ni coatings on AISI 304 suitable for applications requiring enhanced surface durability and enables tailoring of nickel coating microstructure and surface topography to achieve improved functional properties on AISI 304 stainless steel. Recommended follow-up work includes quantitative wear testing.

3.3 Electrodeposition of binary and ternary Cobalt-Vanadium alloy coatings

The development of efficient, stable, and economically viable electrode materials for hydrogen evolution reaction (HER) remains a critical challenge in modern electrochemical technologies. In alkaline electrolysis, which accounts for a substantial share of industrial hydrogen production, the cathode material must possess high catalytic activity, corrosion resistance, and mechanical durability under harsh operating conditions. Although platinum-group metals exhibit superior catalytic performance, their limited availability and high cost motivate the search for alternative non-precious materials with comparable functional characteristics [206].

Cobalt-based alloys have attracted increasing attention as promising electrocatalysts for HER due to their favorable electronic structure, catalytic activity, and mechanical stability. Alloying cobalt with transition metals such as iron and vanadium has been shown to modify the electronic environment, promote synergistic catalytic effects, and enhance both durability and resistance to aggressive media. Vanadium-containing alloys in particular exhibit unique features, including improved catalytic behavior associated with variable oxidation states, and enhanced corrosion resistance properties attributed to the formation of protective layers on the surface.

Electrochemical deposition is known to be a versatile and scalable method for obtaining uniform composite and alloy coatings with tunable microstructure, composition, and functional properties [207, 208]. However, stable incorporation of vanadium into electrodeposited alloys is technically challenging due to the low tendency of vanadium ions to undergo electrochemical reduction. Recent studies report that pulse electrolysis can enhance co-deposition of refractory elements by promoting localized supersaturation, increasing nucleation rates, and enabling additional chemical reduction processes during relaxation periods.

Despite these advancements, comprehensive understanding of the co-deposition behavior, structural features, and electrocatalytic properties of Co-V and Co-Fe-V coatings obtained from citrate electrolytes remains insufficient. In particular, the effects of pulse parameters on vanadium incorporation, microstructure formation, hydrogen evolution kinetics, and corrosion resistance require systematic investigation.

The present work aims to address these gaps by conducting a detailed study on the synthesis of Co-V and Co-Fe-V alloy coatings under stationary and pulse electrolysis regimes. The research focuses on the influence of electrolyte composition, current density, temperature, and pulse characteristics on:

(i) alloy composition and current efficiency,
(ii) surface morphology and microstructure,
(iii) microhardness, and
(iv) electrocatalytic and corrosion behavior in alkaline media.

Special attention is given to elucidating the mechanisms of vanadium incorporation and the role of pulse deposition in enhancing HER activity.

The findings demonstrate that pulse electrolysis significantly increases vanadium content, mechanical strength, and electrocatalytic performance, ultimately enabling the formation of Co-V coatings with HER activity approaching that of

platinum. These results highlight the potential of pulse-deposited Co-V alloys as highly efficient and cost-effective cathode materials for industrial hydrogen production and other electrochemical applications.

3.3.1 Research Methods

Given the complexity of forming multicomponent coatings and the uncertainty associated with achieving optimal functional properties, solving such problems has a clearly defined practical orientation related to the needs of modern industry. The demand for advanced materials and coatings with enhanced performance characteristics makes it essential to understand and control the quantitative and phase composition, surface morphology, and corresponding properties of electrodeposited layers. Despite the large number of investigations in this field, issues related to process control and regulation of coating structure remain highly relevant. Consequently, a justified selection of research methods represents an important aspect of this work.

Binary and ternary alloy coatings were deposited onto low-carbon steel substrates (grades St3 and 08KP). To verify the results of X-ray phase analysis, some coatings were deposited onto copper substrates (grade M1). Before the electrodeposition process, surface preparations were carried out on all substrates according to standard procedures, including mechanical treatment, degreasing, etching, surface activation, and rinsing. Mechanical treatment was used to remove surface defects and reduce roughness by grinding with abrasive paper (No. 0). Degreasing and improved wettability were achieved by treatment in sodium carbonate solution followed by rinsing. Corrosion products were removed by chemical etching: M1 copper was treated in diluted nitric acid, while low-carbon steels were etched in diluted sulfuric acid or a 1:1 mixture of sulfuric and hydrochloric acids. The final step was thorough rinsing with distilled water.

Insoluble anodes made of 12X18H10T stainless steel were used, with a cathode-to-anode area ratio of (1:5) - (1:10). The anode preparation included mechanical treatment with abrasive paper #0, followed by etching it in diluted sulfuric acid, alternatively with a one-to-one sulfuric–hydrochloric mixture, and subsequently rinsing with distilled water. A platinum electrode served as an auxiliary electrode for kinetic studies.

Vanadium-containing cobalt alloy coatings were deposited from citrate electrolytes with various concentrations of V_2O_5. High-purity analytical-grade reagents were used for preparing all solutions. The pH of the electrolytes was monitored using a pH-150M meter with an ESL-6307 glass electrode.

Electrochemical measurements were carried out in a standard cell (YASE-2) equipped with a thermostat controlled by a PT-049 regulator and resistance thermometer. Solutions were homogenized by uniform heating and magnetic stirring (MM-5). Stationary electrode potentials were recorded using high-impedance voltmeters V2-36 and V7-35 (input resistance $\geq 10^{10}$ Ω). Polarization measurements were performed with a PI-50-1.1 potentiostat in a thermostated three-electrode setup. The working potential and waveform were controlled by a PR-8 programmer. Potential sweep rates ranged from 2×10^{-3} to 1×10^{-1} V/s. Dynamic curves were recorded and processed using specialized software.

Galvanostatic deposition was performed using a B5-47 DC power supply, while pulse unipolar deposition employed a PI-50-1.1 potentiostat with PR-8 programming. Vanadium-containing cobalt coatings were deposited at 35-40 °C under galvanostatic conditions at 5-12 A/dm² using cobalt anodes. The current efficiency (η) was determined gravimetrically, assuming that all metals were reduced to their metallic state. Theoretical mass gain was calculated considering the electrochemical equivalents of alloying elements. The kinetics and rate-limiting steps of deposition were analyzed by voltammetry using polarization curves. Diagnostic criteria included the product of the transfer coefficient and electron number ($\alpha \cdot z$), the Semerano criterion (Xs), and the reaction order (pi).

The chemical composition of the coatings was determined by X-ray fluorescence spectroscopy using a portable SPRUT spectrometer. Measurements were taken at a minimum of three points, and results were averaged; the measurement error did not exceed ±1 wt%. Additional verification was performed via energy-dispersive X-ray spectroscopy (EDS) using an Oxford INCA Energy 350 analyzer (15 keV electron beam) integrated into a scanning electron microscope (SEM).

Surface morphology was studied using a ZEISS EVO 40XVP SEM. Secondary electrons were used to obtain high-resolution, high-contrast images at magnifications of 100-5000×. Image processing was conducted with SmartSEM software. Visual inspection under laboratory conditions was performed with an MBS-9 optical microscope at 15× magnification.

Surface roughness was investigated by AFM using an NT-206 SPM in contact mode with a CSC-37 probe and B-type cantilever. Scanning areas of 40×40 μm, 20×20 μm, 10×10 μm, and 5×5 μm were recorded at a resolution of 256×256 pixels. Central regions of the samples were selected for imaging. The relief was reconstructed as 2D/3D topography maps (height represented by color) and 2D torsion maps reflecting lateral friction. Grain size, shape, and anisotropy were determined from surface profiles, height distribution histograms, slope angle distributions, and orientation of surface normals. The similarity of surface characteristics across different areas allowed extrapolation to the entire coating.

Phase composition was determined by X-ray diffraction (XRD) using a DRON-2 diffractometer with monochromatic Fe-Kα (λ = 1.5405 Å) and Co-Kα (λ = 1.7902 Å) radiation. Diffraction patterns were recorded in step-by-step mode with $\Delta(2\theta)$ = 0.1°, exposure time 20 s per point, at 35 kV and 20 mA. Phases were identified by comparing interplanar spacings and relative intensities with PCPDFWIN database standards.

Corrosion behavior was evaluated by EIS (Electrochemical impedance spectroscopy) in in a 3.5% solution of NaCl using a two-electrode planar configuration. Measurement records were carried out with an Autolab PGSTAT301N (Metrohm Autolab) which is equipped with an FRA-2 module within the frequency range 10^{-2} - 10^{6} Hz. Data acquisition and analysis were performed in Autolab 4.9 and ZView 2.0, respectively. Equivalent circuit modeling was used to interpret impedance spectra.

Microhardness of the coatings and substrates was measured using a PMT-3 microhardness tester by the Vickers method at loads of 0.02–0.2 kg with a dwell time

of 10 s. Measurements were conducted after 24-hour aging at room temperature on coatings at least 30 μm thick, with at least three indentations per sample; results were averaged.

3.3.2 Formation of coatings by direct (stationary) electrolysis

Cobalt-vanadium (Co-V) coatings were deposited from a citrate-based electrolyte (electrolyte No. 1, Table 11) [210] onto steel substrates at 35-40 °C under a constant current density of 5-12 A/dm² using soluble cobalt anodes.

Table 11 - Electrolyte compositions for the electrolytic deposition of vanadium-containing alloys

Electrolyte components	**Concentration range, mol/dm³**	**pH of electrolytic bath**
Electrolyte No. 1. Co-V		
$CoSO_4 \cdot 7H_2O$	0.15-0.2	2.8-3.3
V_2O_5 (in terms of metal)	0.1-0.2	
$Na_3Cit \cdot 2H_2O$	0.3-0.4	
Electrolyte No. 2. Co-Fe-V		
$CoSO_4 \cdot 7H_2O$	0.15-0.2	3-4
V_2O_5 (in terms of metal)	0.1-0.2	
$Fe_2(SO_4)_3 \cdot 9H_2O$	0.075-0.15	
$Na_3Cit \cdot 2H_2O$	0.3-0.4	
Na_2SO4	0.1	
H_3BO_3	0.1	

At a ligand concentration of 0.3 mol/dm³, the vanadium content in the deposits lies within 0.1-0.5 wt.% depending on both the V_2O_5 concentration in the solution and the applied current density. It was established that increasing the current density and the vanadium concentration in the electrolyte leads to enrichment of the coating with this element. Visual examination confirmed that the obtained coatings are dense, bright, and free from internal stresses or microcracks. Increasing the ligand concentration to 0.4 mol/dm³ promotes stronger complexation of cobalt, which in turn increases the vanadium incorporation into the coating to 0.6-1.2 wt.%. The trend of rising vanadium content with current density remained unchanged. The current efficiency decreased from 67% at 5 A/dm² to 51% at 12 A/dm². This behavior is expected considering the electrocatalytic nature of cobalt-based alloys. Notably, these values exceed those reported previously by other researchers [209].

3.3.3 Electrodeposition of ternary Co-Fe-V alloys

Ternary Co-Fe-V coatings were deposited on steel substrates from electrolyte No. 2 (Table 11) [211] at 20-30 °C and under a constant current density of 5-12 A/dm² using insoluble X18H10T steel anodes. For electrolyte No. 2 containing 0.3 mol/dm³

ligand, the deposited coatings consisted of 45-50 wt.% Fe, 50-55 wt.% Co, and 0.1-0.4 wt.% V. All previously identified trends relating vanadium incorporation to current density remained valid for the ternary alloy system. Upon increasing the ligand concentration to 0.4 mol/dm³, the vanadium content increased to 0.2-0.6 wt.% while the Fe and Co contents were 40-42 wt.% and 58-60 wt.%, respectively. This indicates that competition between Co and Fe during co-deposition intensifies at higher ligand concentrations. A further increase in vanadium concentration (electrolyte composition, mol/dm³: 0.4 Cit^{3-}; 0.2 Co^{2+}; 0.15 Fe^{3+}; V_2O_5 equivalent to 0.2 mol/dm³ metal) resulted in coatings containing 40-42 wt.% Fe, 58-60 wt.% Co, and 0.4-0.9 wt.% V. As the current density increased, the current efficiency decreased from 65% at 5 A/dm² to 55% at 12 A/dm².

3.3.4 Structural characteristics of Co-V coatings

X-ray diffraction patterns of Co-V coatings deposited at 10-12 A/dm² (Figure 40) showed differences only in peak intensities; the phase composition remained essentially unchanged. The coatings represent a solid solution of vanadium in α-Co.

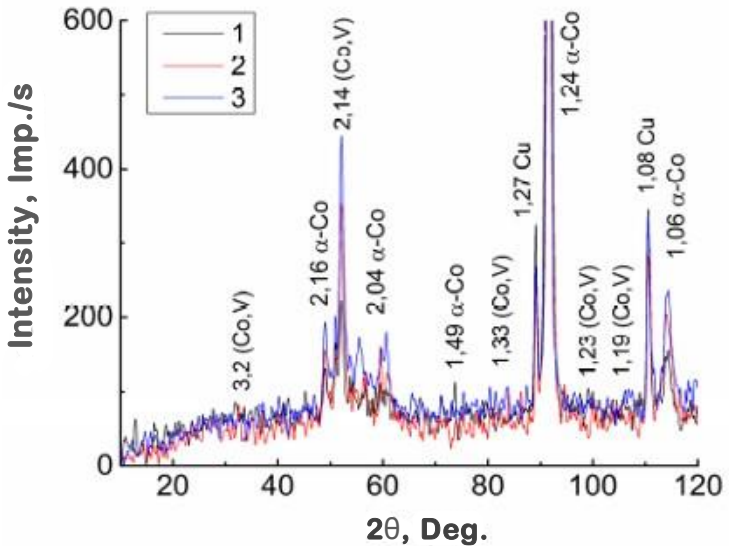
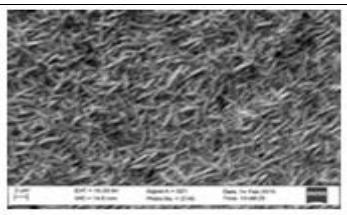
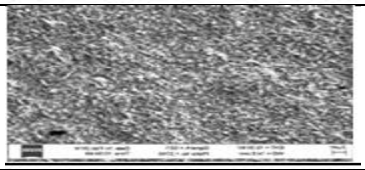
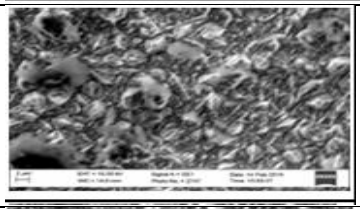
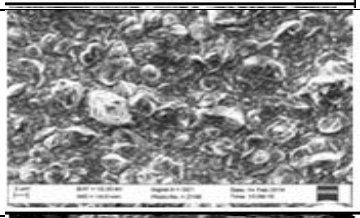
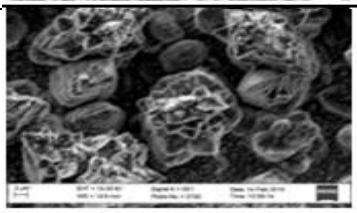
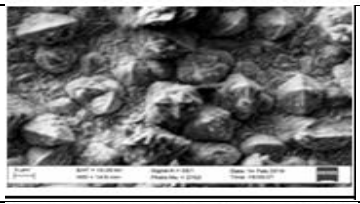
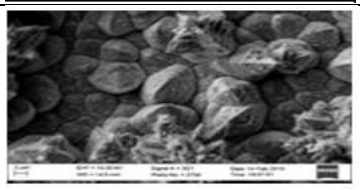
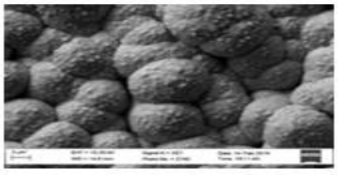


Figure 40 - X-ray diffraction patterns of Co-V coatings of the compositions, at. %: 1) Co - 99.2; V - 0.8; 2) Co - 99.0; V - 1.0; 3) Co - 98.8; V - 1.2

Notably, with increasing vanadium content, reflections in the 50°-60° 2θ range became more pronounced, and a slight halo appeared, indicating partial amorphization of the structure. The influence of current density on surface morphology and microhardness was particularly pronounced (Table 12).

Table 12 - Microhardness of Co-V coatings

Sample No.	j, A/dm^3	Coating composition			SEM, X5000	Microhardness HV, kg/mm^2
1	7	Element	Wt.%	at. %		73.26
		C	4.33	17.85		
		O	0.76	2.34		
		V	0.39	0.38		
		Co	94.52	79.43		
2	8	C	4.42	18.16		84.49
		O	0.76	2.34		
		V	0.23	0.23		
		Co	94.59	79.28		
3	9	C	4.52	18.45		242.8
		O	0.91	2.79		
		V	0.40	0.39		
		Co	94.17	78.37		
4	10	C	3.32	14.20		294.13
		O	0.61	1.97		
		V	0.62	0.62		
		Co	95.45	83.21		
5	11	C	3.12	13.38		268.02
		O	0.8	2.59		
		V	0.72	0.72		
		Co	95.36	83.31		
6	12	C	2.89	12.56		268.7
		O	0.53	1.72		
		V	0.9	0.93		
		Co	95.68	84.79		
7	13	C	2.89	12.56		260.71
		O	0.53	1.72		
		V	0.9	0.93		
		Co	95.68	84.79		
8	14	C	2.67	11.72		278.5
		O	0.44	1.46		
		V	0.86	0.87		
		Co	96.73	85.95		

SEM observations revealed that at 7-8 A/dm², the coatings had a fine needle-like microcrystalline structure with low vanadium content and relatively low microhardness (Samples 1 and 2, Table 12). Interestingly, the oxygen content in Co-V alloys was the lowest among all synthesized coatings, whereas carbon levels were substantially

higher. As the current density increased to 9-10 A/dm², the vanadium content approximately doubled, while carbon content decreased. The surface became more textured, forming conglomerates and globules of varying shapes, accompanied by a threefold increase in microhardness (samples 3 and 4). At 11-12 A/dm², the vanadium content reached up to 1.2 at.% (metal basis). The coating surfaces (samples 5 and 6) exhibited conglomerates 2-5 μm in size growing outward from the substrate. The morphology became more heterogeneous: zones of fine microcrystalline texture alternated with crystals of distinct geometries.

At still higher current densities (13-14 A/dm²), the vanadium content stabilized at 0.9-1.0 at. %, and the decreasing trend in carbon content persisted. Samples 7 and 8 exhibited a uniformly globular surface, where grain conglomerates developed into spheroids 4-7 μm in diameter with crystalline structure alternating with regions of other crystal morphologies. Microhardness remained within 270-280 kg/mm², indicating that vanadium content and surface morphology are the key factors determining the mechanical properties of electrodeposited V-containing cobalt coatings.

3.3.5 Formation of Co-V coatings in pulse electrodeposition mode

The preliminary experimental results served as the basis for a detailed investigation of the electrodeposition of Co-V alloy coatings from a citrate electrolyte under both steady-state and pulse current conditions. The application of a pulse mode is grounded in the hypothesis that, during the pause period, additional chemical reduction of vanadium occurs. This reduction is expected to proceed via adsorbed hydrogen atoms formed during the electrochemical steps of the current pulse. The participation of these hydrogen adatoms in the reduction of oxovanadium ions should increase both the vanadium content in the Co-V alloy and the current efficiency.

Pulse electroplating introduces several technological features; therefore, they are briefly discussed here. Co-V alloy coatings were deposited from a citrate-based electrolyte containing 0.4 mol/dm³ $Na_3C_6H_5O_7 \cdot 2H_2O$, 0.1 mol/dm³ $CoSO_4 \cdot 7H_2O$, and 0.1 mol/dm³ vanadium(V) oxide. Electrodeposition was conducted at 35–40 °C and pH 3–3.5 using a unipolar pulse current with an amplitude of 2–10 A/dm². The pulse and pause durations were varied in the range 5×10^{-3} – 5×10^{-2} s. For comparison and validation, steady-state galvanostatic deposition was also performed at 1–15 A/dm². The resulting coating thickness was 6-9 μm. Prior to deposition, copper electrodes with an area of 2 cm² were mechanically polished and degreased. Electrolysis in galvanostatic mode was conducted using a B5-47 power supply, while pulse deposition was performed using a PI-50-1.1 pulse generator equipped with a PR-8 programmer. Measurement data were processed using 2D plots (Python 3.7) and 3D diagrams (MS Excel).

Effect of current density and temperature

It was experimentally established that Co-V coatings do not form at current densities up to 5 A/dm² and temperatures of 20-30 °C, in either steady-state or pulse deposition modes [212]. Increasing the temperature to 35-40 °C enabled coating formation in steady-state mode, yielding alloys with a vanadium content of 0.007-0.017% and a current efficiency of 11-19% (Table 13). The maximum vanadium

content was achieved at j_k = 10 A/dm². Further temperature increases did not enhance vanadium incorporation or current efficiency. Therefore, 35-40 °C was identified as the optimal deposition temperature.

Table 13 - Dependence of vanadium content in the Co-V coating and current efficiency on current density

Current density, A/dm²	**Vanadium content, %**	**Current efficiency, %**
6	0.007	11
8	0.010	14
10	0.017	19
12	0.014	17
14	0.013	13

Subsequently, Co-V coatings (Figure 41) were obtained under pulse conditions. The resulting deposits were of satisfactory quality-fine-crystalline, uniform, light gray, and glossy.

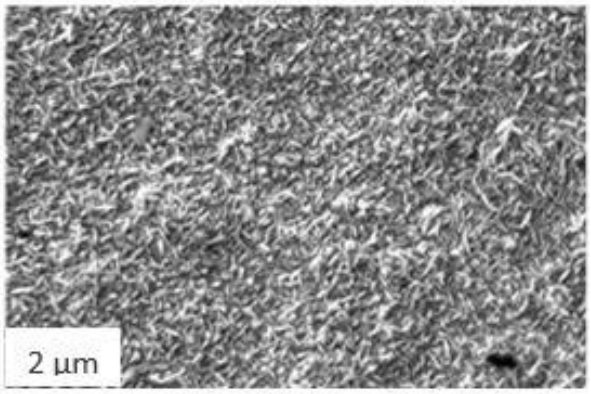


Figure 41 - Surface morphology of Co-V coating (x5000)

3.3.6 Effect of pulse parameters on alloy composition and efficiency

The relationships between vanadium content, current amplitude, and pulse-to-pause ratio are shown in the 3D diagrams in Figures 42 and 43. As seen in Figure 42, vanadium incorporation above 1 wt.% occurs at current densities of 6-7 A/dm², with a maximum of 1.45-1.5% at 6 A/dm². Increasing the pause duration from 5×10^{-3} to 5×10^{-3} s (at constant pulse duration) increases vanadium content from 1.026% to 1.124%, supporting the hypothesis of additional chemical reduction of vanadyl ions by adsorbed hydrogen atoms formed during the pulse. A current efficiency above 50% is achieved at 5-7 A/dm², with a maximum of 80% at 7 A/dm² (Figure 42) when using the longest pause duration (5×10^{-2} s). This further confirms the contribution of hydrogen adatoms to the secondary reduction of vanadium species. At 10 A/dm², vanadium content decreases (Figure 43), and coating quality deteriorates due to intensified hydrogen evolution. Thus, the optimal deposition conditions are a current density of 5-7 A/dm² and pulse/pause durations of 1×10^{-2} - 5×10^{-2} s, producing coatings with maximum vanadium content and high current efficiency.

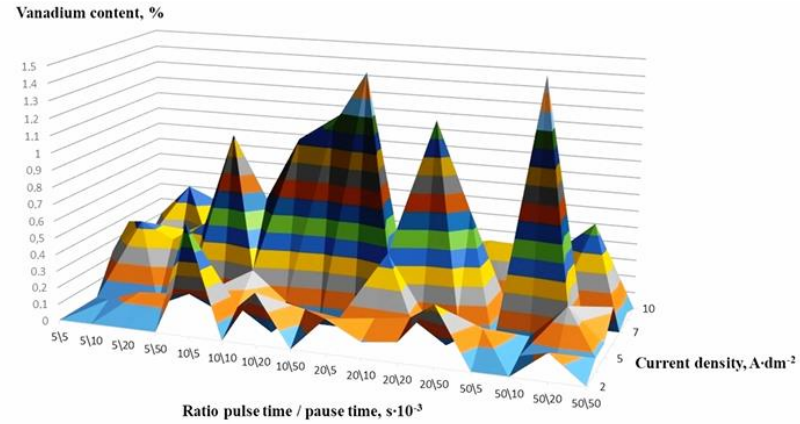


Figure 42 - Dependence of vanadium content in the alloy on current density and the pulse/pause time ratio

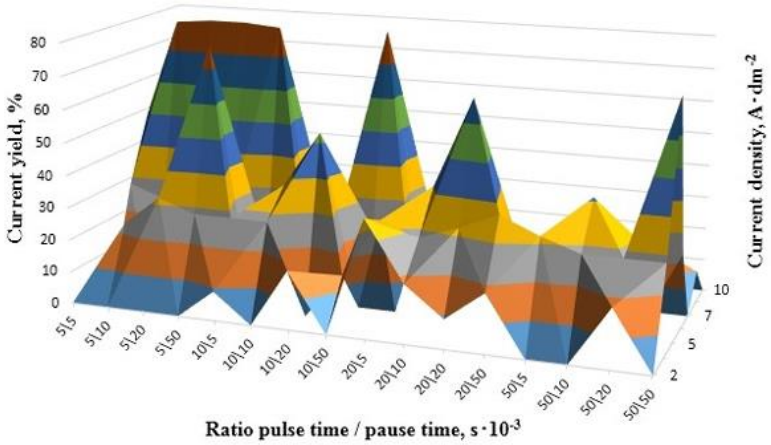


Figure 43 - Dependence of coating current efficiency on current density and the pulse/pause time ratio

3.3.7 Electrocatalytic properties towards the hydrogen evolution reaction (HER)

HER kinetics were studied in 2.5 M NaOH, a typical electrolyte for industrial hydrogen production [213, 214]. Cathodic polarization curves for steel (St.20) electrodes coated with Co and Co-V are shown in Figure 44. The materials can be ranked by decreasing electrode polarization in the following order:

Co coating → Co-V (0.2-0.4 wt.% V) → Co-V (0.5-0.7 wt.% V) → Co-V (0.8-1.0 wt.% V)

Hydrogen evolution begins at -0.88 to -0.95 V on Co-V coated electrodes and at -1.1 V on pure Co coatings. The overpotential for HER on Co-V coatings is 0.15-0.2 V lower than on pure cobalt. Analysis of Tafel plots (Figure 45) enabled determination of HER kinetic parameters (Table 14). The reduced overpotential is attributed to the catalytic activity of vanadium. Increasing vanadium content further decreases the overpotential.

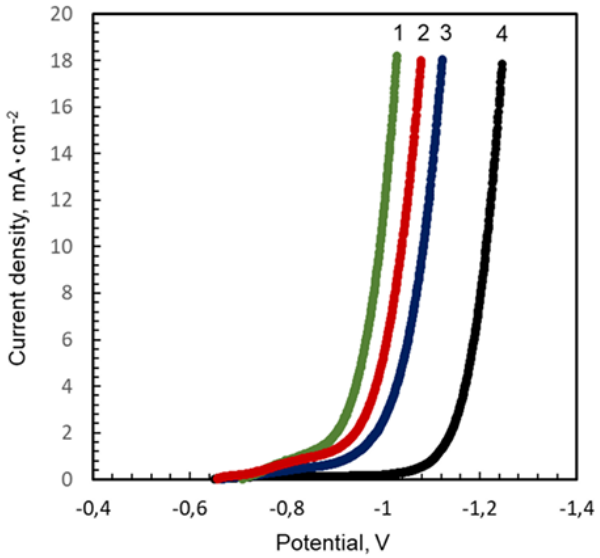


Figure 44 - Cathodic polarization curves of hydrogen evolution in a 2.5M NaOH solution on electrodes: 1) Co-V coating (0.8-1.0 wt. % V); 2) Co-V coating (0.5-0.7 wt. % V); 3) Co-V coating (0.2-0.4 wt. % V); 4) Co coating

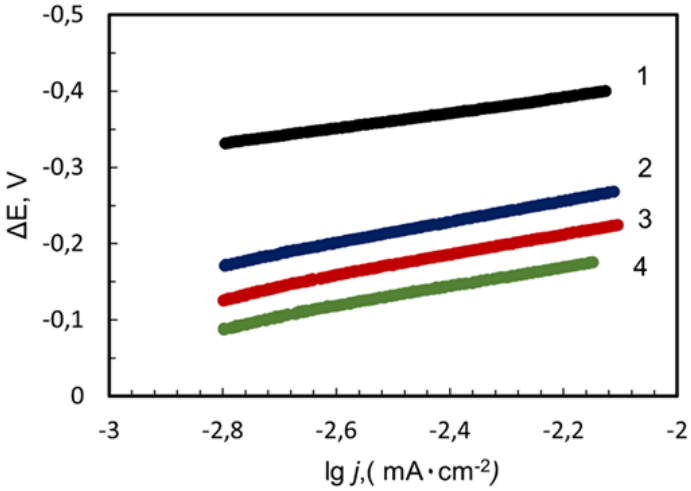


Figure 45 - Overvoltage vs. logarithm of current density in a 2.5M NaOH solution for electrodes: 1) Co coating; 2) Co-V coating (0.2-0.4 wt. % V); 3) Co-V coating (0.5-0.7 wt. % V); 4) Co-V coating (0.8-1.0 wt. % V)

Table 14 - Kinetic parameters of the hydrogen evolution reaction on the studied cathodes

Electrode material	**Vanadium content, wt.%**	***a*, V**	***b*, V**	**–lgj0, A/cm^2**
Pt	-	-0.31	-0.1	3.1
Art. 20 with Co coating	-	-0.61	-0.1	6.12
Art. 20 with Co coating	0.2-0.4	-0.56	-0.139	4.03
	0.5-0.7	-0.51	-0.139	3.67
	0.8-1.0	-0.46	-0.132	3.48

The exchange current density (j_0), a universal kinetic descriptor independent of applied current, reflects intrinsic catalytic activity. j_0 values for Co-V coatings are significantly higher than for cobalt, confirming their superior electrocatalytic behavior. Notably, HER overpotential and exchange current density for Co-V coatings containing 0.8-1 wt.% V are comparable to those of platinum electrodes in alkaline media (Table 12).

3.3.8 Microhardness and mechanical properties

The microhardness of the coatings is 150-200 kg·mm^{-2} higher than that of cobalt deposited from sulfate electrolytes (Figure 46). Increasing vanadium content enhances microhardness, improving operational durability, especially under harsh chemical environments.

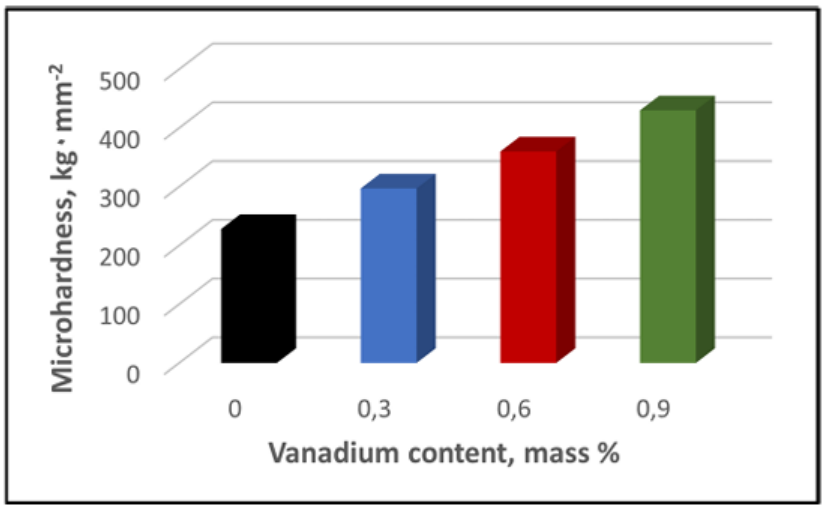


Figure 46 - Dependence of the microhardness of the Co-V coating on the vanadium content, wt.%

3.3.9 Deposition from vanadyl sulfate-containing electrolytes

To further study and improve vanadium incorporation, V_2O_5 was replaced with $VOSO_4$, which exhibits higher solubility and promotes more rapid citrate complex formation [212]. This modification simplifies electrolyte preparation and improves stability. The resulting deposits were uniform, microcrystalline, light gray, semi-glossy, and slightly rough (Figure 47).

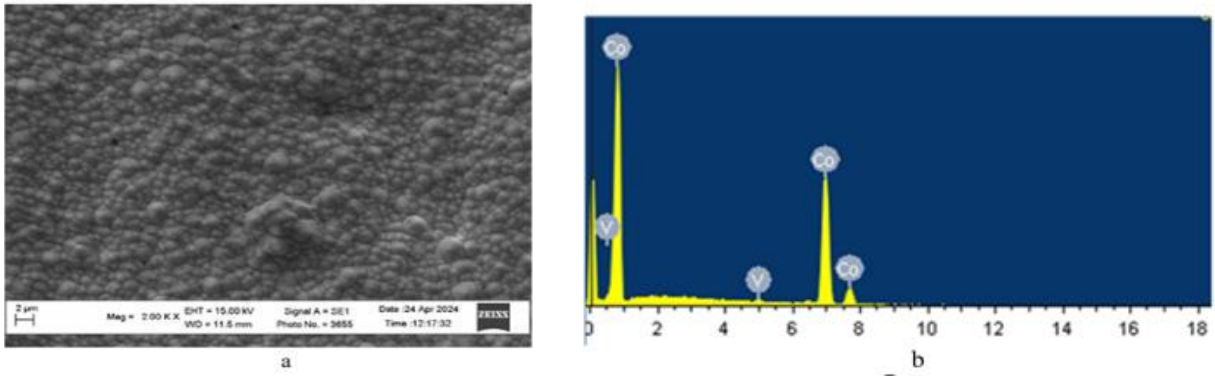


Figure 47- Surface morphology (a) and X-ray spectrum (b) of a cobalt-vanadium coating with a vanadium content of 0.75 wt.%

Vanadium content ranged from 0.7-1.5 wt.%, with a maximum of 1.5 wt.% at j_k = 10 A/dm² (Figure 48).

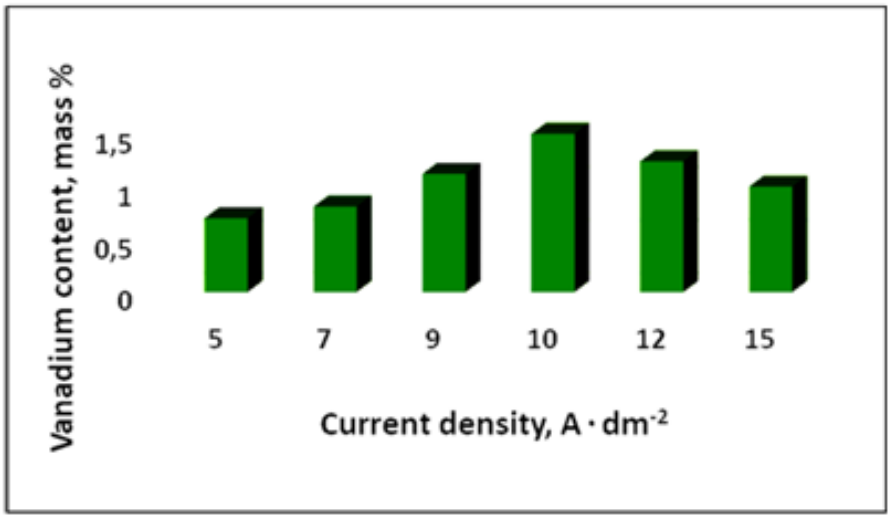


Figure 48 - Dependence of vanadium content in alloys on current density

Hydrogen evolution polarization curves and Tafel plot analyses (Figures 49 and 50; Table 15) confirm the enhanced catalytic properties of these composite coatings. When vanadium content is increased, further reduction of overpotential occurs. The Tafel slope b for the Co-V alloy coatings is close to the classical value for cobalt in alkaline medium (b ≈ 0.14), which indicates that hydrogen evolution reaction proceeds via the Volmer-Heyrovsky mechanism with a rate-limiting discharge step. Exchange current densities again confirm higher catalytic activity relative to pure cobalt. The performance of Co-V (0.7-1.5 wt.% V) closely matches that of platinum, confirming its potential as a cost-effective alternative for hydrogen production [215].

Microhardness values exceed those of cobalt coatings by 100-150 kg·mm² (Figure 51), attributed to intermetallic formation and improved surface morphology.

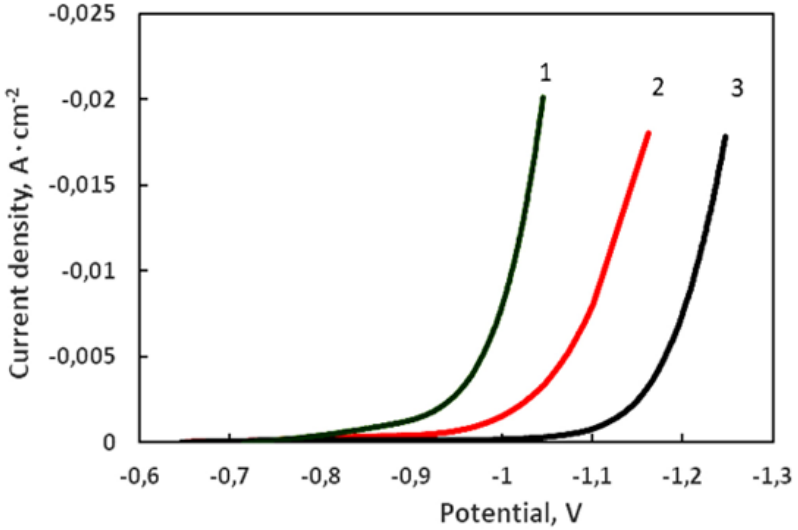


Figure 49 - Cathodic polarization curves of hydrogen evolution for electrodes with the following coatings: 1) Co-V 1.5; 2) Co-V 0.7; 3) Co

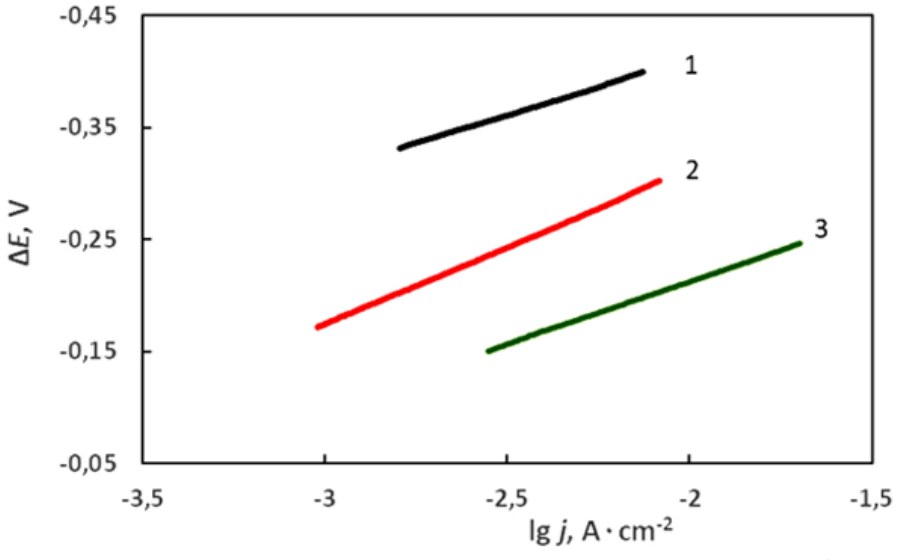


Figure 50 - Overvoltage versus logarithm of current density for coated electrodes: 1) Co; 2) Co-V 0.7; 3) Co-V1.5

Table 15 - Kinetic parameters of the hydrogen evolution reaction for the studied cathodes

Electrode materials	**Vanadium content, wt.%**	***a*, V**	***b*, V**	**–lgj0, A/cm^2**
Pt	-	-0.31	-0.1	3.1
Co	-	-0.6	-0.14	4.3
Co coating	-	-0.61	-0.12	5.1
Co-V coating	0.7	-0.58	-0.14	4.1
	1.5	-0.5	-0.141	3.5

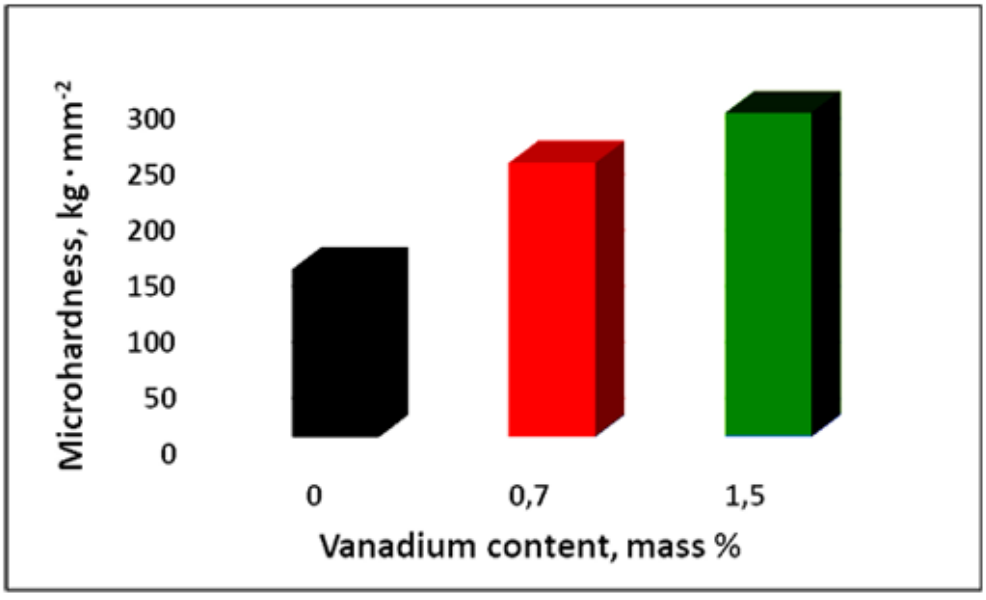


Figure 51 - Dependence of the microhardness of the Co-V coating on the vanadium content, wt.%

3.3.10 Corrosion resistance

Electrochemical corrosion tests indicate that increasing vanadium content enhances corrosion resistance compared to cobalt (Figure 52). As vanadium increases, corrosion potential shifts negatively, while corrosion current decreases, indicating reduced corrosion rate. Vanadium's robust oxide films contribute to this improvement.

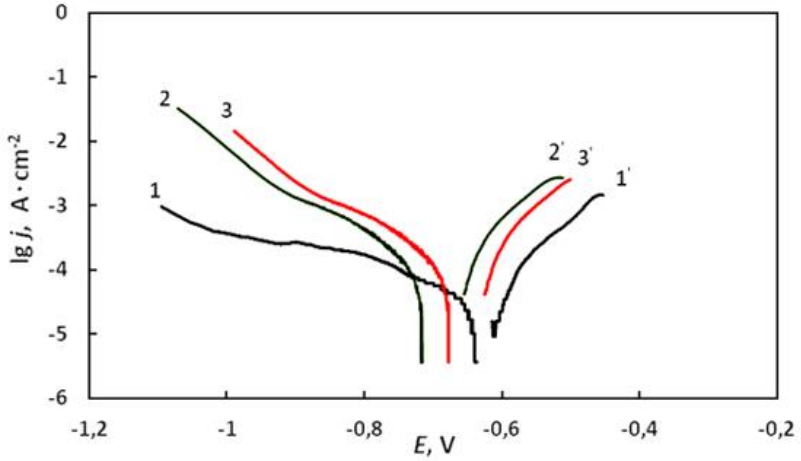


Figure 52 - Cathode (1, 2, 3) and anodic (1', 2', 3') polarization curves for steel electrodes with the following coating: 1, 1') Co; 2, 2') Co-V 1.5; 3, 3') Co-V 0.7 in alkaline media

In alkaline media, corrosion potentials shift negatively because of suppression of the cathodic reaction by surface passivation with poorly soluble hydroxides of cobalt which hinder depolarizer access (Table 16). Despite vanadium being relatively costly, small additions significantly improve protective properties [215, 216].

Table 16 - Corrosion indicators of steel and the coatings studied

Coating material	**Vanadium content, mass %**	***Ecorr*, V**	**lg jcor, A/cm^2**
Steel	-	-0.32	-2.80
Co	-	-0.61	-4.10
Co-V	0.7	-0.65	-4.25
	1.5	-0.70	-4.50

3.9.11 Summary

The results conclusively confirm the predicted functional properties of Co-V alloy coatings. Electrodes modified with Co-V demonstrate enhanced electrocatalytic activity toward HER, improved microhardness, and superior corrosion resistance. These coatings can be recommended as efficient, cost-effective cathode materials for industrial hydrogen production, contributing to substantial reductions in both energy consumption and material costs.

4 CONCLUSIONS

Electrochemical deposition parameters, particularly bath temperature and current density, were shown to critically influence the formation, microstructural evolution, and functional behavior of chromium-graphene composite and Ni-Cu and Co-V alloy coatings. For chromium-graphene composite coatings on low-carbon steel, deposition temperatures of 15–60 °C (±2 °C) have a significant effect on coating thickness, surface morphology, and graphene incorporation, with an optimum deposition temperature at 45 °C (±2 °C) yielding uniform, adherent coatings with enhanced functional properties. In Ni- and Co- based systems, precise control of current density-under direct current and pulse electrolysis was essential to obtain dense, defect-free deposits and regulate hydrogen evolution and alloying behavior, confirming that optimized electrochemical parameters govern coating nucleation, growth, and integrity.

Comprehensive microstructural analyses (SEM/EDS, XRD, and AFM) demonstrated that coating structure and composition are governed by electrochemical synthesis conditions. Cr–graphene composite coatings exhibited temperature-dependent surface roughness and carbon content, with maximum graphene incorporation and refined Cr(200) texture 45 °C (±2 °C). Optimized Ni-Cu coatings formed compact nanocrystalline layers with a dominant fcc Ni(111) texture and ~17 crystallite size, while Co-V coatings consisted of vanadium solid solutions in α-cobalt with partial amorphization at higher vanadium contents under pulse electrolysis.

Functional testing revealed strong structure-property relationships. Cr-graphene coatings showed maximum microhardness and corrosion resistance at the optimal temperature due to grain refinement the barrier effect of graphene. Nanocrystalline Ni-Cu coatings combined surface compactness and uniformity, while Co-V coatings exhibited significantly increase microhardness and enhanced electrolytic activity for hydrogen evolution, approaching that of platinum, alongside improved corrosion resistance.

Overall, the results demonstrate that rational optimization of electrochemical synthesis enables the production of high-performance coatings. Cr-graphene and Ni-Cu composites are confirmed as durable protective coatings, and Co-V electrodeposited coatings emerge as efficient, corrosion resistant and cost-effective alternatives to noble metal cathodes for industrial hydrogen production, thereby demonstrating their practical and technological significance.

LIST OF REFERENCES USED

1 Lv H., Pan Q., Song Y., Liu X.-X., Liu T. A review on nano-/microstructured materials constructed by electrochemical technologies for supercapacitors // Nano-Micro Letters. – 2020. – Vol. 12, № 1. – P. 118.

2 V. M. V., Nageswaran G. Review – direct electrochemical synthesis of metal organic frameworks // Journal of The Electrochemical Society. – 2020. – Vol. 167, № 15. – P. 155527.

3 Li Z., Sun Q., Qian P., Hu K., Zha Z., Wang Z. Electrochemical synthesis of α,α-dihaloacetophenones from terminal alkyne derivatives // Chinese Chemical Letters. – 2020. – Vol. 31, № 7. – P. 1855–1858.

4 Zhao H.-B., Zhuang J.-L., Xu H.-C. Electrochemical synthesis of benzimidazoles via dehydrogenative cyclization of amidines // ChemSusChem. – 2021. – Vol. 14, № 7. – P. 1692–1695.

5 Jimenez-Villegas S., Kelly S. R., Siahrostami S. SnO_2-supported single metal atoms: a bifunctional catalyst for the electrochemical synthesis of H_2O_2 // Journal of Materials Chemistry A. – 2022. – Vol. 10, № 11. – P. 6115–6121.

6 Ye W., Guo X., Ma T. A review on electrochemically synthesized copper-based catalysts for electrochemical reduction of CO_2 to C_2+ products // Chemical Engineering Journal. – 2021. – Vol. 414. – P. 128825.

7 Wu T., Fan W., Zhang Y., Zhang F. Electrochemical synthesis of ammonia: progress and challenges // Materials Today Physics. – 2021. – Vol. 16. – P. 100310.

8 Wang B., Li T., Gong F., Othman M. H. D., Xiao R. Ammonia as a green energy carrier: electrochemical synthesis and direct ammonia fuel cell – a comprehensive review // Fuel Processing Technology. – 2022. – Vol. 235. – P. 107380.

9 Breitkopf C., Swider-Lyons K. Electrochemical science – historical review // Springer handbook of electrochemical energy / Ed. C. Breitkopf, K. Swider-Lyons. – Berlin; Heidelberg: Springer, 2017. – P. 1–9.

10 Hatch C. E., Chain W. J. Electrochemically enabled total syntheses of natural products // ChemElectroChem. – 2023. – Vol. 10, № 11. – P. e202300140.

11 Boudjemaa A. History, progress, and development of electrocatalysis // Methods for electrocatalysis: advanced materials and allied applications / Ed. Inamuddin, R. Boddula, A. M. Asiri. – Cham: Springer, 2020. – P. 401–424.

12 Malapit C. Electrosynthesis for the development of selective organic reactions // ECS Meeting Abstracts. – 2024. – Vol. MA2024-01, № 41. – P. 2336.

13 Frolov V. Yu., Bolotin S. N., Panyshkin V. T. Electrochemical synthesis of complex compounds of transition elements with carboxyl- and carbonyl-containing ligands // Russian Journal of Applied Chemistry. – 2005. – Vol. 78, № 6. – P. 897–902.

14 Saleh H. M., Hassan A. I. Synthesis and characterization of nanomaterials for application in cost-effective electrochemical devices // Sustainability. – 2023. – Vol. 15, № 14. – P. 10891.

15 Sbei N., Hardwick T., Ahmed N. Green chemistry: electrochemical organic transformations via paired electrolysis // ACS Sustainable Chemistry & Engineering. – 2021. – Vol. 9, № 18. – P. 6148–6169.

16 Kamble C., Jadhav V. V., Mane R. S. Electrodeposition of metal oxide nanostructures // Solution methods for metal oxide nanostructures / Ed. R. Mane, V. Jadhav, A. Al-Enizi. – Elsevier, 2023. – P. 197–220.

17 Martin P. Introduction to surface engineering and functionally engineered materials. – Chichester: John Wiley & Sons, 2011. – 560 p.

18 Manoj A., Saurabh A., Narala S. K. R., Saravanan P., Natu H. P., Verma P. C. Surface modification of grey cast iron by laser cladding for automotive brake disc application // Wear. – 2023. – Vol. 532–533. – P. 205099.

19 Zhang X., Wan K., Subramanian P., Xu M., Luo J., Fransaer J. Electrochemical deposition of metal–organic framework films and their applications // Journal of Materials Chemistry A. – 2020. – Vol. 8, № 16. – P. 7569–7587.

20 Li R. et al. Electrodeposition: synthesis of advanced transition metal-based catalyst for hydrogen production via electrolysis of water // Journal of Energy Chemistry. – 2021. – Vol. 57. – P. 547–566.

21 Akbarpour M. R., Gharibi Asl F., Rashedi H. Pulse-reverse electrodeposition of Ni–Co/graphene composite films with high hardness and electrochemical behaviour // Diamond and Related Materials. – 2023. – Vol. 133. – P. 109720.

22 Jin P., Sun C., Zhang Z., Zhou C., Williams T. Fabrication of the Ni–W–SiC thin film by pulse electrodeposition // Surface and Coatings Technology. – 2020. – Vol. 392. – P. 125738.

23 Li C., Xia F., Ma C., Li Q. Research on the corrosion behavior of Ni–SiC nanocoating prepared using a jet electrodeposition technique // Journal of Materials Engineering and Performance. – 2021. – Vol. 30, № 8. – P. 6336–6344.

24 Shi X., Kang M., Fu X., Feng H., Zhang C., Liu Y. Wear resistance of electrodeposited Ni–Mn–SiC composite coatings // Coatings. – 2021. – Vol. 11, № 1. – P. 72.

25 Walsh F. C., Ponce de Leon C. A review of the electrodeposition of metal matrix composite coatings by inclusion of particles in a metal layer: an established and diversifying technology // Transactions of the Institute of Metal Finishing. – 2014. – Vol. 92, № 2. – P. 83–98.

26 Protsenko V. S., Butyrina T. E., Bogdanov D. A., Korniy S. A., Danilov F. I. Electrochemical synthesis of Ni/TiO_2 composite coatings from deep eutectic solvent and electrocatalytic characteristics of deposits // Surface Engineering and Applied Electrochemistry. – 2022. – Vol. 58, № 5. – P. 440–450.

27 Bakhit B., Akbari A. Effect of particle size and co-deposition technique on hardness and corrosion properties of Ni–Co/SiC composite coatings // Surface and Coatings Technology. – 2012. – Vol. 206, № 23. – P. 4964–4975.

28 Hessam R., Najafisayar P., Rasouli S. S. A comparison between growth of direct and pulse current electrodeposited crystalline SnO_2 films: electrochemical properties for application in lithium-ion batteries // Materials for Renewable and Sustainable Energy. – 2022. – Vol. 11, № 3. – P. 259–266.

29 McCormack A. G., Pomeroy M. J., Cunnane V. J. Microstructural development and surface characterization of electrodeposited nickel/yttria composite coatings // Journal of The Electrochemical Society. – 2003. – Vol. 150, №. 5. – P. C356.

30 Mandati S., Sarada B. V., Dey S. R., Joshi S. V. Pulsed electrochemical deposition of $CuInSe_2$ and $Cu(In,Ga)Se_2$ semiconductor thin films // Semiconductors: Growth and Characterization. – 2018. – P. 109.

31 Kale M. B., Borse R. A., Mohamed A. G. A., Wang Y. Electrocatalysts by electrodeposition: recent advances, synthesis methods, and applications in energy conversion // Advanced Functional Materials. – 2021. – Vol. 31, № 25. – P. 2101313.

32 Akbarpour M. R., Gharibi Asl F. Fabrication of high-performance graphene/nickel–cobalt composite coatings using ultrasonic-assisted pulse electrodeposition // Ceramics International. – 2023. – Vol. 49, № 9. – P. 13829–13835.

33 Xia F., Li C., Ma C., Li Q., Xing H. Effect of pulse current density on microstructure and wear property of Ni–TiN nanocoatings deposited via pulse electrodeposition // Applied Surface Science. – 2021. – Vol. 538. – P. 148139.

34 Krajaisri P., Puranasiri R., Chiyasak P., Rodchanarowan A. Investigation of pulse current densities and temperatures on electrodeposition of tin–copper alloys // Surface and Coatings Technology. – 2022. – Vol. 435. – P. 128244.

35 Fan H., Zhao Y., Jiang J., Wang S., Shan W. Effects of deposition parameters on the microstructure and properties of jet-electrodeposited Ni–La_2O_3 composite coatings // Journal of Materials Science: Materials in Electronics. – 2020. – Vol. 31, № 16. – P. 13919–13925.

36 Chen Y. et al. Effects of deposition current density, time and scanning velocity on scanning jet electrodeposition of Ni–Co alloy coating // Journal of Manufacturing Processes. – 2023. – Vol. 101. – P. 458–468.

37 Deshmukh V. K., Rajput M. S., Narang H. K. A systematic review on high speed selective jet electrodeposition manufacturing // World Journal of Engineering. – 2022. – Vol. 21, № 2. – P. 275–292.

38 Walsh F. C., Wang S., Zhou N. The electrodeposition of composite coatings: diversity, applications and challenges // Current Opinion in Electrochemistry. – 2020. – Vol. 20. – P. 8–19.

39 Zhang H., Wang J., Chen S., Wang H., He Y., Ma C. Ni–SiC composite coatings with improved wear and corrosion resistance synthesized via ultrasonic electrodeposition // Ceramics International. – 2021. – Vol. 47, № 7. – P. 9437–9446.

40 Kerr C., Barker D., Walsh F., Archer J. The electrodeposition of composite coatings based on metal matrix–included particle deposits // Transactions of the Institute of Metal Finishing. – 2000. – Vol. 78, № 5. – P. 171–178.

41 Azizi-Nour J., Nasirpouri F. Exploiting magnetic sediment co-electrodeposition mechanism in Ni–Al_2O_3 nanocomposite coatings // Journal of Electroanalytical Chemistry. – 2022. – Vol. 907. – P. 116052.

42 Li Y. J., Zhang X. Z., Zhi C. C. Kinetics of Ni/nano-SiO_2 codeposition on the sintered NdFeB surface // Strength of Materials. – 2021. – Vol. 53, № 1. – P. 134–144.

43 Nasirpouri F., Alipour K., Daneshvar F., Sanaeian M.-R. Electrodeposition of anticorrosion nanocoatings // Corrosion protection at the nanoscale / Ed. S. Rajendran et al. – Elsevier, 2020. – P. 473–497.

44 Torkamani A. D., Velashjerdi M., Abbas A., Bolourchi M., Maji P. Electrodeposition of nickel matrix composite coatings via various boride particles: a review // Journal of Composites and Compounds. – 2021. – Vol. 3, № 7. – P. 4.

45 Elboughdiri N. Electrolytic co-deposition mechanisms, texture layers, and residual stresses in nanocomposite coatings processes: a review // Advanced Chemical Engineering Science. – 2023. – Vol. 13, № 2. – P. 207.

46 Karthik R., Mani R., Manikandan P. Tribological studies of Ni–SiC and Ni–Al2O3 composite coatings by pulsed electrodeposition // Materials Today: Proceedings. – 2021. – Vol. 37. – P. 701–706.

47 Kumar N., Kishore K., Yadav S., Sharma P. Characterisation of Ni–Al2O3 composite coatings at different Al2O3 concentrations // Materials Today: Proceedings. – 2024.

48 Heragh M. F., Eskandarinezhad S., Dehghan A. Ni–Cu matrix composite reinforced with CNTs: preparation, characterization, wear and corrosion behavior, inhibitory effects // Journal of Composites and Compounds. – 2020. – Vol. 2, № 4.

49 Tizgadam M., Hengsberger S., Rasooli A., Ahmadiyeh S. Influence of Si3N4 nanoparticles on morphology, hardness and corrosion resistance of electrodeposited Ni–Co–Si3N4 // International Journal of Electrochemical Science. – 2022. – Vol. 17, № 10. – P. 221062.

50 Gao M., Pei Z., Song G., Liu Z., Li H., Gong J. Wear resistance of Ni/nano-Al2O3 composite coatings by brush electroplating // Journal of Materials Science. – 2024. – Vol. 59, № 16. – P. 7009–7027.

51 Li Y., Zhang K., Zhang M., Zhang Y., Wu T., Zhao H. Effect of current density on properties of sol-enhanced Ni–P–Al_2O_3 composite coating // International Journal of Electrochemical Science. – 2020. – Vol. 15, № 3. – P. 2752–2765.

52 John A., Saeed A., Khan Z. A. Influence of the duty cycle of pulse electrodeposition-coated Ni–Al_2O_3 nanocomposites on surface roughness properties // Materials. – 2023. – Vol. 16, № 6. – P. 2192.

53 Góral A., Nowak M., Berent K., Kania B. Influence of current density on microstructure and properties of electrodeposited nickel–alumina composite coatings // Journal of Alloys and Compounds. – 2014. – Vol. 615. – P. S406–S410.

54 Rezgui I., Belloufi A., Mihi A. Experimental investigation of the corrosion resistance of Ni–Al2O3 composite coatings obtained by electrodeposition // UPB Scientific Bulletin. Series B. – 2020. – Vol. 82, № 1.

55 Chen L., Wang L., Zeng Z., Xu T. Influence of pulse frequency on the microstructure and wear resistance of electrodeposited Ni–Al_2O_3 composite coatings // Surface and Coatings Technology. – 2006. – Vol. 201, № 3. – P. 599–605.

56 Rao H. et al. Electrodeposition of high-quality Ni/SiC composite coatings by using binary non-ionic surfactants // Molecules. – 2023. – Vol. 28, № 8. – P. 3344.

57 Li G. et al. Investigation on microstructure and properties of the electrodeposited Ni–SiC composite coating // Coatings. – 2023. – Vol. 13, № 4. – P. 695.

58 Li B., Su J., Li J., Wang Y. Comparison of the effect of mechanical and ultrasonic agitation on the properties of electrodeposited Ni–Co/ZrO_2 composite coatings // Metals. – 2023. – Vol. 13, № 3. – P. 478.

59 Aruna S. T., Latha S., Lakshmi R. V. Multifunctional properties of electrodeposited nickel composite coating containing nanosized monoclinic zirconia particles // Journal of Metallurgy and Materials Science. – 2020. – Vol. 66, № 1–2. – P. 77–91.

60 Algailani H. M., Mahmoud A. K., Al-Kaisy H. A. Fabrication of Ni–ZrO_2 nanocomposite coating by electroless deposition technique // Engineering and Technology Journal. – 2020. – Vol. 38, № 5A. – P. 649–655.

61 Xiong C. et al. Improving the properties of Ni–ZrO_2 composite coatings by sol-enhanced electroplating // International Journal of Electrochemical Science. – 2018. – Vol. 13, № 11. – P. 11049–11057.

62 Arghavanian R., Parvini Ahmadi N. Electrodeposition of Ni–ZrO_2 composite coatings and evaluation of particle distribution and corrosion resistance // Surface Engineering. – 2011. – Vol. 27, № 9. – P. 649–654.

63 Qiu Y., Jiang G.-Y. Study on friction, wear and thermal insulation properties of laser deposition Ni/ZrO_2 // Optik. – 2021. – Vol. 247. – P. 167783.

64 Ma C., Wang C., Xia F., Wang Q., Yan P., Zhang Y. Microstructure, wear and corrosion resistances of Ni–ZrO_2–CeO_2 nanocoatings // Ceramics International. – 2024. – Vol. 50, № 12. – P. 20949–20957.

65 Benea L. Electrodeposition and tribocorrosion behaviour of ZrO_2–Ni composite coatings // Journal of Applied Electrochemistry. – 2009. – Vol. 39, № 10. – P. 1671–1681.

66 Laszczyńska A., Winiarski J., Szczygieł B., Szczygieł I. Electrodeposition and characterization of Ni–Mo–ZrO_2 composite coatings // Applied Surface Science. – 2016. – Vol. 369. – P. 224–231.

67 Novytska N., Zaverach I. Composition, topography and electrocatalytic properties of Ni–TiO2 composite coatings // Materials Today: Proceedings. – 2022. – Vol. 50. – P. 442–447.

68 Salehi M., Mozammel M., Emarati S. M., Alinezhadfar M. The role of TiO_2 nanoparticles on the topography and hydrophobicity of electrodeposited Ni–TiO_2 composite coating // Surface Topography: Metrology and Properties. – 2020. – Vol. 8, № 2. – P. 025008.

69 Li Y., Song P., Wang W., Lei M., Li X. Microstructure and wear resistance of a Ni–WC composite coating on titanium grade 2 obtained by electroplating and electron beam remelting // Materials Characterization. – 2020. – Vol. 170. – P. 110674.

70 Tehrani H. M., Shoja-Razavi R., Erfanmanesh M., Hashemi S. H., Barekat M. Evaluation of the mechanical properties of WC–Ni composite coating on an AISI 321 steel substrate // Optics and Laser Technology. – 2020. – Vol. 127. – P. 106138.

71 Zhao S., Yang L., Huang Y., Xu S. A novel method to fabricate Ni/WC composite coatings by laser wire deposition: processing characteristics, microstructural evolution and mechanical properties under different wire transfer modes // Additive Manufacturing. – 2021. – Vol. 38. – P. 101738.

72 Mbugua N. S., Kang M., Zhang Y., Ndiithi N. J., Bertrand G. V., Yao L. Electrochemical deposition of Ni, Ni–Co alloy and Ni–Co–ceramic composite coatings: a critical review // Materials. – 2020. – Vol. 13, № 16. – P. 3475.

73 Al Farisi M. S., Hertel S., Wiemer M., Otto T. Aluminum patterned electroplating from AlCl3–EMImCl ionic liquid towards microsystems application // Micromachines. – 2018. – Vol. 9, № 11. – P. 589.

74 Chen S. et al. Effect of deposition parameters for Ni–Au coatings on corrosion protection properties of 2A12 aluminum alloy // Materials. – 2025. – Vol. 18, № 5. – P. 969.

75 Jiang Y., Chen C.-Y., Chang T.-F. M., Luo X., Yamane D., Sone M. Electrodeposition of Ni–Co alloys and their mechanical properties by micro-Vickers hardness test // Electrochem. – 2021. – Vol. 2, № 1. – P. 1–9.

76 dos Santos É. S. et al. Electrochemical fabrication of Ni–Co alloy over a wide pH range using sodium citrate as a complexing agent // Coatings. – 2025. – Vol. 15, № 2. – P. 138.

77 Song Z. et al. Effect of current density on the performance of Ni–P–ZrO2–CeO2 composite coatings prepared by jet electrodeposition // Coatings. – 2020. – Vol. 10, № 7. – P. 616.

78 Jiang Y. et al. Electrodeposition and micro-mechanical property characterization of nickel–cobalt alloys toward design of MEMS components // Electrochem. – 2022. – Vol. 3, № 2. – P. 198–210.

79 Reddah I. et al. Experimental investigation and optimization of the electrodeposition parameters of Ni–Al2O3 composite coating using the Taguchi method // Coatings. – 2025. – Vol. 15, № 4. – P. 482.

80 Bielicka M., Lubecka M., Wasilewska A., Klekotka U., Kalska-Szostko B. Optimization of measurement conditions in SEM microscopy: a case study // Measurement. – 2025. – Vol. 253. – P. 117513.

81 Sheiati S., Behboodi S., Ranjbar N. Segmentation of backscattered electron images of geopolymers using convolutional autoencoder network // Expert Systems with Applications. – 2022. – Vol. 206. – P. 117846.

82 Quirk J., Rothmann M., Li W., Abou-Ras D., McKenna K. P. Grain boundaries in polycrystalline materials for energy applications: first principles modeling and electron microscopy // Applied Physics Reviews. – 2024. – Vol. 11, № 1. – P. 011308.

83 Zhan Z., Liu Y., Wang W., Du G., Cai S., Wang P. Atomic-level imaging of beam-sensitive COFs and MOFs by low-dose electron microscopy // Nanoscale Horizons. – 2024. – Vol. 9, № 6. – P. 900–933.

84 Vijayalakshmi V. J., Katyal A., K. D., Kansal A., Dasarathy A. K., Sharma N. S. Investigating the factors influencing image formation in scanning electron microscopy // International Conference on Computer Communication and Network Technology. – 2024.

85 Carrijo-Gonçalves G. A., da Silva B. P., Aoki I. V., Veloso T. C., Capelossi V. R. Co-deposition of natural particles in the acidic zinc electroplating process // Surface and Coatings Technology. – 2024. – Vol. 482. – P. 130703.

86 Valerio T.L., Boaron C.K., Marchesi L.F., da Silva B.J.G., Vidotti M. Interfacial characterization of poly(pyrrole) films doped with SiO_2 nanoparticles and their use as electrosorptive phase of caffeine // Electrochim. Acta. – 2023. – Vol. 474. – P. 11.

87 da Conceição Luiz L., Bell M.J.V., Batista R.T., de Freitas R.P., da Rocha R.A., Moreira S.I., Moraes M.N., dos Anjos V.D.C. Use of scanning electron microscopy with energy dispersive spectroscopy to detect metallic contamination in candies // Food Packag. Shelf Life. – 2021. – Vol. 28. – P. 100649.

88 Shereef A., Kunjumon J., Jose A.K., Tomy M., Akram W., Jebin R.P., Maity T., Sajan D. Synthesis, magnetic properties, and electrochemical evaluation of La2NiMnO6 double perovskite as electrode materials for supercapacitor applications // Ceram. Int. – 2024. – Vol. 50, №. 9. – P. 15756 -15766.

89 Javaheri V., Haiko O., Sadeghpour S., Valtonen K., Kömi J., Porter D. On the role of grain size on slurry erosion behavior of a novel medium-carbon, low-alloy pipeline steel after induction hardening // Wear. – 2021. – Vol. 476. – P. 203678.

90 Yao J., Jin T., Li Y., Xiao S., Huang B., Jiang J. Electrochemical performance of Fe2(SO4)3 as a novel anode material for lithium-ion batteries // J. Alloys Compd. – 2021. – Vol. 886. – P. 161238.

91 Liang L., Zhang J., Sumpter B. G., Tan Q.-H., Tan P.-H., Meunier V. Low-frequency shear and layer-breathing modes in Raman scattering of two-dimensional materials // ACS Nano. – 2017. – Vol. 11, № 12. – P. 11777–11802.

92 Cançado L. G. et al. Science and metrology of defects in graphene using Raman spectroscopy // Carbon. – 2024. – Vol. 220. – P. 118801.

93 Frost M. et al. Diamond precipitation dynamics from hydrocarbons at icy planet interior conditions // Nature Astronomy. – 2024. – Vol. 8, № 2. – P. 174–181.

94 Paul T., Choudhury D. R., Ghosh D., Saha C. Advancements in optical sensors for explosive materials identification: a comprehensive review // Results in Chemistry. – 2024. – P. 101602.

95 Xu Q., Ding N., Ma D., Lin H., Lin B., Ma X., Yang J., Guo L. Portable Hadamard-Transform Raman Spectrometer: A Powerful Analytical Tool for Point-of-Care Testing // Analytical Chemistry. – 2024. – Vol. 96, №. 30. – P. 12217–12224.

96 Ettabib M.A., Liu Z., Zervas M.N., Bartlett P.N., Wilkinson J.S. Waveguide-enhanced Raman spectroscopy // Nature Reviews Methods Primers. – 2024. – Vol. 4, №. 1. – P. 5.

97 Cao Y., Wang Z., Meng X., Li D., Xiong W., Mao G. Study on all solid-state 213 nm laser Raman spectrometer // Results in Optics. – 2023. – Vol. 13. – P. 100561.

98 Zhu X., Xu T., Lin Q., Duan Y. Technical development of Raman spectroscopy: from instrumental to advanced combined technologies // Applied Spectroscopy Reviews. – 2014. – Vol. 49, №. 1. – P. 64–82.

99 Alghamdi H., Concepcion B., Baliga S., Misra P. Synthesis, spectroscopic characterization and applications of tin dioxide // Contemporary Nanomaterials in Material Engineering Applications. – Cham: Springer International Publishing, 2020. – P. 285–318.

100 Sathish S., Kumaravelu T.A., Yang C.J., Jayapalan R.R., Nirmala R., Dong C.L., Lin B.H., Navamathavan R. Enhancing supercapacitor performance with biomass-derived activated carbon interlinked CoS2 embedded graphitic carbon nitride // Journal of Alloys and Compounds. – 2024. – Vol. 985. – P. 174076.

101 Ibrahim O., Toner M., Flint S., Byrne H. J., Lyng F. M. The potential of Raman spectroscopy in the diagnosis of dysplastic and malignant oral lesions // Cancers. – 2021. – Vol. 13, № 4. – P. 619.

102 Tittel J., Knechtel F., Ploetz E. Conquering Metal–Organic Frameworks by Raman Scattering Techniques // Advanced Functional Materials. – 2024. – Vol. 34, No. 43. – P. 2307518.

103 Khamoushi K. Structure and properties of rare earth neodymium zinc titanate // arXiv preprint. – 2015. – arXiv:1502.07530.

104 Safavi M.S., Walsh F.C. The electrodeposition of particle-metal matrix composite coatings to meet tribological and corrosion challenges // Advances in Colloid and Interface Science. – 2025. – P. 103584.

105 Wang X., Zhao W., Shi T., Cheng L., Hu S., Zhou C., Cui L., Li N., Liaw P.K. A Review on Tribological Wear and Corrosion Resistance of Surface Coatings on Steel Substrates // Coatings. – 2025. – Vol. 15, №. 11. – P. 1314.

106 Huang L., Deng X., Wang Q., Jia Y., Li C., Wang Z. Solidification and sliding wear behavior of low-alloy abrasion-resistant steel reinforced with TiC particles // Wear. – 2020. – Vol. 458. – P. 203444.

107 Hu K., Gao T., Xu Q., Yang H., Ma X., Nie J., Liu X. Investigation of the microstructures and mechanical properties of the Al–xSi–yAlNp composite by a diffusion method // Materials Science and Engineering: A. – 2020. – Vol. 788. – P. 139634.

108 Wang S., Yuan J., Han W., Yin Z. Microstructure and mechanical properties of B4C-TiB2 composite ceramic fabricated by reactive spark plasma sintering // International Journal of Refractory Metals and Hard Materials. – 2020. – Vol. 92. – P. 105307.

109 Zhang Z., Deng J., Wang R., Wu J., Tian R., Ma K. Two-step mask in-situ forming (CFx)n-TiO2/ZrO2 alternate coatings with different width ratios by electrohydrodynamic atomization // Surfaces and Interfaces. – 2024. – Vol. 44. – P. 103818.

110 Davami K., Doroudi A., Hunt T., Tavangarian F., Beck S., Beheshti A. High-velocity laser accelerated deposition: Microstructure and mechanical properties of the aluminum-steel bonding interface // Surface and Coatings Technology. – 2024. – Vol. 494. – P. 131509.

111 Sharma P., Seidel J. Scanning probe microscopy of functional materials surfaces and interfaces // Advanced Materials Interfaces. – 2016. – P. 63–125.

112 Shvedov M., Sherstyukova E., Kandrashina S., Inozemtsev V., Sergunova V. Atomic Force Microscopy and Scanning Ion-Conductance Microscopy for Investigation of Biomechanical Characteristics of Neutrophils // Cells. – 2024. – Vol. 13, No. 21. – P. 1757.

113 Kurki L., Oinonen N., Foster A.S. Automated structure discovery for scanning tunneling microscopy // ACS Nano. – 2024. – Vol. 18, №. 17. – P. 11130–11138.

114 Tiss B., Martínez-Martínez D., Mansilla C., Cunha L. Advanced UV Shielding for Cork: A comparative study of ZnO and TiO2 films through colorimetric and FTIR techniques // Applied Surface Science. – 2025. – Vol. 685. – P. 162038.

115 Chen X., Ni C. Experimental isothermal section phase diagram of Ho–Fe–In at 773 K and magnetic properties of Ho12Fe2.08In2.92 alloy // Rare Metals. – 2021. – Vol. 40, №. 4. – P. 987–994.

116 Wu M.W., Hu Z.F., Yang B.B., Tao Y., Liu R.P., Ma C.M., Zhang L. Additive manufacturing of Cu-Al-Mn shape memory alloy with enhanced superelasticity // Rare Metals. – 2023. – Vol. 42, №. 12. – P. 4234–4245.

117 Jappes J. T. W., Brintha N. C., Khan M. A., Christo N. J. Effect of modified method of coating on particle incorporation and wear resistance of nickel–phosphorus–diamond composite coatings // Materials Today: Proceedings. – 021. – Vol. 45. – P. 1509–1513.

118 Jena G., Philip J. A review on recent advances in graphene oxide-based composite coatings for anticorrosion applications // Progress in Organic Coatings. – 2022. – Vol. 173. №.. 107208.

119 Wu H., Cheng L., Liu C., Lan X., Zhao H. Engineering the interface in graphene oxide/epoxy composites using bio-based epoxy–graphene oxide nanomaterial to achieve superior anticorrosion performance // Journal of Colloid and Interface Science. – 2021. – Vol. 587. – P. 755–766.

120 Xue Y., Wang S., Xue Y., Cao L., Nie M., Jin Y. Robust self-cleaning and marine anticorrosion super-hydrophobic Co–Ni/CeO2 composite coatings // Advanced Engineering Materials. – 2020. – Vol. 22, №. 11. – P. 2000402.

121 Snizhnoi G., Pulina T., Solidor N., Yar-Mukhamedova G., Imanbayeva A., Zellele D., Mussabek G. Patterns and Mechanisms of Pitting of Heat Exchangers Made of AISI 321 and 08Kh18N10T Steels During their Operation in Recycled Water // Eurasian Chemico-Technological Journal. -2025. -Vol. 27, №. 4. -P. 305-313.

122 Randis R., Darmadi D. B., Gapsari F., Sonief A. A., Akpan E. D., Ebenso E. E. The potential of nanocomposite-based coatings for corrosion protection of metals: A review // Journal of Molecular Liquids. – 2023. – Vol. 390. – P. 123067.

123 Greshta V. L., Narivskyi O., Dzhus A., Vynar V., Yar-Mukhamedova G., Mukashev K., Beissen N., Mussabek G., Imanbayeva A., Zelele D., Atchibayev R. Corrosion behaviour of magnesium alloys NZ30K and NZ30K alloyed with silver in the model solution of the osteosynthesis process // Eurasian Physical Technical Journal. – 2024. – Vol. 21, №. 3(49). – P. 29-36.

124 Nenastina T., Sakhnenko M., Oksak S., Yar-Mukhamedova G., Zellele D., Mussabek G., Imanbayeva A. Study of complexation patterns in the system Ni^{2+}, MoO_4^{2-}, $P_2O_7^{4-}$, Cit^{3-} for the development of poly-ligand electrolytes // Eurasian Chemical-Technological Journal. – 2024. – Vol. 26, №. 3. –P. 155-160.

125 Raviprabha K., Bhat R. S. Corrosion inhibition of mild steel in 0.5 M HCl by substituted 1,3,4-oxadiazole // Egyptian Journal of Petroleum. – 2023. – Vol. 32, №. 2. – P. 1–10.

126 Dabees S., Mirzaei S., Kaspar P., Holcman V., Sobola D. Characterization and evaluation of engineered coating techniques for different cutting tools: Review // Materials. – 2022. – Vol. 15, №. 16. –P. 5633.

127 Yar-Mukhamedova G., Sakhnenko N., Karakurkchi A., Yermolenko I., Kemelzhanova A., Zellele D**.** Electrochemical and Mechanical Properties of Iron-Based Nanocomposites // Advanced and Novel Technologies - Interdisciplinary Collaboration in Materials Science (ANTICM 2025), Springer Nature, Zaporizhzhia, Ukraine. -2025. -P. 215 – 220.

128 Xin T., Pei H., Shucai Y. Coating and micro-texture techniques for cutting tools // Journal of Materials Science. – 2022. – Vol. 57, №. 36. – P. 17052–17104.

129 Sabzi M., Mousavi Anijdan S.H., Shamsodin M., Farzam M., Hojjati-Najafabadi A., Feng P., Park N., Lee U. A review on sustainable manufacturing of ceramic-based thin films by chemical vapor deposition (CVD): Reaction kinetics and deposition mechanisms // Coatings. – 2023. – Vol. 13, №. 1. –P. 188.

130 Gupta G., Tyagi R. K., Rajput S. K., Saxena P., Vashisth A., Mehndiratta S. PVD-based thin film deposition methods and characterization/property of different compositional coatings: A critical analysis // Materials Today: Proceedings. – 2021. – Vol. 38. – P. 259–264.

131 Ye Z., Li J., Liu L., Ma F., Zhao B., Wang X. Microstructure and wear performance enhancement of carbon nanotubes reinforced composite coatings fabricated by laser cladding on titanium alloy // Optics and Laser Technology. – 2021. – Vol. 139. –P. 106957.

132 Yar-Mukhamedova G., Sakhnenko N., Korogodskaya A., Stepanova I., Karakurchi A., Zellele D., Wang W. Y., Imanbayeva A. Synthesis and properties of polyfunctional coatings on aluminum and titanium alloys // Physical Sciences and Technology. -2025. -Vol. 12, №. 3-4. -P. 41-49.

133 Garg R., Gonuguntla S., Sk S., Iqbal M.S., Dada A.O., Pal U. and Ahmadipour M. Sputtering thin films: Materials, applications, challenges and future directions // Advances in Colloid and Interface Science. - 2024. -Vol. 330. №.. 103203.

134 Joseph A., Kirubasankar B., Mathew A. M., Narayanasamy M., Yan C., Angaiah S. Influence of pulse reverse current parameters on electrodeposition of copper–graphene nanocomposite coating // Applied Surface Science Advances. – 2021. – Vol. 5. –P. 100116.

135 Saini Singh G., Mehta S., Singh H., Dixit S. A review on mechanical behaviour of electrodeposited Ni-composite coatings // International Journal on Interactive Design and Manufacturing (IJIDeM). – 2023. – Vol. 17, №. 5. – P. 2247–2258.

136 Fayyaz O., Bahgat Radwan A., Sliem M. H., Abdullah A. M., Hasan A., Shakoor R. A. Investigating the properties of electrodeposited Ni–P–ZrC nanocomposite coatings // ACS Omega. – 2021. – Vol. 6, №. 49. – P. 33310–33324.

137 Zellele D. M., Yar-Mukhamedova G. S., Rutkowska-Gorczyca M. A review on properties of electrodeposited nickel composite coatings: Ni–Al_2O_3, Ni–SiC, Ni–ZrO_2, Ni–TiO_2 and Ni–WC // Materials. – 2024. – Vol. 17, №. 23. –P. 5715.

138 Okonkwo B. O., Jeong C., Jang C. Advances on Cr and Ni electrodeposition for industrial applications: A review // Coatings. – 2022. – Vol. 12, №. 10. –P. 1555.

139 Yar-Mukhamedova G. S., Zellele D. M., Rutkowska-Gorczyca M., Makhambet I., Mussabek G., Atchibayev R., Kemelzhanova A. Advancements in coating methods and properties of titanium-based composite coatings: A review // ES Materials and Manufacturing. – 2025. – Vol. 28. №. 1569.

140 Bastakys L., Marcinauskas L., Milieška M., Kalin M., Kėželis R. Tribological properties of Cr_2O_3, Cr_2O_3–SiO_2–TiO_2 and Cr_2O_3–SiO_2–TiO_2–graphite coatings deposited by atmospheric plasma spraying // Coatings. – 2023. – Vol. 13, №. 2. –P. 408.

141 Nebogatikov R. S., Pichidze S. Ya. Structure and properties of the SiO2–Cr2O3 coatings obtained by pulsed magnetron sputtering onto a ZrO2 ceramic substrate // Inorganic Materials: Applied Research. – 2024. – Vol. 15, №. 5. – P. 1289–1299.

142 Shakiba S., Khabbazi N. S., Tabrizi A. T., Aghajani H. Enhancing the electroplated chromium coating for corrosion protection of aluminum by adding graphene oxide // Surface Engineering and Applied Electrochemistry. – 2022. – Vol. 58, №. 2. – P. 202–209.

143 Zellele D. M., Gulmira S. Yar-Mukhamedova, and Małgorzata Rutkowska-Gorczyca. Effect of Deposition Temperature on Morphology and Corrosion Resistance of Electrodeposited Chromium-Graphene Composite Coatings // ES Materials and Manufacturing. – 2025. – Vol. 31, №. 1966.

144 Mahmoudi D., Taghizadeh Tabrizi A., Aghajani H. Study of the variation of surface topography and corrosion resistance of Cr–GO nanocomposite coatings by addition of GO nanoparticles // Surface Topography: Metrology and Properties. – 2021. – Vol. 9, №. 1. –P. 015025.

145 Mohamed M. E., Mekhaiel P. S., Mahgoub F. M. Construction of superhydrophobic graphene-based coating on steel substrate and its ultraviolet durability and corrosion resistance properties // Scientific Reports. – 2023. – Vol. 13, №. 1. –P. 590.

146 Özkan D., Erarslan Y., Kıncal C., Gürlü O., Yağcı M. B. Wear and corrosion resistance enhancement of chromium surfaces through graphene oxide coating // Surface and Coatings Technology. – 2020. – Vol. 391. –P. 125595.

147 Tseluikin V., Dzhumieva A., Yakovlev A., Mostovoy A., Lopukhova M. Electrodeposition of graphene oxide modified composite coatings based on nickel–chromium alloy // Crystals. – 2021. – Vol. 11, №. 4. –P. 415.

148 Zhu Y. et al. An improved Hummers method to synthesize graphene oxide using much less concentrated sulfuric acid // Chinese Chemical Letters. – 2022. – Vol. 33, №. 10. – P. 4541–4544.

149 Salverda M., Thiruppathi A. R., Pakravan F., Wood P. C., Chen A. Electrochemical exfoliation of graphite to graphene-based nanomaterials // Molecules. – 2022. – Vol. 27, №. 24. –P. 8643.

150 Marcano D. C. et al. Improved synthesis of graphene oxide // ACS Nano. – 2010. – Vol. 4, №. 8. – P. 4806–4814.

151 Moon I. K., Lee J., Ruoff R. S., Lee H. Reduced graphene oxide by chemical graphitization // Nature Communications. – 2010. – Vol. 1. –P. 73.

152 Stankovich S. et al. Synthesis of graphene-based nanosheets via chemical reduction of exfoliated graphite oxide // Carbon. – 2007. – Vol. 45, №. 7. – P. 1558–1565.

153 Xue Y., Zhu L., Chen H., Qu J., Dai L. Multiscale patterning of graphene oxide and reduced graphene oxide for flexible supercapacitors // Carbon. – 2015. Vol. – 92. – P. 305–310.

154 Basha G. M. T., Venkateshwarlu B. Influence of carbon nanotubes reinforcement on characteristics of thermally sprayed ceramic coatings // Surface Review and Letters. – 2021. – Vol. 28, №. 2. – P. 2050052.

155 Usef A. P., Bhajantri V., Kannoth V., Jambagi S. C. Influence of carbon nanotube reinforcement on the heat transfer coefficient, microstructure, and mechanical properties of a die-cast Al–7Si–0.35Mg alloy // Journal of Alloys and Compounds. – 2021. – Vol. 888. – P. 160844.

156 V. S., S. B., Praveen B. M., Devendra B. K. The effect of graphene content on the corrosion and mechanical properties of an electrodeposited Ni–graphene coating // Applied Surface Science Advances. – 2022. – Vol. 11. – P. 100310.

157 Sundaramali G., Aiyasamy J. P., Karthikeyan S., Kandavel T. K., Arulmurugan B., Rajkumar S., Sharma S., Li C., Dwivedi S. P., Kumar A., Singh R. Experimental investigations of electrodeposited Zn–Ni, Zn–Co, and Ni–Cr–Co-based novel coatings on AA7075 substrate to ameliorate the mechanical, abrasion, morphological, and corrosion properties for automotive applications // Reviews on Advanced Materials Science. –2023. –Vol. 62, №. 1. –P. 20220324.

158 Osuchowska E., Buczko Z. Zn–Cr pulse plated alloy coatings for corrosion protection // Transactions of the IMF. –2024. –Vol. 102, №. 1. –P. 38–42.

159 Meng L., Hu Q., Shi C., Huang C. Roles of graphene additives in optimizing the microstructure and properties of Ni–Cr–graphene coatings // Coatings. –2020. – Vol. 10, №. 2. –P. 104.

160 Zellele D. M., Microstructural and corrosion resistance properties of electrodeposited chromium–graphene composite coatings under varying deposition temperatures // Materials of the XVI International Symposium on Combustion Plasma and Chemistry, Physics and Chemistry of Carbon and Nano Energetic Materials. Almaty, Kazakhstan, 1–3 October. –P. 181.

161 Guan T., Zhang N. Recent advances in electrodeposition of nickel-based nanocomposites enhanced with lubricating nanoparticles // Nanomanufacturing and Metrology. –2024. –Vol. 7, №. 1. –P. 25.

162 Zellele D. M., Yar-Mukhamedova G. S., Rutkowska-Gorczyca M. Effects and applications of additives in Nickel electrodeposition: A review // ES Materials and Manufacturing. – 2026. – Vol. 31, – P. 2080.

163 Fattah M., Morin S. Microstructure, corrosion, and hardness properties of Ni coatings electrodeposited from a deep eutectic solvent-based electrolyte // Journal of Materials Engineering and Performance. –2025. –Vol. 34, №. 17. –P. 18560–18576.

164 Aghaee Malayeri M., Koohestani H., Tajally M. Improving the properties of nickel/graphene oxide coated copper plate by changing the electroplating process conditions // Results in Engineering. –2023. –Vol. 18. -P. 101167.

165 Bigos A., Wolowicz M., Janusz-Skuza M., Starowicz Z., Szczerba M. J., Bogucki R., Beltowska-Lehman E. Citrate-based baths for electrodeposition of nanocrystalline nickel coatings with enhanced hardness // Journal of Alloys and Compounds. –2021. –Vol. 850. -P. 156857.

166 Sowmiyanarayanan A., Krishnamurthy S., Kandasubramanian B., Balu P. K. Current trends in multifunctional nanocomposite coatings through electrodeposition for aerospace and strategic defense // Advanced Engineering Materials. –2025. –Vol. 27, №. 13. -P. 2402668.

167 Awasthi S., De S., Pandey S. K. Electrodeposited carbon nanostructured nickel composite coatings: A review // Heliyon. –2024. –Vol. 10, №. 8. -P. e26051.

168 Omoegun O., Fayomi O., Ayoola A., Agboola O. Chemical deposition and corrosion perspectives on the development of pipe union steel in automobile industry // International Journal of Advanced Manufacturing Technology. –2024. –Vol. 131, №. 9. P. 4611–4620.

169 Ojo A. A., Dharmadasa I. M. Electroplating of semiconductor materials for applications in large area electronics: A review // Coatings. –2018. –Vol. 8, №. 8. -P. 262.

170 Sui Y., Sun C., Sun J., Pu B., Ren W., Zhao W. Stability of an electrodeposited nanocrystalline Ni-based alloy coating in oil and gas wells with the coexistence of H2S and CO2 // Materials. –2017. –Vol. 10, №. 6. -P. 632.

171 Khorsand S., Raeissi K., Ashrafizadeh F. Corrosion resistance and long-term durability of super-hydrophobic nickel film prepared by electrodeposition process // Applied Surface Science. –2014. –Vol. 305. –P. 498–505.

172 Zhou Z., Ma B., Zhang X., Tang L., Lin X., Hu C., Ren K. Enhanced corrosion resistance and self-cleaning properties of superhydrophobic nickel coating fabricated by one-step electrodeposition // Ceramics International. –2023. –Vol. 49, №. 8. –P. 13109–13118.

173 Liu Z., Zhang Q., Zhang X., Yu Z., Mao Q., Nie J., Zhao Y. Electrodeposition of nanocrystalline Ni and NiCr alloy coatings: Effects of Cr content on microhardness and wear resistance improvement // Journal of Materials Research and Technology. – 2024. –Vol. 30. –P. 3584–3593.

174 Xie D., Wu W., Huang J., Wang X., Zhang Y., Wang Z., Jiang P., Tang L., Wu F., Wang Q. Effect of electrodeposited Cu interlayer thickness on characterizations and adhesion force of Ni/Cu/Ni coatings on polyetherimide composite substrates // International Journal of Adhesion and Adhesives. –2024. –Vol. 129. -P. 103580.

175 Mušicki M., Mitrović N., Rethas S., Mladenović I. O., Petković S., Radojević V., Lamovec J. S. Evaluation of adhesion performance of electrodeposited nickel coatings on copper and molybdenum substrates using different techniques // Proceedings of the 12th International Conference on Electrical, Electronic and Computing Engineering (IcETRAN). –2025. –P. 1–6.

176 Kumar A., Sharma R., Kumar S., Verma P. A review on machining performance of AISI 304 steel // Materials Today: Proceedings. –2022. –Vol. 56. –P. 2945–2951.

177 Kumar R., Das A. K. A comprehensive review of AISI 304 steel based on different thick coating process // Materials Today: Proceedings. –2024. –Vol. 98. –P. 180–186.

178 Banovic S. W., Barmak K., Marder A. R. Microstructural characterization and hardness of electrodeposited nickel coatings from a sulphamate bath // Journal of Materials Science. –1998. –Vol. 33, №. 3. –P. 639–645.

179 Boukhrouiete A., Boumendjel S., Sobhi N.-E.-H. Effect of current density on the microstructure and morphology of the electrodeposited nickel coatings // Turkish Journal of Chemistry. –2021. –Vol. 45, №. 5. –P. 1599–1608.

180 Hu Y., Lam S., Lodhi M. J. K., Spencer B. W., Teng F., Hosemann P. Experimental evaluation of interfacial bonding strength between 304 stainless steel substrate and electrodeposited nickel coating using mesoscale mechanical testing methods // JOM. –2025. –Vol. 77, №. 5. –P. 3513–3525.

181 Keramatian A., Enayati M. H., Sayyedan F., Torkian S. Investigating the effect of current density on electrodeposited Ni–TiC–WC composite coating and evaluating the corrosion resistance of the coating and substrate in NaCl solution // Iranian Journal of Materials Science and Engineering. –2025. –Vol. 22, № 2.

182 Mandich N. V. Surface preparation of metals prior to plating // Metal Finishing. – 2002, – Vol. 101, – №. 9, – P. 8-22.

183 Rudnik E. Black nickel coatings: From plating techniques to applications // Coatings. –2024. –Vol. 14, №. 12. -P. 1588.

184 Zhang F., Liu S., Wang F. Nucleation and growth behaviors of nickel coating by jet electrodeposition under the combined effect of convection and vertical distribution // Journal of Physical Chemistry C. –2022. –Vol. 126, №. 34. –P. 14669–14679.

185 Lin Y.-P., Selman J. R. Electrodeposition of Ni–Zn alloy. II. Electrocrystallization of Zn, Ni, and Ni–Zn alloy // Journal of the Electrochemical Society. –1993. –Vol. 140, №. 5. –P. 1304.

186 Nikitin V. S., Ostanina T. N., Rudoi V. M., Kuloshvili T. S., Darintseva A. B. Features of hydrogen evolution during electrodeposition of loose deposits of copper, nickel and zinc // Journal of Electroanalytical Chemistry. –2020. –Vol. 870. -P. 114230.

187 Egbuhuzor M. O., Akalezi C. O., Ulaeto S. B., Njoku D. I., Onyeachu B. I., Oguzie E. E. Electro-deposited nanocomposite coatings and their behaviours against aqueous and high-temperature corrosion: A review // Hybrid Advances. –2024. –Vol. 5. -P. 100180.

188 Juodkazis K., Juodkazytė J., Vilkauskaitė R., Jasulaitienė V. Nickel surface anodic oxidation and electrocatalysis of oxygen evolution // Journal of Solid State Electrochemistry. –2008. –Vol. 12, №. 11. –P. 1469–1479.

189 Li J., Li P., Li J., Tian Z., Yu F. Highly-dispersed Ni–NiO nanoparticles anchored on an SiO2 support for enhanced CO methanation performance // Catalysts. –2019. –Vol. 9, №. 6. -P. 506.

190 Wu B., Tan B., Tan G., Zeng M., Luo J., Hu G., Hao Z., Lai S., Liu B. Electroless deposition of Ni–P/Au coating on Cu substrate with improved corrosion resistance // RSC Advances. –2021. –Vol. 11, №. 62. –P. 39153–39168.

191 Arnaudova M., Lefterova E., Rashkov R. Corrosion behavior of electrodeposited nickel-based coatings with W, Mo, and TiOx // Journal of Solid State Electrochemistry. –2024. –Vol. 28, №. 5. –P. 1657–1670.

192 Monshi A., Foroughi M. R., Monshi M. R. Modified Scherrer equation to estimate more accurately nano-crystallite size using XRD // World Journal of Nano Science and Engineering. –2012. –Vol. 2, №. 3. –P. 154–160.

193 Haušild P., Čech J., Karlík M., Legros M., Nohava J., Merle B. Indentation size effect in electrodeposited nickel with different grain size and crystal orientation // Crystals. –2023. –Vol. 13, №. 9. -P. 1385.

194 Matsui I., Watanabe A., Takigawa Y., Omura N., Yamamoto T. Microstructural heterogeneity in the electrodeposited Ni: Insights from growth modes // Scientific Reports. –2020. –Vol. 10, №. 1. -P. 5548.

195 Philipsen H. et al. Nucleation and growth kinetics of electrodeposited Ni films on Si(100) surfaces // Electrochimica Acta. –2017. –Vol. 230. –P. 407–417.

196 Nasehnejad M., Nabiyouni G. Role of substrate on the fractal characteristics of nanostructure surfaces of electrodeposited nickel thin films // Physica Status Solidi B. –2024. –Vol. 261, №. 8. -P. 2400109.

197 Parnian M. J., Jafarniya V., Marenco A. J., Paulson S., Birss V. I. Controlling the surface properties of electrodeposited Ni films // ECS Meeting Abstracts. –2020. –Vol. MA2020-01, №. 20. –P. 1224.

198 Guo F., Yu X., Wang M. The dependence and evolution mechanism of surface structure of electrodeposited Ni films on wettability // Journal of the Electrochemical Society. –2020. –Vol. 167, №. 6. -P. 063506.

199 Yu X., Wang M., Wang Z., Gong X., Guo Z. The structure evolution mechanism of electrodeposited porous Ni films on NH4Cl concentration // Applied Surface Science. –2016. –Vol. 360. –P. 502–509.

200 Zellele D. M., Rutkowska-Gorczyca M. Electrochemical synthesis and functional properties of metal and alloy-based composition coatings // Recent Contributions to Physics. –2024. –Vol. 88, №. 1. –P. 41–48.

201 Zellele D., Sakhnenko M., Nenastina T., Yar-Mukhamedova G. Electrolytic nickel alloys: Status and prospects // Proceedings of the XXXIII International Scientific-Practical Conference MicroCAD-2025. Kharkiv, Ukraine, –2025. –P. 1882.

202 Zellele D., Zhamanbayeva G., Kemelzhanova A., Atchibayev R., Kurmangaliyeva V. Microstructure, tribological and corrosion resistance properties of

Ni composite coatings prepared via electrodeposition // International Multidisciplinary Scientific GeoConference (SGEM 2025). –2025. –Vol. 6, №. 1. –P. 57–63.

203 de Souza R. F., Del Pozzo A. S., Giuliano A. D., Silvestrin G., De Micheli L., Soares E. P., Giovedi C., Terremoto L. A., Somessari S. L., Neto A. O., Calvo W. In-operando 3D visualization of nickel electrodeposition and mass transport phenomena // International Journal of Electrochemical Science. –2025. –Vol. 20, №. 8. -P. 101090.

204 Wang C.-C., Ziegler K. J., Narayanan R. Understanding electrodeposition instabilities // ECS Meeting Abstracts. –2014. –Vol. MA2014-01, №. 43. –P. 1663.

205 Hao F., Verma A., Mukherjee P. P. Electrodeposition stability of metal electrodes // Energy Storage Materials. –2019. –Vol. 20. –P. 1–6.

206 Яр-Мухамедова Г. Ш., Ведь М. В., Сахненко Н. Д., Степанова И. И., Желавская Ю. А., Корогодская А. Н., Мукашев К., Мурадов А. Д., Зеллеле Д. Функциональные покрытия сплавами и нанокомпозитами для экотехнологий: синтез и свойства: монография. Алматы: Казахский национальный университет имени аль-Фараби, 2025. 110 с.

207 Zellele D., Electrodeposited iron-based composition coatings // Proceedings of the International Scientific Conference of Students and Young Scientists “Farabi Alemi”. Almaty, Kazakhstan, 3–5 April 2025. P. 447.

208 Makhambet I., Zellele D. Development of recommendations for corrosion-resistant nano-CEC applications // Proceedings of the International Scientific Conference of Students and Young Scientists “Farabi Alemi”. Almaty, Kazakhstan, 3–5 April 2025. P. 448.

209 Shao I., Vereecken P. M., Chien C. L., Cammarata R. C., Searson P. C. Electrochemical deposition of FeCo and FeCoV alloys // Journal of the Electrochemical Society. –2003. –Vol. 150, №. 3. –P. C184.

210 Patent 11879 Republic of Kazakhstan; Yar-Mukhamedova G., Sakhnenko N., Imanbaeva A., Kemelzhanova A., Zellele D., Atchibayev R., Pospelov A., Zhelavskaya Y., Zyubanova S., Wang Y., Shen C. Method for depositing a cobalt-vanadium alloy coating, 06.03.2026, Bulletin №. 9.

211 Patent 10580 Republic of Kazakhstan; Yar-Mukhamedova G., Sakhnenko N., Mukashev K., Imanbayeva A., Zellele D., Nenastina T., Mussabek G., Pospelov A. Method for applying coatings with iron–cobalt–vanadium alloy, 19.02.2025, Bulletin №. 22.

212 Ehsan M. A., Hakeem A. S., Sharif M., Rehman A. Direct deposition of amorphous cobalt–vanadium mixed oxide films for electrocatalytic water oxidation // ACS Omega. –2019. –Vol. 4, №. 7. P. 12671–12679.

213 Bairachniy B., Zhelavska Y., Smirnova O., Pilipenko A., Finohenov O. Study of electrocatalytic activity of the vanadium-containing materials for the hydrogen evolution reaction // Materials Today: Proceedings. –2022. –Vol. 50. –P. 448–451.

214 Bairachnyi V., Rudenko N., Zhelavska Y., Pilipenko A. Using aluminum alloys in the electrochemical hydrogen production // Materials Today: Proceedings. –2019. –Vol. 6. –P. 299–304.

215 Sakhnenko M. D., Ved’ M. V., Ermolenko I. Y., Hapon Y. K., Kozyar M. O. Design, synthesis, and diagnostics of functional galvanic coatings made of multicomponent alloys // Materials Science. –2017. –Vol. 52, №. 5. –P. 680–686.

216 Nenastina T. O., Ved’ M. V., Sakhnenko M. D., Proskurina V. O., Zyubanova S. I. Corrosion resistance of composite coatings based on the alloys of cobalt with refractory metals // Materials Science. –2021. –Vol. 56, №. 5. –P. 634–641.